

UNIVERSITÄTSKLINIKUM HAMBURG-EPPENDORF

Zentrum für Operative Medizin
Klinik und Poliklinik für Unfall-, Hand- und Wiederherstellungschirurgie

Prof. Dr. med. Karl-Heinz Frosch

Role of Tgif1 in osteoclast differentiation and bone resorption

Dissertation

zur Erlangung des Doktorgrades Dr. rer. biol. hum. / PhD
an der Medizinischen Fakultät der Universität Hamburg.

vorgelegt von:

Miki Maeda, *M.Sc.*
aus Chiba, Japan

Hamburg 2018

(wird von der Medizinischen Fakultät ausgefüllt)

**Angenommen von der
Medizinischen Fakultät der Universität Hamburg am:** 20.03.2019

**Veröffentlicht mit Genehmigung der
Medizinischen Fakultät der Universität Hamburg**

Prüfungsausschuss, der/die Vorsitzende: Prof. Dr. Eric Hesse

Prüfungsausschuss, zweite/r Gutachter/in: Prof. Dr. Stefan Linder

Prüfungsausschuss, dritte/r Gutachter/in: _____

Table of Content

1	Introduction	1
1.1	Bone anatomy	2
1.2	Bone development	4
1.3	Bone remodeling and modeling	4
1.4	Aging-related bone disease	6
1.5	Osteoporosis	7
1.6	Osteopetrosis and Osteosclerosis	7
1.7	RANKL/RANK signaling cascade	8
1.8	Osteoblasts and Osteocytes	9
1.8.1	Runt-related transcription factor 2 (Runx2)	10
1.8.2	Osterix	11
1.8.3	Activating transcription factor 4 (ATF4)	11
1.8.4	Sclerostin	11
1.8.5	Osteopontin (OPN)	12
1.8.6	Parathyroid hormone 1 receptor (PTH1R), Parathyroid hormone/parathyroid hormone-related protein/peptide receptor	13
1.9	Osteoclast precursors	13
1.10	Osteoclasts	15
1.11	Tartrate-resistant acid phosphatase (TRAP)	17
1.12	Cathepsin K	18
1.13	Dendritic cell-specific transmembrane protein (DC-STAMP) and Osteoclast stimulatory transmembrane protein (OC-STAMP)	18
1.14	Src	19
1.15	TNF receptor-associated factors (TRAFs)	21
1.16	Transforming growth factor beta (TGF- β) receptor signaling	22
1.17	Sma and Mad related (Smad) signaling	23
1.18	Nuclear factor of activated T cells (NFATc1)	23
1.19	Nuclear factor kappa B (NF- κ B)	24
1.20	Activator protein 1 (AP-1)	25
1.21	Treatment of osteoporosis	26
1.21.1	Anti-resorptive drugs for the treatment of osteoporosis	26
1.21.1.1	Bisphosphonates	26
1.21.1.2	Denosumab	27
1.21.2	Anabolic drugs for the treatment of osteoporosis	28

Table of Contents

1.21.2.1	Teriparatide	28
1.21.2.2	Abaloparatide	28
1.21.2.3	Romosozumab	29
1.22	TG-interacting factor 1 (Tgif1)	29
2	Hypothesis and Aims	32
2.1	Hypothesis	33
2.2	Aims.....	33
3	Materials and Methods	34
3.1	Chemicals, equipment and consumables	35
3.2	Kits.....	39
3.3	DNA ladders and protein standards	39
3.4	Enzymes.....	40
3.5	Oligonucleotides	40
3.5.1	Primers	40
3.5.2	GapmeR oligonucleotides	42
3.6	Antibodies.....	43
3.7	Live cell imaging	45
3.8	Electronic data processing	45
3.9	Mice	46
3.9.1	Tgif1 ^{+/-} and Tgif1 ^{loxP/+} mice	46
3.9.2	LysM-Cre;Tgif1 ^{loxP/loxP} mice	47
3.9.3	Ctsk-Cre;Tgif1 ^{loxP/loxP} mice	47
3.10	Cell biology methods	47
3.10.1	Medium and solutions for cell culture.....	47
3.10.2	Cell culture	48
3.10.3	Trypsinization.....	48
3.10.4	Cell counting	48
3.10.5	Bone marrow isolation and BMM culture.....	48
3.10.6	Colony Forming Unit (CFU) assay	49
3.10.7	Primary osteoblast isolation from the long bones	49
3.10.8	Primary osteoblast isolation from calvariae	49
3.10.9	Osteoblast differentiation and mineralization	50
3.10.10	Osteoclast differentiation.....	50
3.10.11	Pit formation assay	51
3.10.12	Pit volume analysis	51
3.10.13	Osteoclast differentiation with Okadaic acid.....	52

Table of Contents

3.11	Biochemical methods.....	52
3.11.1	Staining of cell culture	52
3.11.1.1	TRAP staining.....	52
3.11.1.2	Alkaline Phosphatase (ALP) staining.....	53
3.11.1.3	Alizarin Red staining.....	53
3.11.2	Immunocytochemistry.....	54
3.11.2.1	Actin staining	54
3.11.3	Flow cytometry	54
3.11.4	Protein extraction (Total cell lysate preparation).....	55
3.11.5	Nuclear/Cytoplasmic Fractionation.....	56
3.11.6	Measurement of protein concentration.....	56
3.11.7	Sodium Dodecyl Sulfate (SDS)- Poly-Acrylamide Gel Electrophoresis (PAGE)	57
3.11.8	Transferring.....	58
3.11.9	Immunoblotting.....	59
3.11.10	Mild retrieving of western blot membrane	60
3.12	Molecular biology methods	60
3.12.1	Alkaline digestion for the isolation of genomic DNA	60
3.12.2	Genotyping.....	61
3.12.2.1	Preparation.....	61
3.12.2.2	Tgif1 genotyping	62
3.12.2.3	Ctsk-Cre genotyping.....	63
3.12.2.4	LysM-Cre genotyping	63
3.12.3	RNA extraction	64
3.12.4	Synthesis of complementary DNA (cDNA).....	65
3.12.5	Quantitative real-time polymerase chain reaction (qRT-PCR).....	65
3.12.6	Inhibition of mRNA function by GapmeR.....	66
3.12.7	<i>In silico</i> analysis	67
3.13	<i>In vivo</i> analysis.....	68
3.13.1	<i>In vivo</i> sample collection.....	68
3.13.2	Dehydration of bone samples.....	68
3.13.3	Infiltration of bone samples.....	69
3.13.4	MMA embedding	69
3.13.5	Staining of tissue sections	69
3.13.5.1	von Kossa/van Giesson staining.....	69
3.13.5.2	Toluidine blue staining.....	71
3.13.5.3	TRAP staining.....	71

Table of Contents

3.13.6	Histomorphometry	72
3.13.7	Micro-computed tomography (μ CT) scan	72
3.13.7.1	<i>In vivo</i> scan.....	72
3.13.7.2	<i>Ex vivo</i> scan.....	73
3.13.8	μ CT analysis.....	73
3.14	Ethics.....	73
3.15	Statistics	74
4	Results	75
4.1	RANKL and M-CSF stimulation increases <i>Tgif1</i> expression in osteoclasts.....	76
4.2	Osteoclast-targeted deletion of <i>Tgif1</i>	77
4.3	Analysis of <i>LysM-Cre⁺;Tgif1^{loxP/loxP}</i> mice	78
4.3.1	<i>In vitro</i> phenotype	78
4.3.1.1	<i>Tgif1</i> expression in osteoclasts.....	78
4.3.1.2	Differentiation of osteoclasts from <i>LysM-Cre⁺;Tgif1^{loxP/loxP}</i> mice	78
4.3.2	<i>In vivo</i> phenotype	80
4.3.2.1	Bone phenotype of young <i>LysM-Cre⁺;Tgif1^{loxP/loxP}</i> mice.....	80
4.3.2.2	Bone phenotype of aged <i>LysM-Cre⁺;Tgif1^{loxP/loxP}</i> mice	81
4.4	Analysis of <i>Ctsk-Cre⁺;Tgif1^{loxP/loxP}</i> mice.....	82
4.4.1	<i>In vitro</i> phenotype	82
4.4.1.1	<i>Tgif1</i> expression in osteoclasts.....	82
4.4.1.2	Osteoclast differentiation of <i>Ctsk-Cre⁺;Tgif1^{loxP/loxP}</i> BMMs	82
4.4.1.3	<i>Tgif1</i> expression and differentiation of osteoblasts isolated from <i>Ctsk-Cre⁺;Tgif1^{loxP/loxP}</i> mice	84
4.4.2	Bone mass kinetics of <i>Ctsk-Cre⁺;Tgif1^{loxP/loxP}</i> mice	85
4.4.3	Bone phenotype of young <i>Ctsk-Cre⁺;Tgif1^{loxP/loxP}</i> mice	86
4.4.4	Bone phenotype of aged <i>Ctsk-Cre⁺;Tgif1^{loxP/loxP}</i> mice.....	89
4.5	<i>In vitro</i> osteoclast phenotype of <i>Tgif1</i> -deficient BMMs.....	91
4.6	Osteoclast precursors	92
4.7	Osteoclast fusion.....	93
4.8	Actin ring formation in osteoclasts.....	95
4.9	Osteoclast resorption activity	97
4.10	RANKL and M-CSF signaling pathways	98
4.11	RANK and <i>c-fms</i> receptors.....	99
4.12	Signaling cascades	100
4.13	Protein Phosphatase 2A (PP2A)	102
4.14	Okadaic acid (OKA)	105

Table of Contents

4.15	Silencing by GapmeR	107
4.15.1	PP2A-C β -targeting GapmeR.....	107
4.15.2	Tgif1-targeting GapmeR	108
4.15.3	Targeting Tgif1 and PP2A-C β using GapmeRs.....	111
4.16	<i>In silico</i> analysis of the PP2A-C β promoter	112
5	Discussion	115
6	List of Abbreviations.....	122
6.1	Generic Abbreviations	123
6.2	Abbreviations in Histomorphometry	129
6.3	Abbreviations of Peptide sequence/Amino acid sequence	130
7	Bibliography.....	131
8	Summary	147
8.1	Summary in English	148
8.2	Summary in German.....	150
9	List of Publications and Author Contributions	152
9.1	Publications	153
9.2	Abstracts	154
10	Acknowledgement.....	155
11	Curriculum Vitae.....	163
12	Declaration	166
12.1	Declaration in English.....	167
12.2	Declaration in German	168

List of Tables

Table 3.1. Chemicals	35
Table 3.2. Equipment	37
Table 3.3. Consumables	38
Table 3.4. Kits	39
Table 3.5. Enzymes	40
Table 3.6. Primers	40
Table 3.7. GapmeRs	43
Table 3.8. Primary antibodies	43
Table 3.9. Secondary antibodies	45
Table 3.10. Vybrant™ Cell-Labeling Solutions	45
Table 3.11. Softwares.....	45
Table 3.12. Online programs and databases.....	46
Table 4.1. Tgif1 potential binding sites on the promoter region of PP2A-C β gene (Ppp2cb)	113
Table 6.1. Generic Abbreviations	123
Table 6.2. Abbreviations in Histomorphometry.....	129
Table 6.3. Abbreviations of Peptide sequence	130

List of Figures

Fig. 1.1. Schematic image of a cross-section of bone.....	4
Fig. 1.2. Bone remodeling cycle.	6
Fig. 1.3. Signaling cascades in osteoclastogenesis.....	9
Fig. 1.4. Osteoblast differentiation.....	10
Fig. 1.5. Schematic alteration of cell surface markers during differentiation from hematopoietic stem cell to osteoclast.	15
Fig. 1.6. Schematic important factors in osteoclast differentiation.....	17
Fig. 1.7. The structure of c-Src family tyrosine kinase.	20
Fig. 1.8. Schematic functional TRAF proteins.....	22
Fig. 1.9. Functional domains of TGIF.....	31
Fig. 3.1. Schematic GapmeR designs by Exiqon algorithm.....	43
Fig. 3.2. Transferring membrane in order.	59
Fig. 3.3. Agarose gel electrophoresis for Tgif1 genotyping.....	62
Fig. 3.4. Agarose gel electrophoresis for Ctsk-Cre genotyping.	63
Fig. 3.5. Agarose gel electrophoresis for LysM genotyping.....	64

Fig. 4.1. Tgif1 expression increases in osteoclasts during differentiation and in response to RANKL and M-CSF stimulation.	77
Fig. 4.2. Osteoclast differentiation is impaired in LysM-Cre ⁺ ;Tgif1 ^{loxP/loxP} osteoclasts <i>in vitro</i>	79
Fig. 4.3. LysM-Cre ⁺ ;Tgif1 ^{loxP/loxP} mice have no striking phenotype at 8 weeks of age.	81
Fig. 4.4. LysM-Cre ⁺ ;Tgif1 ^{loxP/loxP} mice have a tendency towards an increased bone mass compared to control mice at 36 weeks of age.	82
Fig. 4.5. Osteoclast differentiation is impaired in Ctsk-Cre ⁺ ;Tgif1 ^{loxP/loxP} BMMs <i>in vitro</i>	84
Fig. 4.6. Osteoblast differentiation is impaired in Ctsk-Cre ⁺ ;Tgif1 ^{loxP/loxP} calvarial osteoblasts <i>in vitro</i>	85
Fig. 4.7. Deletion of Tgif1 in osteoclasts protects from age-related bone loss.	86
Fig. 4.8. Ctsk-Cre ⁺ ;Tgif1 ^{loxP/loxP} mice have a low turnover bone phenotype at 8 weeks of age.	88
Fig. 4.9. Aged Ctsk-Cre ⁺ ;Tgif1 ^{loxP/loxP} mice have a higher bone mass than controls due to a decreased osteoclast activity.	90
Fig. 4.10. Loss of Tgif1 impairs osteoclast differentiation.	92
Fig. 4.11. The osteoclast progenitor cell population is unchanged in Tgif1 ^{-/-} mice.	93
Fig. 4.12. Tgif1 supports osteoclast fusion.	95
Fig. 4.13. Actin ring formation is delayed in Tgif1 ^{-/-} osteoclasts.	96
Fig. 4.14. Tgif1 deficiency reduces osteoclast function.	98
Fig. 4.15. High concentration of RANKL does not restore the impaired differentiation of Tgif1 ^{-/-} osteoclasts.	99
Fig. 4.16. RANK, c-fms and TRAF6 expressions are unchanged in Tgif1 ^{-/-} osteoclast precursors.	100
Fig. 4.17. Phosphorylated ERK1/2 is decreased in Tgif1 ^{-/-} BMMs.	102
Fig. 4.18. PP2A catalytic subunit β expression is increased in Tgif1 ^{-/-} BMMs.	104
Fig. 4.19. PP2A catalytic subunit is increased in Tgif1 ^{-/-} osteoclast precursor cells.	105
Fig. 4.20. PP2A inhibitor Okadaic acid restores the impaired ERK1/2 phosphorylation in Tgif1 ^{-/-} BMM and recovers the impaired differentiation of Tgif1 ^{-/-} osteoclasts.	106
Fig. 4.21. Silencing of PP2A increases phosphorylated ERK1/2.	108
Fig. 4.22. Silencing of Tgif1 increases the abundance of the catalytic subunit of PP2A.	110
Fig. 4.23. Silencing of PP2A rescues the impaired differentiation of Tgif1-deficient osteoclasts.	112
Fig. 4.24. Tgif1 regulates PP2A-C β expression to sustain phosphorylated ERK1/2 downstream of RANKL and M-CSF stimulation.	114

1 Introduction

Bones comprising the skeleton play important roles, including but not limited to providing mechanical support, protecting inner organs, interacting with tendons and muscles to facilitate locomotion, support of hematopoiesis, control of mineral homeostasis and the regulation of distant organs¹⁻⁴. The integrity and function of the bone tissue is maintained in a coordinated and balanced manner by tissue-specific cells such as osteoclasts, osteoblasts and osteocytes⁵. Bone-forming osteoblasts are of mesenchymal origin and differentiate into matrix-embedded osteocytes, lining cells residing on the bone surface or undergo apoptosis⁵. Bone-resorbing osteoclasts are multinucleated cells arising from the hematopoietic lineage⁶. Since the activities of osteoblasts and osteoclasts are tightly regulated under physiological conditions, any deregulation may cause pathological disturbances for instance aging-related bone loss⁷.

1.1 Bone anatomy

The human skeleton comprises approximately 200 bones⁸. Bones are covered from the outside and the inside by fibrous connective tissue membranes called periosteum and endosteum, respectively (Fig. 1.1)⁹. The thick outer periosteum is densely innervated by sensory nerves. It serves as an insertion site and provides the holdfast of tendons and ligaments, allows the appositional growth and protects the bone from damage. The endosteum contains abundant osteoprogenitor cells derived from bone marrow and blood vessels and also contributes to bone formation and remodeling.

Based on morphology, bones can be divided into different categories. For instance, long bones (e.g. femur, tibia, humerus) are tubular bones with a diaphysis in the middle and metaphyses at both ends that are separated from the epiphyses by growth plates for longitudinal growth. While the diaphysis mainly consists of cortical bone, the metaphyses and epiphyses have a thin cortical bone but contain abundant trabecular bone. In short bones (e.g. carpal and tarsal bones), epiphyses and diaphysis cannot be distinguished. Flat bones (e.g. scapula,

sternum, ilium) are rather thin and irregular bones (e.g. vertebra, sacrum, coccyx) do not belong to any of the aforementioned categories. Furthermore, some bones fall into a special category like pneumatic bones (e.g. mastoid and paranasal sinuses) that contain air-filled cavities. Sesamoid bones (e.g. patella) are embedded in muscles or tendons and help redirecting muscle forces.

While trabecular bone is mainly located within the epiphyses and metaphyses, the outer shell of bones usually consists of densely packed cortical bone. Cortical bone contains osteons. Osteons comprise a central Haversian canal that contain vessels and nerve fibers and is surrounded by concentric collagen lamellae. Haversian canals are connected by Volkmann's canals, traversing the cortical bone (Fig. 1.1)¹⁰. In the adult human skeleton, cortical bone accounts for 80% and cancellous bone for 20% of the total bone mass⁸. While cortical bone provides most of the mechanical stability, trabecular bone is metabolically more active and subject to a higher remodeling rate⁸.

Bone tissue interacts with many other tissues and organ systems, one of which is the hematopoietic system⁴. Although active hematopoietic red bone marrow is present in almost all bones in early childhood, it is replaced by bone marrow adipose in particular in the long bones starting around puberty¹¹⁻¹³. Nevertheless, hematopoiesis continues to be active throughout adulthood in flat and irregularly shaped bones including vertebra, sternum, ribs and the ilium^{14,15}.

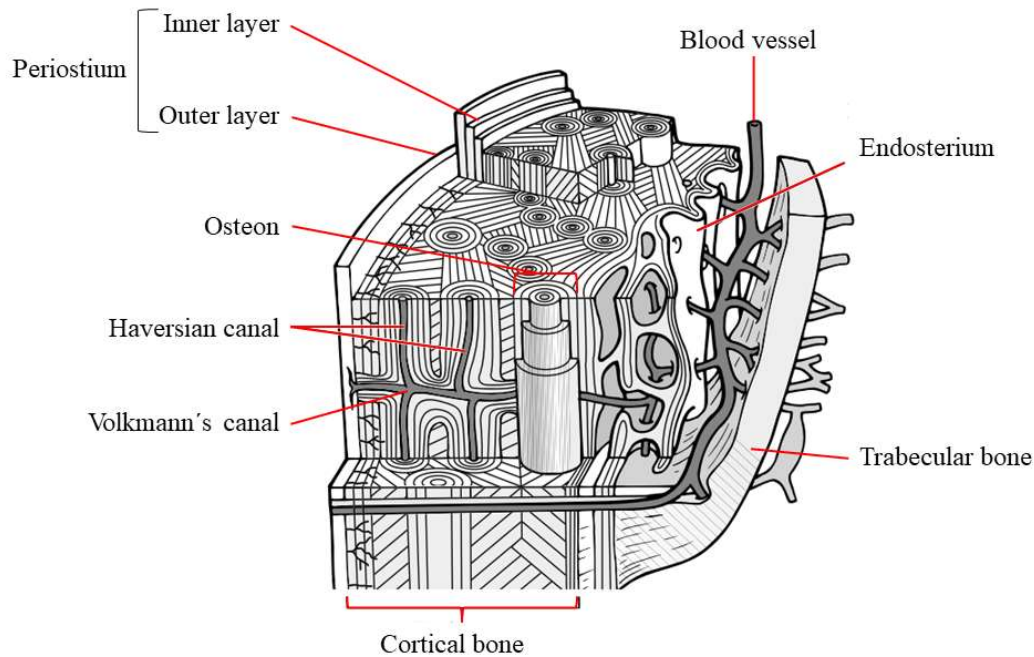


Fig. 1.1. Schematic image of a cross-section of bone. Mature cortical bones are constructed from osteons. The osteon is surrounded by lamellae (bone layer plate) concentrically around Haversian canal. Cortical bone is enclosed outside and inside by periosteum and endosteum, respectively. Arterial vessels, veins and nerve fibers run through Haversian canal and Volkmann's canal. Modified from Korkia, *Journal of Bodywork and Movement Therapies* (2002) 6 (3): 156-169; Figure 4⁹.

1.2 Bone development

Development of bones at embryonic stages follows two main principles, intramembranous ossification and endochondral bone formation¹⁶. Intramembranous ossification initiates from neural crest cells that directly differentiate into matrix-producing osteoblasts. Based on this process, flat bones, bones of the skull, the clavicle and the mandible are formed¹⁷. Endochondral bone formation involves mesenchymal cells that form an intermediate cartilage template, which then becomes ossified. This process forms all other bones and is closely recapitulated in fracture healing^{18,19}.

1.3 Bone remodeling and modeling

To preserve the mechanical integrity, bones are constantly destructed and rebuilt in a coordinated and balanced manner throughout the life. Remodeling of the mineralized tissue is

executed by matrix-forming osteoblasts and bone-resorbing osteoclasts (Fig. 1.2)^{20,21}. The remodeling cycle is often activated by local damage like micro-cracks, which attract and activate cells of the monocyte-macrophage lineage that expand and differentiate into osteoclasts. After the bone matrix is resorbed by osteoclasts, mesenchymal precursor cells migrate into the resorption zone and differentiate into osteoblasts. This reverses matrix resorption into the formation of osteoid, a type I collagen rich matrix that starts to mineralize. While osteoid is deposited, osteoblasts can become entrapped into the newly formed matrix and differentiate into osteocytes with a densely connected canalicular network^{22,23}. Alternatively, osteoblasts can become flat lining cells covering the new bone surface or undergo apoptosis²⁴. The molecular mechanisms regulating the entry into one fate or the other are not yet fully elucidated. At the cellular level, molecular cues link the activities between osteoblasts, osteocytes and osteoclasts. For instance, osteoblasts and osteocytes secrete factors like Receptor activator of NF- κ B Ligand (RANKL) that binds to the RANK receptor expressed by osteoclast precursor cells and mature osteoclasts and stimulate osteoclast differentiation and activity²⁵. This stimulatory signal can be antagonized by osteoprotegerin (OPG) that is secreted by osteoblasts and acts as a soluble decoy receptor of RANKL²⁶. In addition, osteoblasts secrete many more factors that altogether act to regulate osteoclast function²⁷. The reciprocal process by which osteoclasts influence osteoblast activity by soluble factors or cell-cell interactions is referred to “coupling”²⁸.

Bone remodeling always occurs on surfaces and starts with resorption, followed by formation. It is the main principle of bone turnover during adulthood and all participating cell types combined form the basic multicellular unit (BMU)^{28,29}. In contrast to bone remodeling, bone modeling is a process by which bone matrix is deposited without prior resorption. This more direct process of bone formation contributes to the appositional bone growth and participates in the mode of action by which pharmacological agents stimulate bone mass

accrual. Bone modeling is highly activated during development and growth but remains at a lower level during life³⁰.

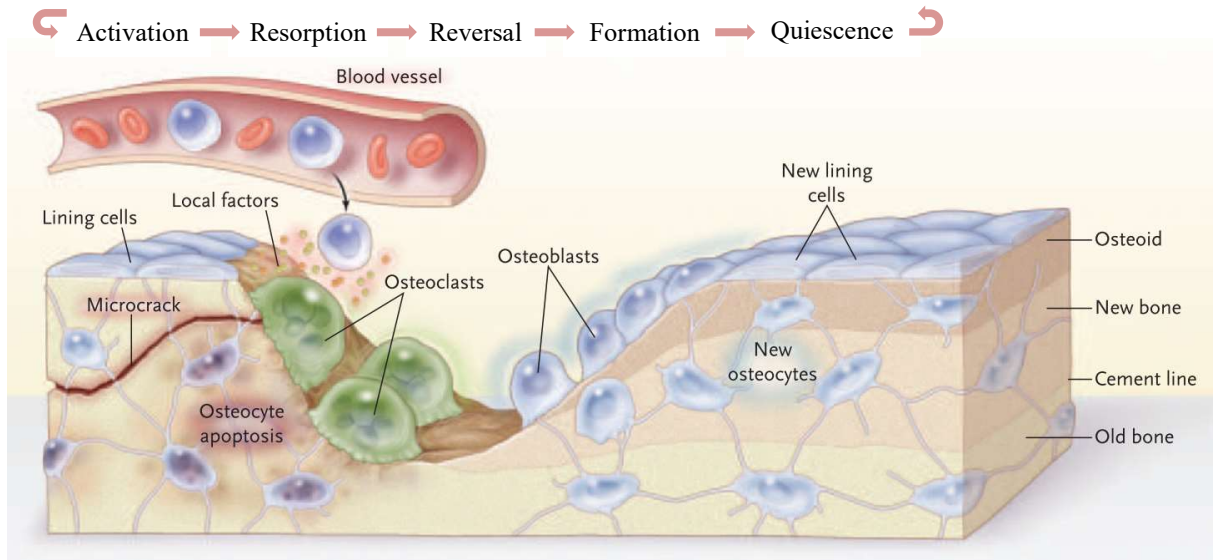


Fig. 1.2. Bone remodeling cycle. Bone is continuously remodeled in the skeleton in order to maintain the integrity of the tissue. Bone remodeling consists from five phases; activation, resorption, reversal, formation and quiescence. In the first phase, lining cells and osteocytes release local factors that attract osteoclast progenitors, for example, in response to microcracks. Osteoclast progenitors are stimulated to differentiate to osteoclasts for resorbing bones. During resorption, osteoclasts digest mineral matrix of old bone. Following resorption, mesenchymal cells are recruited to differentiate into osteoblasts (the reversal phase). Osteoblasts fill the resorption cavity with osteoid, which is mineralized. Following bone deposition, osteoblasts can differentiate to osteocytes embedded in the new bone matrix, turn to bone-lining cells, or undergo apoptosis. The border between old bone and new bone remains as cement line. Modified from Ego Seeman and Pierre D. Delmas, *New England Journal of Medicine* (2006) **354**: 2250-61; Figure 2³¹.

1.4 Aging-related bone disease

Bone strength (i.e. resistance to fracture) is determined by bone quality, bone mineral density and bone mass³¹. Bone mineral density is calculated by the content of minerals divided by the bone area. Bone mass is measured by the bone volume divided by total volume and determined by the balance between bone-forming osteoblasts and bone-resorbing osteoclasts³². Bone quality, bone mineral density and bone mass change during aging³³. For example, sexual hormone deficiency induces high resorption by osteoclasts especially in postmenopausal women. During aging, osteoblast activity and the amount of bone formed decreases, while osteoclast activity and the amount of bone resorbed increases³⁴.

1.5 Osteoporosis

Osteoporosis is the most common bone disease characterized by a decrease in bone mass and a decline in bone architecture, leading to an enhanced bone fragility and an increased fracture risk³⁵. Around the world, osteoporosis causes more than 8.9 million fractures annually, resulting in an osteoporotic fracture every 3 seconds³⁶. Osteoporotic fractures mainly occur at the wrist, spine and hip⁹. Particularly at the hip and spine, the incidence of osteoporotic fracture increases with age in both women and men. These fractures are also associated with an increased risk for subsequent fractures and an increased morbidity and mortality³⁷.

Clinically, bone mineral density (BMD) is non-invasively assessed by dual-energy X-ray absorptiometry (DXA) at the hip and the lumbar spine. BMD is transformed into a T-score, which reflects the number of standard deviations (SD) above or below the mean BMD compared to a healthy young adult reference group³⁸. The World Health Organization (WHO) defined the diagnosis of osteoporosis if the T-score is -2.5 or below³⁵. Based on WHO criteria, a T-score between -1 and -2.5 is considered as osteopenia.

In addition to postmenopausal osteoporosis, secondary forms of osteoporosis exist that can for instance be due to the use of glucocorticoids or a prolonged bed rest³⁹. Secondary osteoporosis also represents a tremendous health problem with a great societal impact^{40,41}.

1.6 Osteopetrosis and Osteosclerosis

Apart from aging-related bone loss due to active osteoclast-mediated bone resorption like in osteoporosis, lack of or dysfunction of osteoclasts may induce a high bone mass phenotype causing skeletal diseases such as osteopetrosis⁴². In contrast to osteopetrosis, a high bone mass phenotype due to an increased osteoblast-mediated bone formation is referred as osteosclerosis⁴³.

1.7 RANKL/RANK signaling cascade

RANKL is a member of the tumor necrosis factor (TNF) family and necessary to prime osteoclast precursors for differentiation. RANKL is a homotrimer having two forms, soluble form or anchored to the cell matrix, which is produced by osteoblasts and osteocytes. OPG is also secreted by osteoblasts as a decoy receptor of RANKL^{44,45}. The balance between RANKL and OPG regulates osteoclast differentiation and function⁴⁶.

RANK signaling is mediated by TNF receptor-associated factors (TRAFs) that activate downstream signaling pathways (Fig. 1.3). At least five signaling cascades mediated by protein kinase such as inhibitor of NF- κ B kinase (IKK), c-Jun N-terminal kinase 1 (JNK1), p38, extracellular signal-regulated kinase (ERK) and Src pathways are induced during osteoclast activation⁴⁷.

The extracellular signal-regulated kinases (ERK1 and ERK2) are widely expressed and modulate proliferation, survival, differentiation, and protein synthesis in multiple cell lineages⁴⁸. Yong-Zheng He *et al.* demonstrated that ERK1 positively regulates osteoclast development and bone resorption, as genetic disruption of ERK1 reduced the osteoclast progenitor cell number, compromised pit formation, and diminished M-CSF-mediated adhesion and migration⁴⁹. On the other hand, Hotokezaka *et al.* claimed that the MEK/ERK pathway negatively regulates osteoclastogenesis while the p38 pathway has a positive effect⁵⁰.

Mutation of the p50/p52 component of NF- κ B or the c-Fos component of activator protein 1 (AP-1) cause osteopetrosis due to an impaired osteoclastogenesis⁵¹⁻⁵³. Activation of NF- κ B and AP-1 can be induced by signaling cascades mediated by IKK1/2 and JNK1, respectively^{54,55}. Mutation of TAK1 inhibits RANKL-mediated activation of both IKK1/2 and JNK1, suggesting that TAK1 is important in the activation of NF- κ B and AP-1⁵⁶.

The stress-activated protein kinase p38 is also involved in the RANKL signaling cascade. p38 is phosphorylated by MAPK-related kinase 6 (MKK6) and the activated p38

activates the microphthalmia-associated transcription factor (MITF), which regulates (TRAP) and Cathepsin K expression^{57,58}.

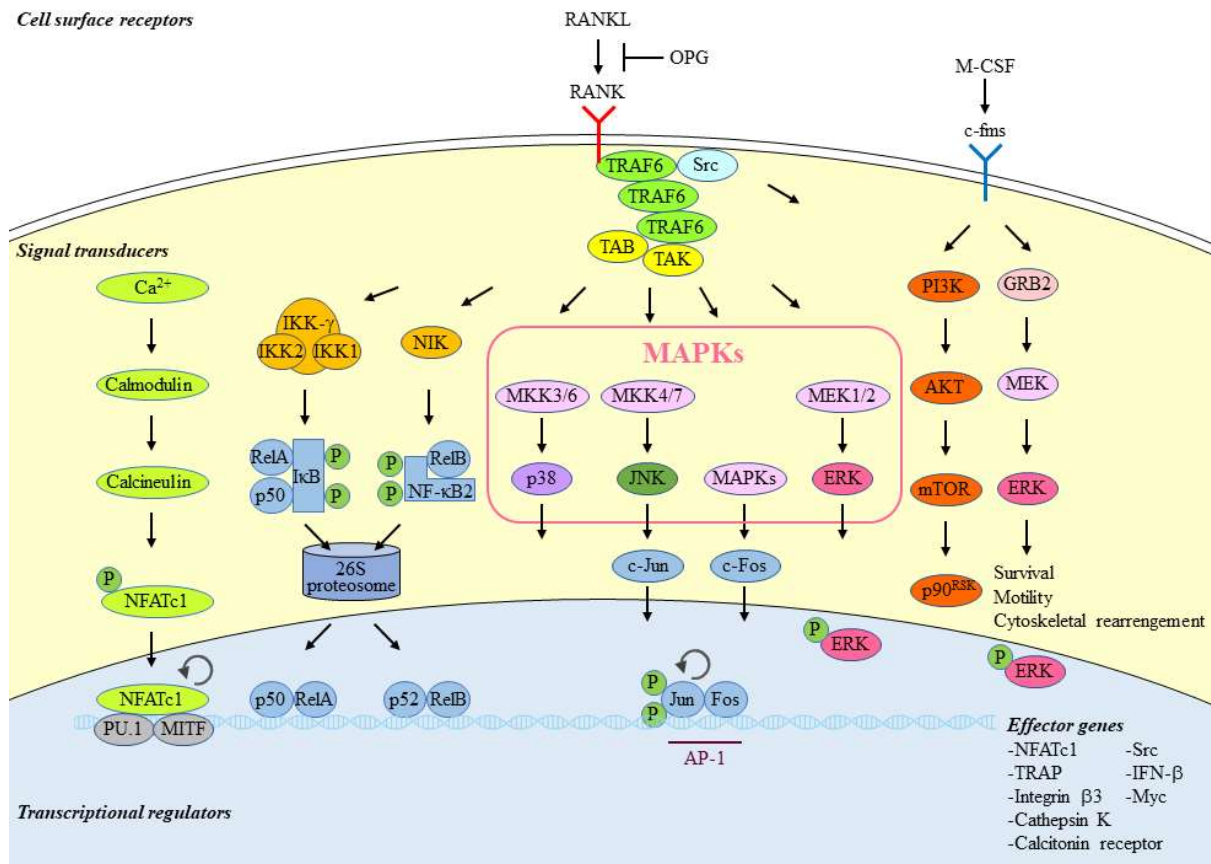


Fig. 1.3. Signaling cascades in osteoclastogenesis. RANKL/RANK and M-CSF/c-fms activates respective signaling pathways. RANKL is an essential cytokine for osteoclastogenesis. M-CSF is involved in cell survival and cytosol organization in macrophages. A transcription factor NFATc1 is activated downstream of the RANKL pathway. Modified from Boyle, Simonet and Lacey, *Nature* (2003) **423**: 337-342, Fig. 3⁴⁷ and from Kikuta and Ishii, *Rheumatology* (2013) **52**: 226-234; Figure 2⁵⁹.

1.8 Osteoblasts and Osteocytes

Osteoblasts arise from mesenchymal stem cells and differentiate under the influence of stimulatory factors like bone morphogenetic proteins (BMPs), transforming growth factor- β (TGF- β) and Wnts⁶⁰⁻⁶⁴. At the terminal differentiation stage, an osteoblast has three fates which is becoming an osteocyte, turning to bone-lining cells or undergoing apoptosis (Fig. 1.4)⁶⁵. Osteocytes have been reported to account for 90-95% of all bone cells and are embedded in the newly formed matrix⁶⁶. These cells form a highly interconnected system of canaliculi and have contact with many other cell types like osteoblasts, osteoclasts, hematopoietic cells, bone lining

cells and also penetrate into the vasculature. In addition to osteoblasts, osteocytes also produce RANKL and are perceived as its main source, thereby affecting bone resorption^{67,68}. Furthermore, osteocytes are the main source of sclerostin expression⁶⁹. Sclerostin is secreted through the lacunar-canalicular network into the local environment and binds to low-density lipoprotein-related protein (Lrp) 5 and 6 on osteoblasts. Binding to Lrp5/6 prevents activation of the canonical Wnt pathway and suppresses osteoblast activity, thereby affecting bone formation⁷⁰.

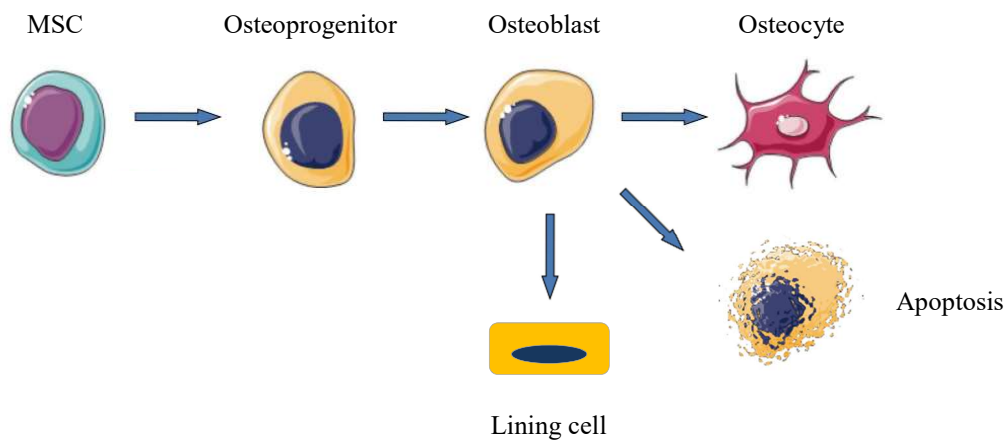


Fig. 1.4. Osteoblast differentiation. Osteoblasts originate from mesenchymal stem cells (MSCs). MSCs differentiate into osteoprogenitor cells and eventually to mature osteoblasts which mineralize the bone matrix. Osteoblasts have three fates, to become osteocytes which embedded in the bone matrix, become resting bone-lining cells or either apoptosis. Modified from Fakhry *et al.*, *World Journal of Stem Cells* (2013) 5(4): 136-148; Figure 1⁷¹.

1.8.1 Runt-related transcription factor 2 (Runx2)

The Runt-related transcription factor 2 (Runx2 or core binding factor alpha 1 (Cbfa1)) is an indispensable transcription factor required for ossification while Runx1 is necessary for hematopoietic stem cell differentiation⁷². Runx2 is expressed in osteoblasts and chondrocytes. In osteoblasts, Runx2 expression is regulated by an enhancer region, which resides approximately 30 kb upstream of the P1 promoter. This enhancer region is activated by Mef2, Tcf7, Sox5/6, Smad1, Sp7 (Osterix), *etc.* in the response to Bone morphogenetic protein (BMP) and Wnt⁷³.

1.8.2 Osterix

Osterix (*Osx*, *Sp7*) is an osteoblast-specific transcription factor essential for osteoblast differentiation and bone formation⁷⁴. *Osx* is induced by BMP-2 and stimulates the expression of osteoblastic makers such as osteocalcin and collagen type I⁷⁵.

Bone formation is strongly inhibited in *Osx* knock-out mice accompanied by a decreased expression of collagen type I, bone sialoprotein (BSP), osteonectin and osteopontin⁷⁴. However, *Runx2* expression in *Osx* knock-out mice is comparable to wild type mice. On the other hand, *Osx* is not expressed in *Runx2* knock-out mice, demonstrating that *Osx* is downstream of *Runx2*⁷⁴.

1.8.3 Activating transcription factor 4 (ATF4)

ATF4 is a member of the cAMP response element-binding protein (CREB) family and transcriptional regulator of the osteocalcin expression⁷⁶. Interactions of ATF4 with a specific enhancer sequence in the Osterix promoter promotes bone formation in the response to parathyroid hormone (PTH)⁷⁷.

ATF4-deficient mice exhibit a marked reduction or delay in mineralization of bones including frontal and parietal bones, clavicles, and long bones. In addition, ATF4-deficient mice exhibit severe osteopenia involving an impaired osteoblast differentiation⁷⁸.

1.8.4 Sclerostin

Sclerostin is a secreted glycoprotein encoded by the *SOST* gene^{79,80}. Sclerostin negatively regulates bone formation by antagonizing the interaction between Wnt ligands and LRP5/6 co-receptors located on osteoblasts, resulting in an inhibition of the canonical Wnt signaling pathway activity⁷⁰. PTH and mechanical stress reduces sclerostin expression, which contributes to the increase in bone formation in response to these stimuli⁸¹⁻⁸⁴. An anti-sclerostin antibody has recently been investigated in Phase III clinical trials for the treatment of postmenopausal osteoporosis⁸⁵. The results demonstrate that the treatment increased BMD in the hip and spine

and significantly reduced the fracture rate at different sites in postmenopausal women with osteoporosis⁸⁵. Thus, the anti-sclerostin antibody is awaited in the clinics as new bone anabolic treatment of osteoporotic bone loss.

1.8.5 Osteopontin (OPN)

OPN is also known as bone sialoprotein 1 (BSP-1), early T-cell activation 1 (ETA1) or secreted phosphoprotein 1 (SPP1). Non-collagen proteins account for 10% of all proteins in bone and OPN accounts for 10% of non-collagen proteins in bone. OPN has a RGD (Arg-Gly-Asp) sequence to bind to integrins, implicating its role in cell adhesion⁸⁶. OPN is highly expressed in differentiated osteoblasts, lining cells and osteocytes. OPN expression is increased in response to 1,25-dihydroxyvitamin D3 and TGF- β stimulation^{87,88}. Although OPN is not essential for osteoclast activity, OPN expression is required at sites of bone resorption to attract osteoclast precursors⁸⁹.

Osteoclast precursors and mature osteoclasts express CD44 and the $\alpha_v\beta_3$ integrin, which is one of the receptors for OPN⁸⁹. Binding of OPN to osteoclast precursors is important for their migration. Binding of OPN to osteoclasts through the β subunit of the $\alpha_v\beta_3$ integrin can activate the FAK-related protein tyrosine kinase 2 (PYK2) through c-Src, which binds PYK2 through SH2 domains⁸⁹. These signaling cascades are important for the formation of the sealing zone, which is important for osteoclast-mediated bone resorption. Osteoclasts are anchored by OPN to the mineral of bone matrix and to the vitronectin receptor on the osteoclast cell membrane⁹⁰. OPN deficient mice show normal development and bone structure but altered osteoclast differentiation *in vitro*⁹¹. OPN knockout mice are resistant to ovariectomy (OVX)-induced bone resorption⁹².

1.8.6 Parathyroid hormone 1 receptor (PTH1R), Parathyroid hormone/parathyroid hormone-related protein/peptide receptor

The type 1 receptor (PTH1R) for PTH and parathyroid hormone-related protein/peptide (PTHrP) is a G protein-coupled receptor that is highly expressed in bone and kidney and mediates the PTH-dependent regulation of mineral ion homeostasis⁹³. In bone, PTH1R is expressed in cells of the osteoblast lineage⁹⁴⁻⁹⁷. The PTH1R also mediates the paracrine actions of PTHrP, which plays an important role in the process of endochondral bone formation^{93,98}. Binding of PTH/PTHrP to PTH1R induces the expression of RANKL by osteoblasts⁹⁹. This mechanism increases bone resorption. Novel PTH receptor ligands have a therapeutic value in the treatment of diseases such as osteoporosis⁹³.

Amizuka *et al.* demonstrated that although *Pthrp*^{-/-} mice die by the time of birth because of a cartilage defect, *Pthrp*^{+/-} mice survive. By 3 months of age, the heterozygous mice were markedly osteoporotic and possessed an increased number of adipocytes in the bone marrow¹⁰⁰. Miao *et al.* found that *Pth*^{-/-} mice have an increased trabecular bone volume due to a diminished PTH-induced osteoclast formation¹⁰¹. However, *Pth*^{-/-};*Pthrp*^{+/-} mice had a reduced trabecular bone volume despite an increased bone volume observed in *Pth*-null mice. These findings suggest that PTH is secreted as a hormone in response to a hypocalcemic signal in order to regulate calcium homeostasis by promoting bone resorption, while PTHrP functions as a bone cytokine that controls bone mass¹⁰¹.

1.9 Osteoclast precursors

Hematopoietic stem cells (HSCs, *Lin*⁻*Sca-1*⁺*c-Kit*⁺*CD34*⁻) give rise to several cell types to further develop into lineage-restricted progenitors¹⁰². Seita and Weissman classified cell types based on the expression pattern of cell surface markers (Fig. 1.5). HSCs lose their self-renewal capacity while upregulating CD34 and become multipotent progenitors (MPPs, *Lin*⁻*Sca-1*⁺*c-Kit*⁺*CD34*⁺), which still retain pluripotency¹⁰². MPPs differentiate into oligopotent progenitors,

common myeloid progenitors (CMPs, $\text{Lin}^- \text{Sca-1}^{\text{lo/-}} \text{c-Kit}^+ \text{CD34}^+ \text{IL-7R}^- \text{Fc}\gamma\text{R}^{\text{lo}}$), megakaryocyte–erythrocyte progenitors (MEPs, $\text{Lin}^- \text{Sca-1}^- \text{c-Kit}^+ \text{CD34}^- \text{IL-7R}^- \text{Fc}\gamma\text{R}^-$) and common lymphoid progenitors (CLPs, $\text{Lin}^- \text{Sca-1}^{\text{lo}} \text{c-Kit}^{\text{lo}} \text{IL-7R}^+ \text{CD27}^+ \text{Flk2}^+$)¹⁰².

CMPs give rise to osteoclast progenitor cells ($\text{c-Kit}^+ \text{CD11b}^{\text{lo/-}}$ and $\text{c-Kit}^+ \text{CD11b}^{\text{lo/-}} \text{c-Fms}^+$ populations) in the bone marrow¹⁰³. Arai *et al.* showed that $\text{c-Kit}^+ \text{CD11b}^{\text{lo/-}} \text{c-Fms}^+$ cells differentiate into macrophage-lineage cells more frequently than the c-Fms^- counterpart which is capable of becoming granulocytes and erythrocytes as well. This result indicates that c-Fms expression specifies the fate of progenitor cells towards monocyte/macrophage-lineage cells¹⁰³.

Macrophage-1 antigen (Mac-1) is also known as the complement receptor 3 (CR3) which consists of CD11b (integrin α_M) and CD18 (integrin β_2). Mac-1 binds to intercellular adhesion molecule-1 (ICAM-1, CD54) for cell adhesion¹⁰⁴. M-CSF stimulation of $\text{c-Kit}^+ \text{CD11b}^{\text{lo/-}} \text{c-Fms}^+$ cells induces RANK expression on these cells, and RANK^+ cells lose c-Kit expression and upregulate CD11b expression¹⁰³. These cells can be defined as late stage of osteoclast precursors. Thus, osteoclast progenitors undergo a stepwise differentiation and finally become $\text{c-Fms}^+ \text{RANK}^+$ progenitors, which are ready for RANKL stimulation¹⁰⁵.

Perkins *et al.* reported that aging-related bone loss in mice is associated with an increased osteoclast progenitor pool, comparing aged (24 months old) mice to young (4-6 months old) mice¹⁰⁶.

Introduction

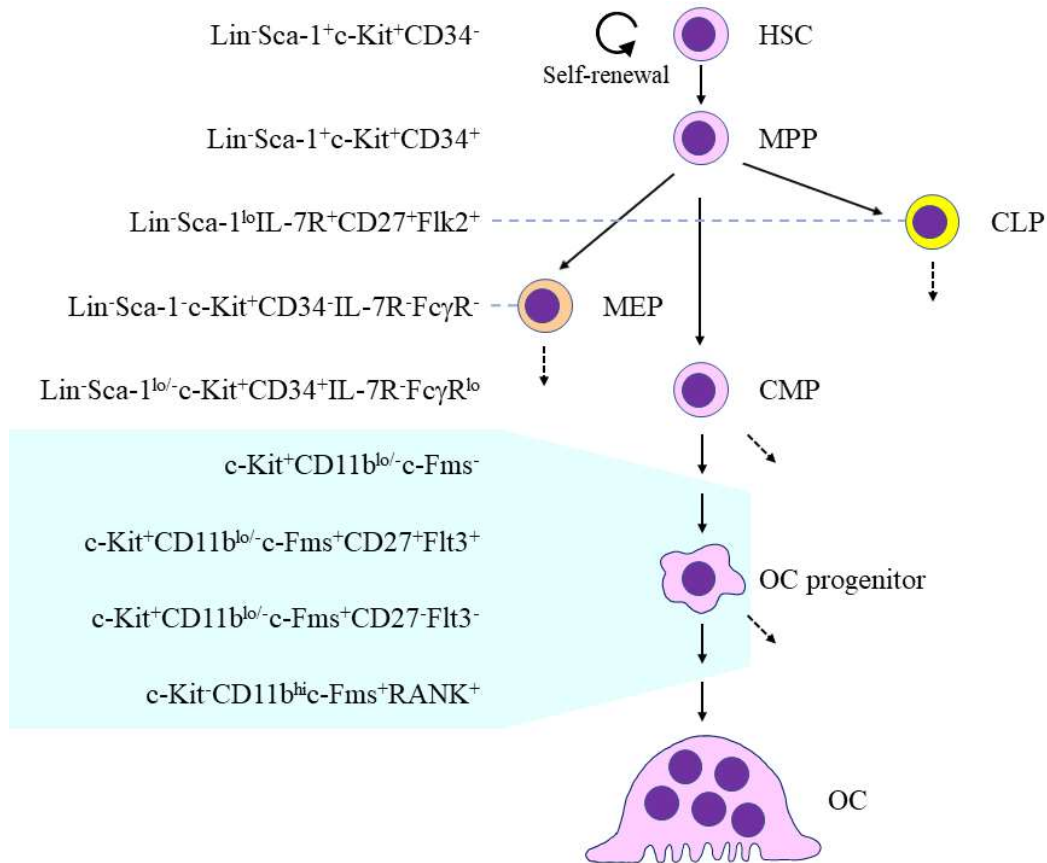


Fig. 1.5. Schematic alteration of cell surface markers during differentiation from hematopoietic stem cell to osteoclast. Osteoclasts originate from hematopoietic stem cells (HSCs). $\text{Lin}^-\text{Sca-1}^+\text{c-Kit}^+\text{CD34}^-$ HSCs are pluripotent and have the capacity for self-renewal. HSCs give rise to oligopotent progenitor cells with CD34 expression. Among oligopotent progenitors, common myeloid progenitor cells (CMPs) are the origin of osteoclasts. During osteoclast differentiation, osteoclast progenitors express c-Fms and RANK, receptors for M-CSF and RANKL, respectively. HSC; hematopoietic stem cell, MPP; multipotent progenitor, MEP; megakaryocyte/ erythrocyte progenitor, CLP; common lymphoid progenitor, CMP; common myeloid progenitor, OC; osteoclast. lo, low, hi, high. Modified from Ono and Nakashima, *Histochemistry and Cell Biology* (2018) **149**: 325–341; Figure 1¹⁰⁵.

1.10 Osteoclasts

Osteoclasts are multinucleated giant cells that arise from the hematopoietic lineage and belong to the group of monocytes/macrophages¹⁰⁷. Bone-resorbing osteoclasts form an actin ring also known as sealing zone and a ruffled border upon adherence to the bone surface¹⁰⁸. Osteoclasts tightly attach to the bone surface and secrete protons and proteases into the resorption lacuna to digest the bone matrix containing hydroxyapatite and type I collagen. Digested proteins are engulfed into trans-cytotic vesicles from the side of the ruffled border of osteoclasts, transported through the cytosol and excreted¹⁰⁹. Thus, bone-resorbing osteoclasts are highly specialized and

unique cells. Osteoclast differentiation is strictly regulated by cytokines, of which some are derived by osteoblasts (Fig. 1.6)²⁵. For instance, RANKL and M-CSF are essential for the formation and function of osteoclasts^{25,26,110}. Osteoblasts express M-CSF and RANKL¹¹¹. M-CSF is a disulfide-linked homodimer and necessary for hematopoietic stem cells to differentiate into macrophages and for ensuring survival and proliferation^{112,113}. RANKL and M-CSF activate various signaling pathways in osteoclast precursor cells, resulting in the activation of the master transcription factor NFATc1¹¹⁴.

Osteoclasts highly express the vitronectin receptor $\alpha_v\beta_3$ integrin, which supports the attachment to the bone surface¹¹⁵. Osteoclasts abundantly express the carbonic anhydrase II (CAII) to secrete protons ($\text{CO}_2 + \text{H}_2\text{O} \rightarrow \text{H}^+ + \text{HCO}_3^-$) for the resorption of the bone matrix and a vacuolar-type H^+ -ATPase (V-ATPase) at ruffled border to transport protons into the resorption zone using energy from adenosine triphosphate (ATP) hydrolysis ($\text{ATP} \rightarrow \text{ADP} + \text{P}_i + \Delta\text{G}$)^{116,117}. Furthermore, chloride is transported into the resorption pits through the chloride channel-7 (ClC-7)¹¹⁸. Proteases such as cathepsin K and matrix metalloproteinase-9 (MMP-9) are transported through the Golgi apparatus and lysosomes into the resorption zone and contribute to the removal of the organic matrix^{119–121}.

Osteoclasts express the RANKL receptor RANK, the M-CSF receptor c-fms and the calcitonin receptor that all contribute to the differentiation and function of osteoclasts^{103,122}. At the signaling level, mitogen-activated protein kinases (MAPKs) play an important role in osteoclastogenesis. Many MAPKs are activated downstream of RANK^{123,124}. Furthermore, p38 α and/or β are involved in osteoclast formation¹²⁵. p38 is important for the induction of the cathepsin K gene⁵⁸. ERK is involved in osteoclast survival since the ERK pathway negatively regulates osteoclastogenesis^{47,50}.

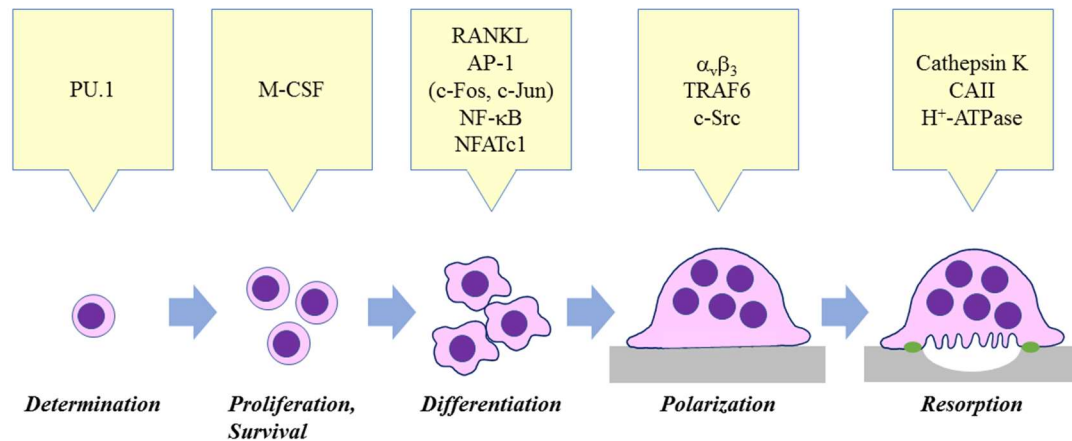


Fig. 1.6. Schematic important factors in osteoclast differentiation. PU.1 commits HSCs to the macrophage lineage. M-CSF is an essential cytokine to generate mature macrophages and to promote osteoclast differentiation. RANKL is an essential cytokine for osteoclast differentiation. AP-1, NF-κB and NFATc1 are important transcription factors in osteoclast differentiation. Integrin $\alpha_v\beta_3$, TRAF6 as well as c-Src are increased in multinucleated osteoclasts. Cathepsin K, Carbonic Anhydrase II (CAII) and H⁺-ATPase are critical enzymes to resorb bone in functional osteoclasts. Modified from Teitelbaum, *Science* (2000) **289**: 1504–1508; Figure 3¹²⁶.

1.11 Tartrate-resistant acid phosphatase (TRAP)

Tartrate-resistant acid phosphatase (TRAP) is highly expressed by osteoclasts, macrophages and dendritic cells. More precisely, macrophages and dendritic cells secrete TRAP-5a while osteoclasts express TRAP-5b¹²⁷. TRAP enzymes degrade phospho-proteins including OPN, thereby contributing to matrix degradation¹²⁸. Beyond its role in osteoclast function, TRAP-staining is useful to identify osteoclasts in histological sections. Furthermore, quantification of TRAP-5b in the serum is of diagnostic use in the clinics as a bone turnover marker^{127,129}. The transcription factors MITF and the related transcription factor E3 (TFE3) interact with the promoter of the TRAP gene and activate its activity in osteoclasts^{130,131}. Mice lacking tartrate-resistant acid phosphatase (Acp5) have disrupted endochondral ossification and mild osteopetrosis¹³².

1.12 Cathepsin K

Cathepsin K is a cystein protease, which is highly expressed in osteoclasts¹³³. Cathepsin K has a high homology to cathepsin L, which is localized in lysosomes. Importantly, cathepsin K can cut triple helical structure of native type I collagen in acidic conditions to resorb bones¹³⁴.

Cathepsin K knockout mice have an osteopetrotic phenotype, which fills the medullary space with cancellous bone and collagen remains on the resorptive bone surface after minerals have been removed from bone by acids¹³⁵. Although osteoclasts also express MMP-9, which has a strong gelatinase activity, MMP-9 knockout mice do not have an osteopetrotic phenotype¹³⁶. Therefore, cathepsin K is indispensable for osteoclasts to digest native collagen. In humans, mutation of the cathepsin K gene (CTSK^{-/-}) causes a skeletal abnormality called pycnodysostosis, which is characterized by short stature and osteopetrosis¹³⁷.

Odanacatib is a selective and reversible cathepsin K inhibitor that reduces osteoclast activity but not the number of osteoclasts¹³⁸. Although odanacatib had been highly expected to be a next generation medicine for osteoporosis, its development has been stopped at Phase 3 due to an increased risk of cardio-vascular side effects¹³⁹.

1.13 Dendritic cell-specific transmembrane protein (DC-STAMP) and Osteoclast stimulatory transmembrane protein (OC-STAMP)

DC-STAMP and OC-STAMP are seven-transmembrane proteins of high similarity that support the fusion of mononuclear precursor cells into multi-nucleated osteoclasts^{140,141}. Interestingly, although mononuclear osteoclast precursor cells from mice bearing a germline deletion of DC-STAMP or OC-STAMP are impaired in their fusion capacity, cells have the ability to form an acting ring as well as a ruffled border and have a resorptive function^{142,143}. DC-STAMP-deficiency causes a complete blockage of cell-cell fusion, but not an alteration of osteoclast differentiation except multi-nucleation, leading to a reduction of the bone-resorbing activity and an osteopetrotic high bone mass phenotype (osteopetrosis) in mice¹⁴⁴. Although OC-

STAMP-deficient mice exhibit a complete lack of cell-cell fusion of osteoclasts, OC-STAMP-deficient mice do not change bone mass compared to control mice¹⁴³. Collectively, DC-STAMP or OC-STAMP-deficient mice do not have a severe *in vivo* osteoclast phenotype, suggesting that although DC-STAMP and OC-STAMP are essential for osteoclasts to fuse, these factors are dispensable for bone resorption^{142,143}.

1.14 Src

The family of *SRC* kinases comprises a group of genes that encode cytoplasmic protein kinases (*SRC*, *FYN*, *YES*, *YRK*, *BLK*, *FGR*, *HCK*, *LCK*, *LYN*, *FRK/RAK*, *IYK/BSK*) that regulate cell growth, differentiation, adhesion, mobility, survival and apoptosis¹⁴⁵. Within the Src family, v-src is a gene, which was discovered in Rous sarcoma virus in chicken as the first identified cancer gene^{146,147}. C-src is a homologous gene of v-src in normal cells and both are tyrosine kinases that phosphorylate tyrosine residues¹⁴⁸. V-Src and c-Src consist of 526 amino acids and 533 amino acids, respectively, and both proteins are approximately 60 kDa in size. c-Src has a cell membrane anchor (region) at its N-terminal end (Fig. 1.7)¹⁴⁹⁻¹⁵¹. Src homology (SH) 3 and SH2 domains recognize prolin-rich sequences and phosphorylated tyrosine residues, respectively, and those are responsible for protein-protein interaction¹⁵². A kinase domain resides at the downstream end after the SH3 and SH2 domains. The kinase domain has the Y416 site, which is auto-phosphorylated in an active status while the Y527 site is phosphorylated in an inactive status¹⁵³. During a steady state, the Y527 residue is phosphorylated by the C-terminal Src kinase (Csk) and binds to the SH2 domain, resulting in an inactive conformation¹⁵³. Upon binding of integrins to the extracellular matrix, Src is activated, phosphorylates the focal adhesion kinase (FAK), paxillin, talin and cortactin, resulting in the formation of a larger adhesive protein complex. Additionally, Src transmits signals to Rho family G proteins, leading to an actin ring formation and the attachment to bone surfaces¹⁵⁴⁻¹⁵⁶. C-Src knockout mice have

an osteopetrotic phenotype with a decreased bone resorption due to an impaired formation of the ruffled border by osteoclasts¹⁵⁷. C-Src knockout osteoclasts also fail to form an actin ring¹⁵⁸.

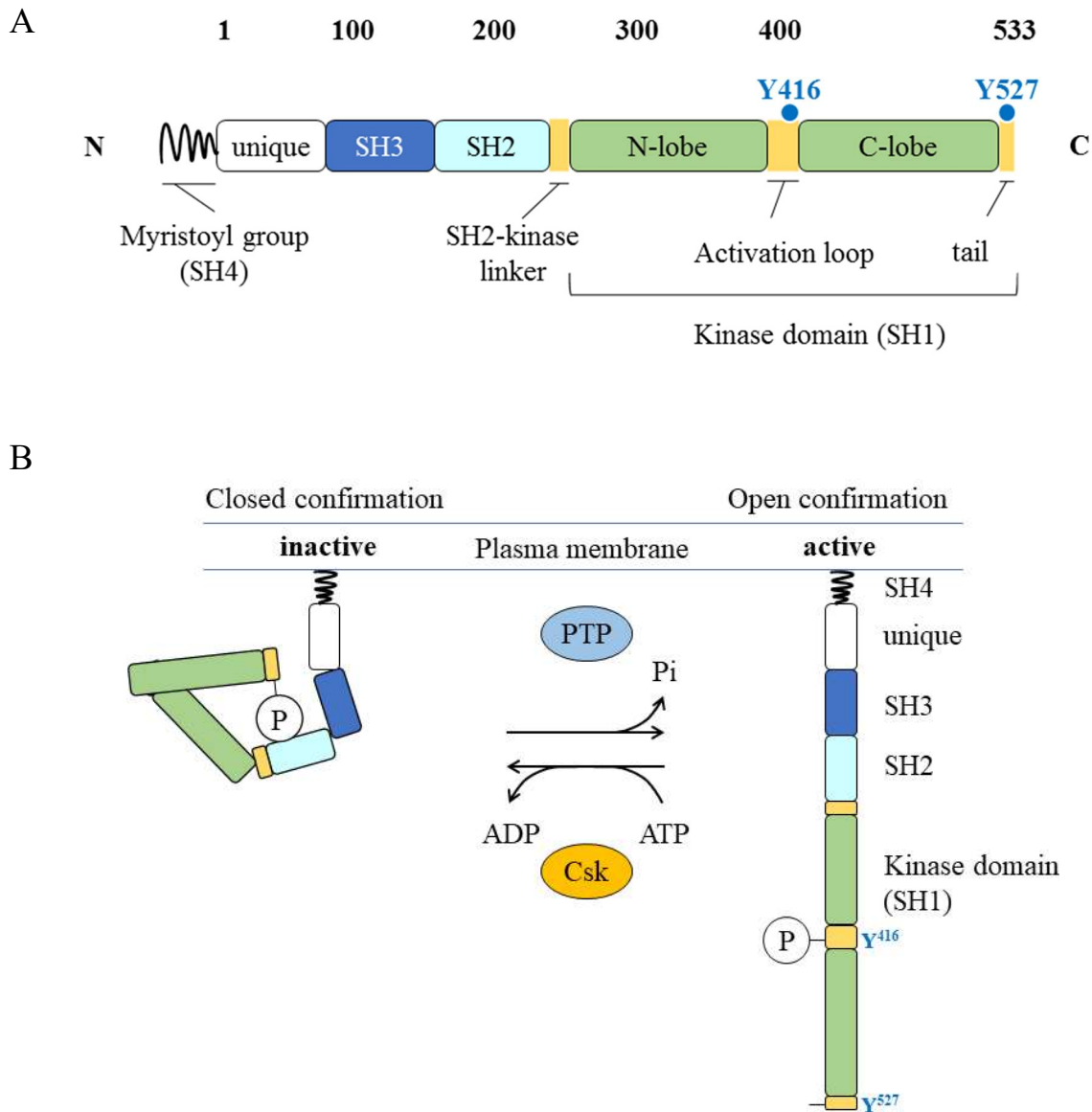


Fig. 1.7. The structure of c-Src family tyrosine kinase. (A) Schematic illustrations of the c-Src. The N-terminal segment includes membrane-localization signal, myristoylation site (also called SH4 domain), followed by “unique” domain which differs among family members. The SH3 and SH2 domains mediate protein-protein interactions in cellular signaling cascades. The SH2 domain binds phosphotyrosine, followed by tyrosin kinase (SH1) domain in order. C-terminal tail includes a critical tyrosine residue 527 (Y⁵²⁷). (B) Activation of c-Src. Phosphorylation of Tyr-527 by a specific kinase Csk inhibits Src catalytic activity by creating an intramolecular binding to the SH2 domain (Left). Dephosphorylation of p-Tyr527 allows the kinase domain to open, exposing Tyr-416 to phosphorylation. In the open state, p-Tyr416 in the activation loop of the kinase domain activates the enzyme (Right). Auto-phosphorylation of Tyr-416 (Y⁴¹⁶) on the activation loop of the kinase domain increases catalytic activity. SH; Src homology, PTP; protein-tyrosine phosphatase, Csk; C-terminal Src family kinase, Pi; inorganic phosphate, ADP; adenosine diphosphate, ATP; adenosine triphosphate, P; phosphorylated. Modified from Horne and Baron *et al.*, *Immunological Reviews* (2005) **208**: 106-125; Figure 3¹⁵⁹ and from Miyazaki and Baron *et al.*, *Modern Rheumatology* (2006) **16**: 68-74; Figure 1¹⁶⁰.

1.15 TNF receptor-associated factors (TRAFs)

Seven TNF receptor-associated factors (TRAF) are identified thus far (TRAF1-7) (Fig. 1. 8)¹⁶¹. TRAF6 not only participates in TNF receptor family signaling, but also in interleukin (IL)-1 receptor and Toll-like receptors (TLRs) signaling¹⁶². Thus, TRAF6 is important for both bone metabolism and the immune system.

The TRAF family members, except TRAF7, have a similar secondary structure including a ring and zinc finger (RZF) region at its N-terminal part and a TRAF domain at the C-terminal end¹⁶³. The ring finger domain is poly-ubiquitinated by ubiquitin-conjugating enzyme Ubc13 and forms complex with Ubc-like protein Uev1A¹⁶⁴. The complex of TRAF6 and Ubc13/Uev1A catalyzes the synthesis of unique polyubiquitin chains linked through lysine-63 (K63) of ubiquitin. Ubiquitinated TRAF6 serves as a signaling scaffold to recruit TGF- β -activated kinase (TAK)-1 via TAK1 binding protein (TAB) 2/3 to activate TAK-1. This polyubiquitin chain synthesis, but not decomposition by the proteasome, activates IKK through the assembly of K63-linked polyubiquitin chains¹⁶⁴. TAK-1 activates MAPKs such as p38 and JNK, resulting in an activation of AP-1 and NF- κ B¹⁶⁵⁻¹⁶⁷. The TRAF domain contains 2 parts, the coiled-coil domain and the TRAF-C domain. Both domains mediate a trimer formation and the binding to receptors and adaptors¹⁶⁸. In addition, the TRAF domain has a meprin and a TRAF homology (MATH) domain, which support polymer formation^{169,170}.

TRAF6 is most upstream of the RANK-dependent signaling pathway. Therefore, a lack of TRAF6 severely attenuates the activation of important transcription factors in osteoclast differentiation such as NF- κ B, AP-1 (Fos/Jun) and NFATc1^{162,171}. Not only TRAF6 but also TRAF1, 2, 3 and 5 bind to RANK^{172,173}. In particular, the TRAF6 binding motif in RANK is closer to the cell membrane than other binding motifs. Thus, TRAF6 binds not only to RANK, but also to c-*Src* to form a complex and to activate phosphoinositide 3-kinase (PI3-K) signaling¹⁷⁴. This signal activates serine/threonine kinase Akt for osteoclast survival¹⁷⁵.

TRAF6 knockout mice have a severe osteopetrosis and incomplete tooth eruption¹⁶². This phenotype is thought to be due to a lack of osteoclast resorption activity or an impaired osteoclast differentiation^{162,176}. In either case, TRAF6 is important for RANK-dependent bone resorption.

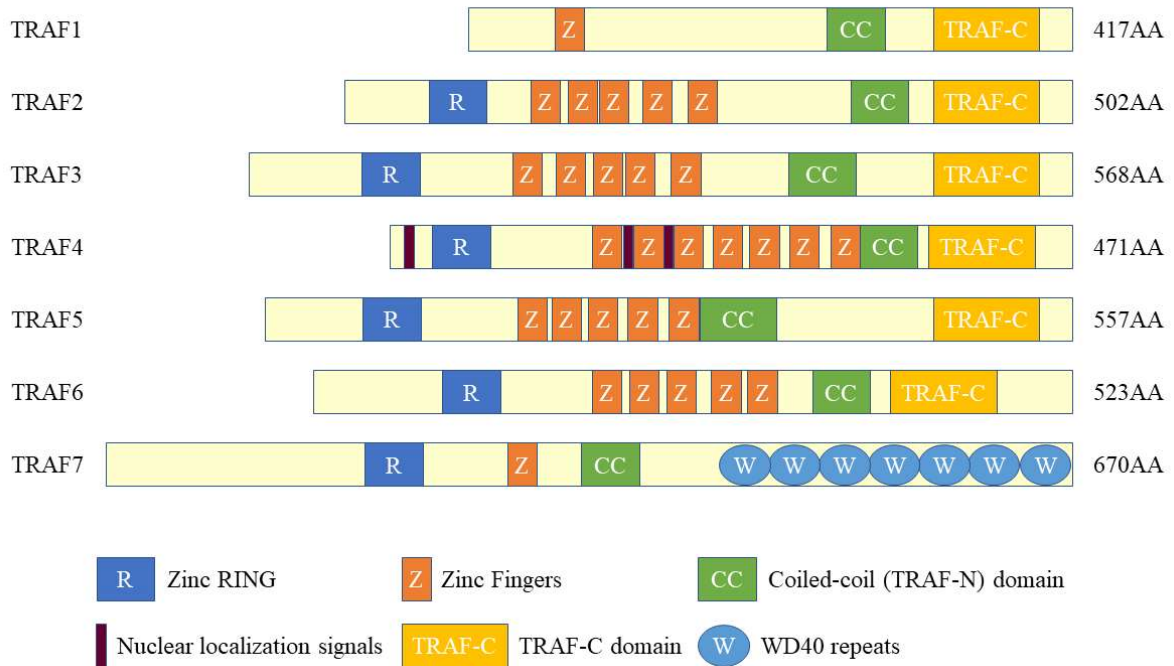


Fig. 1.8. Schematic functional TRAF proteins. The seven human TNFR-associated factor (TRAF) proteins are shown. All TRAFs except TRAF7 contain a C-terminal TRAF domain. All TRAFs except TRAF1 contain an N-terminal RING finger domain (a signature motif of E3 RING finger ubiquitin ligases) and several zinc finger motifs. The TRAF domain contains a coiled-coil region and a C-terminal TRAF-C domain (also known as a meprin and TRAF homology (MATH) domain). AA, amino acids. A WD repeat is approximately 40 amino acids constructed by tryptophan-aspartic acid (W-D) dipeptide.¹⁷⁷ RZF (ring and zinc finger) plays a role of signal activation. Coiled-coil domain and MATH domain are involved in polymerization. TRAF6 binds to RANK and trimerize itself in response to RANKL stimulation. TRAF-C domain contributes to bind to receptors. Modified from Häcker and Karin *et al.*, *Nature Reviews Immunology* (2011) **11**: 457-468; Figure 1¹⁶⁸ and from Xie, *Journal of Molecular Signaling* (2013) **8** (7): 1-31; Figure 1¹⁶³.

1.16 Transforming growth factor beta (TGF- β) receptor signaling

TGF- β is produced by almost every cell. There are five subtypes (β 1- β 5) of TGF- β . TGF- β 1, β 2 and β 3 are accumulated in the bone matrix and bind to the TGF receptor (TGFR), a seven transmembrane receptor¹⁷⁸.

Resorbing osteoclasts release and activate TGF- β from the bone matrix¹⁷⁹. TGF- β contributes to RANKL-induced osteoclastogenesis^{180,181}. TGF- β phosphorylates Smad2 and

Smad3, which translocate into the nucleus together with Smad4, leading to a Smad-dependent transcription, including the expression of the plasminogen activator inhibitor type-1 (PAI-1)¹⁸². PAI-1 is an important physiological regulator of extracellular matrix (ECM) homeostasis and cell motility^{183,184}. TGF- β has also been described to activate other signaling pathways, such as the JNK-dependent and the Smad4-independent pathway¹⁸⁵.

1.17 Sma and Mad related (Smad) signaling

The Smad family proteins are critical mediators of the TGF- β superfamily signaling. Smad2/3 directly associates with the TRAF6-TAB1-TAK1 molecular complex, which is generated in response to RANKL stimulation and plays an essential role in osteoclast differentiation¹⁸⁶. The Mad homology 2 (MH2) domain of Smad3 is necessary for the TRAF6-TAB1-TAK1 complex formation, downstream signal transduction and osteoclast formation¹⁸⁶. Therefore, TGF- β and the binding of Smad3 to the TRAF6-TAB1-TAK1 complex is crucial for RANKL-induced signaling in osteoclasts¹⁸⁶.

1.18 Nuclear factor of activated T cells (NFATc1)

The family of NFAT transcription factors was originally discovered in activated T cells in 1988 and consists of five members; NFATc1 (NFAT2, NFATc), NFATc2 (NFAT1, NFATp), NFATc3 (NFAT4, NFATx), NFATc4 (NFAT3, NFATx) and NFAT5 (TonEBP: tonicity-responsive enhancer-binding protein)¹⁸⁷. All NFAT family members have a DNA-binding domain, which is highly homologous to the NF- κ B/Rel family (RHR: Rel-homology region) domain. NFATc1-4 but not NFAT5 have a DNA-binding domain, which is highly homologous to the N-terminal domain of NFAT family (NHR: NFAT-homology region) and functions as a calcium control domain¹⁸⁸. NHR has many serine residues and those are phosphorylated if the protein is inactive. If the phosphorylated serine residues are dephosphorylated by

calcium/calmodulin-dependent serine phosphatase calcineurin, NFAT translocates into the nucleus and initiates the transcription of target genes^{189,190}.

Upon RANKL stimulation, NFATc1 interacts directly with PU.1 to activate the gene promoter in concert with MTF. p38 MAP kinase phosphorylates NFATc1 but not PU.1 thereby enhancing nuclear accumulation of NFATc1 and the transcriptional activation of RANKL-induced osteoclast-specific genes such as the cathepsin K gene promoter. Asagiri M *et al.* reported in 2005 that NFATc1 is a master transcription factor for osteoclast differentiation, which is recruited to its own promoter resulting in the auto-amplification of NFATc1 during osteoclast differentiation¹⁹¹.

NFATc1-deficient embryonic stem cells fail to differentiate into osteoclasts in response to RANKL stimulation, and overexpression of NFATc1 causes precursor cells to undergo differentiation without RANKL signaling¹⁹². Thus, NFATc1 is identified as a master regulator of osteoclast differentiation¹⁹².

1.19 Nuclear factor kappa B (NF- κ B)

Presently, five mammalian NF- κ B family members are identified and cloned, including p50/p105 (NF- κ B1), p65 (RelA), cRel, p52/p100 (NF- κ B2) and RelB¹⁹³. Those families form homo- or hetero-dimer and are involved in various processes such as inflammation, immune response and carcinogenesis¹⁹⁴.

NF- κ B has a Rel homology domain (RHD) at its N-terminal end. RHD is essential for dimerization, DNA and I κ B binding. p50 and p52 are processed from p105 and p100 by an excision of the C-terminus, respectively¹⁹⁵⁻¹⁹⁸. p105 and p100 have an ankyrin repeat (ANK) structure at the C-terminus, which is highly homologous to I κ B¹⁹⁹. ANK structure masks the nuclear localization signals (NLSs) around the RHD and prevents the translocation into the nucleus²⁰⁰. p65, cRel and RelB have a transcriptional activation (TA) domain at the C-terminus,

while p50 and p52 do not have a TA domain²⁰¹. Therefore, homodimers of p50 or p52 inhibit transcription. However, if p50 or p52 form hetero-dimers with p65 or RelB, transcription of factors stimulating osteoclast differentiation such as NFATc1 is supported²⁰².

Two major ways exist to activate NF- κ B, the canonical pathway and the non-canonical pathway²⁰¹. The canonical pathway causes an activation of the I κ B kinase (IKK) complex as well as phosphorylation and decomposition of I κ B α mainly through p50/p65²⁰¹. The non-canonical pathway signals through p52/RelB, which is processed from p100 in an NF- κ B-inducing kinase (NIK) and IKK α -dependent manner²⁰³. Noteworthy, NFAT transcription factors also contain the RHD and bind to similar DNA sequences as the Rel/NF- κ B dimers, but NFAT proteins generally have not been found to form dimers with Rel and NF- κ B proteins^{201,204}.

Although p50- or p52-deficient mice have no obvious bone phenotype^{205,206}, NF- κ B1/NF- κ B2 (p50/p52) double knockout mice have an impaired tooth eruption and an osteopetrotic phenotype with no osteoclasts^{51,207}. This defect is caused by abnormal osteoclast precursors.

1.20 Activator protein 1 (AP-1)

AP-1 refers to heterodimers of members of the Fos family (c-Fos, Fos-related antigen (Fra)-1, Fra-2, FosB) and Jun family (c-Jun, JunB, JunD), or homodimers of members of the Jun family²⁰⁸. AP-1 factors have a basic leucine zipper structure for DNA binding and dimerization^{209,210}. c-Fos and c-Jun are activated by phosphorylation by JNKs (c-Jun N-terminal kinases) and RSK (ribosomal S6 kinase) or ERK (extracellular signal-regulated protein kinase)²¹¹⁻²¹³. c-Fos is a transcriptional inducer of the *Nfatc1* gene and essential to stabilize NFATc1 production for osteoclast differentiation⁵³. C-Jun, a partner of c-Fos to establish AP-

1 complex also has critical role in NFAT regulation of RANKL-induced osteoclast differentiation²¹⁴.

RANKL induces transcription of Fos11 in a c-Fos-dependent manner, thereby establishing a link between Rank signaling and the expression of AP-1 proteins in osteoclast differentiation²¹⁵. c-Fos and NFATc1 bind to the promoter of TRAP in a cooperative manner²¹⁶.

1.21 Treatment of osteoporosis

Historically, a number of different medications to treat osteoporosis were studied and developed. Parathyroid hormone (PTH; 1-84) is the first bone anabolic agent approved by the FDA for the treatment of osteoporosis. Testosterone treatments are available for osteoporosis in men to increase muscle and bone mass. Selective androgen receptor modulator (SARM) treatment prevents bone loss and reduces body fat in ovariectomized rat²¹⁷. Selective estrogen receptor modulators (SERMs) have a similar effect on bone as the hormone estrogen, helping to maintain the bone mineral density and to reduce the risk of fracture, particularly in the spine²¹⁸. Calcium and vitamin D supplements also help to reduce bone loss in elderly^{219,220}. Active form of vitamin D, Calcitriol improves calcium absorption²²¹. Although Strontium ranelate reduces vertebral fractures as a dual action bone agent (DABA), it is not on the market anymore due to an increased risk of myocardial infarction²²². Hormone replacement therapy (HRT) is not appropriate because of the link between estrogen and female cancers²²³.

1.21.1 Anti-resorptive drugs for the treatment of osteoporosis

1.21.1.1 Bisphosphonates

Bisphosphonates are stable analogs of pyrophosphate and the most commonly used anti-resorptive drugs, which bind to the mineral component of bone and inhibit osteoclast activity^{224,225}. Bisphosphonates are taken up by osteoclasts and induce apoptosis.

Bisphosphonates induce caspase-dependent formation of pyknotic nuclei and cleavage of

Mammalian Sterile 20-like (Mst) kinase 1 to form the active 34-kDa species associated with apoptosis²²⁶. Caspase-3 might be the major effector caspase activated in osteoclasts by bisphosphonate treatment²²⁷. Bisphosphonates are administered orally or intravenously and are divided into two types, the low potency non-nitrogen-containing bisphosphonates (e.g. clodronate) and the potent nitrogen-containing bisphosphonates (e.g. alendronate, zoledronate). The non-nitrogen-containing bisphosphonates become incorporated into molecules of newly formed ATP by the class II aminoacyl-transfer RNA synthetases after uptake by osteoclasts, leading to an accumulation of non-hydrolyzable ATP analogues²²⁸. These non-hydrolyzable ATP analogues inhibit multiple ATP-dependent cellular process, leading to apoptosis²²⁸. The nitrogen-containing bisphosphonates act as inhibitors of farnesyl-pyrophosphatase synthase, which leads to inhibition of the prenylation of many intracellular signaling proteins including Ras²²⁹. Preventing protein prenylation in osteoclasts inhibits bone resorption. Enzymes of the mevalonate pathway or prenyl protein transferases are likely to be the molecular targets of the nitrogen-containing bisphosphonates²²⁹. Bisphosphonates also function to limit both osteoblast and osteocyte apoptosis^{230,231}. Moreover, part of the osteoclast inhibiting effect of bisphosphonates is thought to be mediated through an action on osteoblasts^{232,233}. For example, bisphosphonates may act via osteoblasts to inhibit interleukin-6 (IL-6) production, a cytokine implicated in osteoclastogenesis²³⁴.

1.21.1.2 Denosumab

Denosumab is a human IgG2 monoclonal antibody against RANKL, which interrupts RANK/RANKL interaction and inhibits osteoclast differentiation and function²³⁵. Denosumab binds to the DE (Asp-Glu) loop region of human RANKL²³⁵, which is one of the surface loop structures that forms contacts with RANK on responding cells²⁶. Of note, denosumab does not bind to other TNF family members, such as TNF-related apoptosis-inducing ligand (TRAIL), CD40 ligand (CD40L), TNF- α and TNF- β ²³⁶. Denosumab (60 mg, subcutaneous injection every

6 months) was licensed by FDA for use in postmenopausal women who have high risk of osteoporotic fracture in 2010, and for use in men with high risk of fracture in 2012. Denosumab was at least as effective in increasing BMD at the hip and lumber spine as alendronate (70 mg oral weekly)²³⁷.

1.21.2 Anabolic drugs for the treatment of osteoporosis

1.21.2.1 Teriparatide

Teriparatide is a recombinant fragment of the first 34 amino acids of human parathyroid hormone (PTH; 1-34) with catabolic and anabolic effects on the skeleton depending on the mode of administration²³⁸. Endogenous PTH controls calcium and phosphate homeostasis in bone and kidney⁴. PTH stimulates osteoclast activity, leading to an increase of calcium level in the blood^{239,240}. Although the long-term PTH administration severely decreases bone mass, the intermittent administration of low dose PTH elevates bone formation by increasing osteoblast proliferation and function by suppressing osteoblast apoptosis²⁴¹. Teriparatide is the first anabolic drug for the treatment of osteoporosis approved by FDA in 2002²⁴². Teriparatide therapy is not allowed for more than 2 years, based on the induction of osteosarcoma in a rat model²⁴³.

1.21.2.2 Abaloparatide

Abaloparatide is a PTHrP analog for the treatment of osteoporosis²⁴⁴. It has 41% of homology to PTH (1-34, Teriparatide) and 76% of homology to PTHrP²⁴⁴. Abaloparatide binds to the PTH1R and increases the synthesis of cyclic adenosine monophosphate (cAMP) in osteoblasts like teriparatide. Abaloparatide has been reported to have a greater anabolic capacity than teriparatide since abaloparatide binds to PTH1R less stable than teriparatide²⁴⁵. Compared with placebo, 24 weeks of daily s.c. abaloparatide increases BMD at the lumbar spine, the femoral neck and the total hip. Furthermore, the abaloparatide-induced increase in BMD at the total hip

is greater than with the teriparatide²⁴⁶. Abolaparotide is approved for its use in the clinics in the U.S. but not yet in Europe²⁴⁷.

1.21.2.3 Romosozumab

Bone formation is increased by an activation of the Wnt- β -catenin signaling pathway^{248,249}. Furthermore, β -catenin increases OPG expression thereby suppressing osteoclast differentiation and function²⁵⁰. Sclerostin is expressed by osteocytes and inhibits the Wnt- β -catenin signaling pathway, resulting in a decreased bone formation^{84,251}. Romosozumab is a monoclonal antibody that binds to and inhibits sclerostin, resulting in an increase in bone formation and a decrease in bone resorption²⁵². Therefore, romosozumab is expected as the next generation bone anabolic drug for the treatment of osteoporosis^{85,253}. It is expected to enter the market in early 2019.

Despite the fact that several drugs are available to treat osteoporosis, more and better drugs are still needed in the clinics to improve the current treatment concepts. To reach this goal, more research is necessary to further characterize and understand the cellular and molecular mechanisms that control the differentiation and function of bone cells.

1.22 TG-interacting factor 1 (Tgif1)

TG-interacting factor 1 (Tgif1, Thymine-Guanine interacting factor 1, TGF- β -induced factor 1) is encoded by the *TGIF1* gene located on Chromosome 18. Tgif1 is a member of the three-amino-acid loop extension (TALE) subfamily of homeodomain proteins and a transcriptional repressor and co-repressor of the retinoid and TGF- β signaling pathways^{254,255}. Structurally, the Tgif1 gene consists of four parts, the repression domain (RD) -1 (1-41), the homeodomain (42-137), the RD-2A (138-192) and the RD-2B (208-272) (Fig. 1.9). The RD-1 recruits the C-terminal-binding protein (CtBP) and the RD-2A and RD-2B recruits histone deacetylases (HDACs), thereby repressing transcription. Additionally, the RD-2A has an Axin-binding

domain (144-177), by which Tgif1 can interfere with the assembly of the β -catenin destruction complex in the cytoplasm^{256,257}.

At the functional level, Tgif1 is required for gastrulation and limits the transcriptional response to Nodal signaling during early embryogenesis²⁵⁸. Furthermore, Tgif1 binds directly to DNA or interacts with TGF- β -activated Smads, thereby repressing TGF- β -responsive gene expression. Some Smad co-repressors such as Tgif1 and Smad nuclear interacting protein 1 (SNIP1) repress not only TGF- β /Smad-mediated transcriptional activation, but also Smad-independent transcription²⁵⁹.

Ling Yan and Rizwan Hamid *et al.* explored the role of Tgif1 in murine HSC function by CFU assays *in vitro* and short- and long-term competitive repopulation assays *in vivo*. Tgif1-deficient HSCs exhibits greater self-renewal and were less proliferative and more quiescent than wild-type cells. Thus, Tgif1 regulates quiescence and self-renewal of HSCs²⁶⁰.

Mutations of *TGIF1* in humans causes holoprosencephaly, a severe genetic disorder affecting the craniofacial development, due to aberrant sonic hedgehog (SHH) signaling²⁶¹. Deletion of *Tgif1* in mice results in only relatively mild developmental phenotypes in most strain backgrounds. However, the role of Tgif1 in bone is not fully understood.

The closely related homologue, TG-interacting factor 2 (*TGIF2*) is located on Chromosome 20²⁶². Tgif2 has a DNA-binding homeodomain that is very similar to the one of Tgif1. TGIF2 has two regions of high sequence identity with TGIF1. Contrary to Tgif1, Tgif2 recruits HDAC but not CtBP because it lacks a short amino acid motif, the PLDLS motif²⁶³. Tgif2 also interacts with TGF- β -activated Smads and represses TGF- β -responsive transcription²⁶³. Tgif2-deficient osteoclasts demonstrate a decreased phosphorylation of c-Jun and a decreased transcription of NFATc1 and TRAP in response to RANKL stimulation, resulting in an impaired osteoclast differentiation²⁶⁴. Thus, Tgif2-deficient mice display high bone mass with a decreased bone resorption²⁶⁴.

Our laboratory focuses on the role of Tgif1 in bone cells and the skeleton since the role of Tgif1 in adult bone homeostasis is not known. Previous work of our group has demonstrated that Tgif1 has an important role in osteoblast differentiation, activity and the PTH signaling pathway. Tgif1 knockout mice have a low bone turnover phenotype with a decreased bone formation and a reduced bone resorption²⁶⁵. These results indicate that Tgif1 might have a role in osteoclasts. In this thesis, I am exploring the intrinsic role of Tgif1 in osteoclasts and decipher the underlying molecular mechanism. This work will help to better understand osteoclast function and bone remodeling.

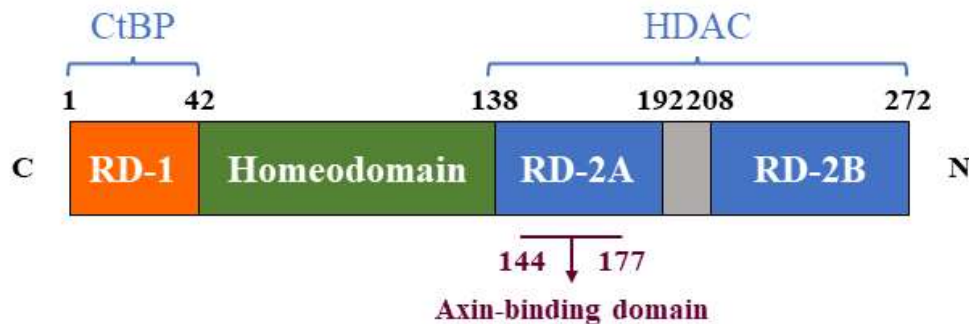


Fig. 1.9. Functional domains of TGIF. TGIF contains repression domain-1 (RD-1; 1-42), homeodomain (43-138), RD-2A (139-192) and RD-2B (208-272). RD-1 recruits C-terminal-binding protein (CtBP). RD-2A and RD-2B recruits to histone deacetylase (HDAC). RD-2A contains axin-binding domain (144-177). Modified from Razzaque and Atfi, *Biochimica et Biophysica Acta* (2016) **1865**: 101-104; Figure 1²⁵⁷.

2 Hypothesis and Aims

2.1 Hypothesis

Bone is a highly dynamic tissue that is constantly remodeled during lifetime. Bone remodeling is tightly regulated by a balanced activity of bone-resorbing osteoclasts and bone-forming osteoblasts. However, during aging the cellular activities become unbalanced with osteoclast activity increasing over osteoblast activity. This may lead to a loss of bone mass and ultimately osteoporosis with subsequent fractures. Since the mechanisms regulating bone remodeling in health and disease are not yet fully elucidated, we aimed to identify novel regulators of bone metabolism. In the context of ongoing research, the laboratory identified the homeodomain protein TG-interacting factor 1 (Tgif1) as a novel and important factor controlling bone remodeling and osteoblast activity in a cell-autonomous manner. Due to a decrease in osteoclast parameters and bone resorption in Tgif1-deficient mice, we hypothesized that Tgif1 might also play an important role in osteoclast differentiation and function as well as in bone resorption. Testing this hypothesis became therefore the subject of my PhD thesis.

2.2 Aims

To test the hypothesis that Tgif1 plays a role in osteoclast differentiation, function and bone resorption, the work of my thesis addresses these specific aims:

- 1) Characterize the bone phenotype upon osteoclast-targeted deletion Tgif1 *in vivo*.
- 2) Determine the role of Tgif1 in osteoclast differentiation and function.
- 3) Identify the molecular mechanisms by which Tgif1 controls osteoclast activity.

3 Materials and Methods

3.1 Chemicals, equipment and consumables

Table 3.1. Chemicals

Chemical	Company
10x TGS (Tris/Glycine/SDS) buffer	Bio-Rad
20% Sodium dodecyl sulfate solution	Sigma
2-Mercaptoethanol (β -ME)	Sigma
2-Methoxyethyl acetate	Merck
2-Propanol	Roth
4x Laemmli sample buffer	Bio-Rad
50x Cleaning concentrate	Bio-Rad
6x DNA loading dye	Thermo
Acetic acid	Sigma
Aceton	Chemsolute
Acid Fuchsin	Sigma
Acrylamide/bisacrylamide (Rotiphorese® Gel 30) (37, 5:1)	Roth
Albumin, from bovine serum (BSA)	Sigma
Alexa Flour™ 488 Phalloidine	Life Technologies
Alizarin Red S	Sigma
Ammonium persulfate (APS)	Sigma
Ampicillin sodium salt	Sigma
Aqua-Poly/Mount®	Polysciences
Benzoyl peroxide (with 25% H ₂ O) for synthesis	Merck
β -Glycerophosphate disodium salt, Pentahydrate	Calbiochem®
Calcein	Sigma
cOmplete, EDTA-free, Protease Inhibitor Cocktail Tablets	Roche
Coomassie(R) Brilliant Blue R-250 Staining Solution	Bio-Rad
Demeclocyclin hydrochloride	Sigma
Dimethylsulfoxide (DMSO)	Sigma
dNTP Mix, 10 mM	Fermentas
DPX Mountant for Histology	Sigma
Ethanol, 70%	TH. Geyer
Ethanol, 80%	TH. Geyer
Ethanol, 96%	TH. Geyer
Ethanol, absolute	Sigma
Ethanol, absolute	Chemsolute
Ethidium bromide drop, 0.025%	Roth
Ethidium bromide drop, 0.5%	Roth
Ethidium Bromide, 10 mg/ml	Roth
Ethylene glycol-bis(2-amino-ethylether)- <i>N,N,N',N'</i> -tetraacetic acid (EGTA)	Fluka
Ethylenediaminetetraacetate (EDTA), Titriplex(R) III	Fluka
Fast blue RR salt	Sigma
Fast red violet LB salt	Sigma

Fetal Bovine Serum (FBS)	gibco®
Ficoll-Paque™ PLUS	GE Healthcare
Formaldehyde solution, 37%	Sigma
Glycerol	Roth
Glycine, ReagentPlus®	Sigma
HBSS (1x), [-]CaCl ₂ , [-]MgCl ₂	gibco®
HEPES (4-(2-hydroxyethyl)-1-piperazineethanesulfonic acid) buffer solution	Sigma
Hydrochloric acid (HCl), 6 mol/L	Millipore
Immersion Oil	Fluka, Sigma
iQTM SYBR® Green Supermix	Bio-Rad
Isofluran, 100% (v/v), Forene®	abbvie
Ketamine, 10%	WDT
L-Ascorbic acid	Sigma
LE Agarose	Biozym
Light green SF	Chroma/Waldeck
Magnesium chloride hexahydrate	Sigma
MEM Alpha Medium (1x), [+]Ribonucleosides, [+]Deoxyribonucleosides, [+]L-glutamine, [+]Phenol red	gibco®
Methanol	J.T.Baker
Methyl methacrylate (MMA) solution	Merck
Milk powder, non-fat dry	Roth
<i>N,N,N',N'</i> -Tetramethylethylenediamine (TEMED)	Sigma
<i>N,N</i> -Dimethylformamide	Sigma
<i>N,N</i> -Dimethyl- <i>p</i> -toluidine for synthesis	Merck
Naphtol AS-MX phosphate disodium salt	Sigma
Nitric acid solution, concentrate	Sigma
Nonidet™ P-40 Substitute	Sigma
Nonylphenyl-polyethyleneglycol acetate for histology	Sigma
PBS pH 7.4 (1x), [-]CaCl ₂ , [-]MgCl ₂	gibco®
Penicillin/Streptomycin, 5,000 U/ml Penicillin, 5,000 µg/ml Streptomycin	gibco®
Permout®	Fisher Chemical
Phosphate buffered saline powder, pH 7.4	Sigma
PhosSTOP, Phosphatase Inhibitor Cocktail Tablets	Roche
Picric acid solution, saturated	Sigma
Ponceau S	Sigma
Precision Plus Protein™ WesternC™ Standards	Bio-Rad
Precision Protein™ Strep Tactin-HRP Conjugate, 5.000x	Bio-Rad
Rompun® (Xylazin injection), 2%	Bayer
Silver nitrate	Merck
Sodium acetate	Sigma
Sodium carbonate	Merck

Sodium chloride	J.T.Baker
Sodium deoxycholate	Sigma
Sodium dodecyl sulfate (SDS) pellets, $\geq 99\%$	Roth
Sodium dodecyl sulfate (SDS) solution, 20% in H ₂ O, BioUltra	Sigma
Sodium hydroxide solution (1N)	Merck
Sodium hypochlorite solution, 12%	Roth
Sodium L-tartrate dibasic dihydrate	Sigma
Sodium thiosulfate	Sigma
SYBR® Select Master Mix for CFX	Applied Biosystems
Toluidine blue O	Chroma/Waldeck
Triton X-100	Sigma
Trizima® base (=Tris)	Sigma
Trizima® hydrochloride (=Tris-HCl)	Sigma
Trypan blue solution	Sigma
Tween 20	J.T.Baker
Vectashield® Mounting medium with 4', 6-Diamino-2-phenylindol (DAPI)	Vector
Water, Molecular Biology Reagent	Sigma
Xylene	Chemsolute

Table 3.2. Equipment

Equipment	Company
Balance	Sartorius, SCALTEC
Block heater	Grant instruments
Cell counter	Bio-Rad
Centrifuge	Eppendorf, Thermo Scientific, Heraeus instruments, Kendro Laboratory Products
Clean bench	Heraeus instruments, Thermo Scientific
Tissue processor	Enno VIETH, Mikrotome GmbH
Confocal microscope	Leica
Electrophoresis chambers	Bio-Rad
Heater	Memmert
Imager	Bio-Rad
Incubators [-]CO ₂	New Brunswick Scientific
Incubators [+]CO ₂	Heraeus instruments, Thermo Scientific
Inverted microscope	Carl-Zeiss
Light microscope	Olympus
Magnetic stirrer	Heidolph instruments, IKA-WERK, Janke & Kundel GmbH & Co. KG., H+P Labortechnik GmbH
Microtome	Leica Biosystems
Microwave	SHARP
μ CT scanner	SCANCO MEDICAL

Optical microscope	BRUKER
Plate reader	Perkin Elmer
pH meter	METTLER TOLEDO
Pipettes	Eppendorf
Power supply	Bio-Rad
Scanner	EPSON
Shaker	GFL, PHOENIX Instrument
Spectrophotometer	PeqLab, Thermo Scientific
Thermocyclers	Eppendorf
Thermocycler Realtime PCR	Bio-Rad
Thermo mixer	Eppendorf
Transfer chamber	novex® by life technologies™
UV Transilluminator	Biometra
Vacuum pump	Servox Medizintechnik GmbH
Vortex	Heidolph instruments
Water bath	Eppendorf
Shaking water bath	GFL

Table 3.3. Consumables

Consumable	Company
Aluminum foil	Carl-Roth
Blotting paper	Whatmann™, GE Healthcare Life Sciences
Cell culture plate (6, 12, 48, 96 well-plate)	Thermo Scientific
Cell lifter	coster®, Corning Incorporated
Cell scraper	Sarstedt
Coverslip	Marienfeld superior
Cuvettes	WHEATON®, T.H.Gayer
Disposable bags	Carl-Roth
Embedding cassettes	MEDITE
Gel electrophoresis comb	Bio-Rad
Gel glass plate	Bio-Rad
Glass pasteur pipette	Carl-Roth
Glass slide	LABSOLUTE®, T.H.Gayer
Glass vial	Carl-Roth
Gloves	Ansell
Laboratory film (Parafilm)	Bemis
Laboratory color tape	TimeMed Labeling System, Inc., Fisher Scientific
Lens paper	Assistant®
Needle	BD
Nitrocellulose blotting membrane	Amersham, GE Healthcare Life Sciences
Pasteur pipette	VWR
PCR plate	Bio-Rad

Pipette tips	Eppendorf, Sarstedt, Biozym
PVDF blotting membrane	Amersham, GE Healthcare Life Sciences
Reaction tube (0.2, 1.5, 2.0, 5.0 ml)	Eppendorf, Sarstedt
Scalpel	BRAUN (Aesculap Division)
Sterile syringe filter (0.22 µm)	Merck Millipore Ltd.
Syringe	BD, BRAUN
Tissue	TORK Universal
Wrap	Carl-Roth

3.2 Kits

Table 3.4. Kits

Kits	Company
Bio-Rad Protein Assay	Bio-Rad
Pierce™ BCA Protein Assay Kit	Pierce (Thermo Fisher Scientific)
CellTiter 96® AQueous One Solution Cell Proliferation Assay	Promega
Clarity™ Western ECL substrate	Bio-Rad
HiSpeed® Plasmid Maxi Kit	QIAGEN
Lipofectamine 3000 Transfection Kit	Invitrogen
ProtoScript® M-MuLV First Strand cDNA Synthesis Kit	New England BioLabs
QIAGEN® Plasmid Maxi Kit	QIAGEN
QIAprep® Spin Miniprep Kit	QIAGEN
QIAquick® Gel Extraction Kit	QIAGEN
Quick Ligation™ Kit	New England BioLabs
RNeasy® Plus Mini Kit	QIAGEN
SuperSignal® West Femto Chemiluminescent Substrate	Pierce (Thermo Fisher Scientific)

3.3 DNA ladders and protein standards

GeneRuler™ DNA Ladder Mix, ready-to-use (10 kb) was purchased from Thermo Fisher Scientific and used to determine the DNA length in DNA electrophoresis. Precision Plus Protein™ WesternC™ Standards were purchased from Bio-Rad and used in western blot analyses to determine the molecular mass of specific proteins.

3.4 Enzymes

Table 3.5. Enzymes

Enzyme	Activity	Company
Collagenase A	0.253 U/mg, lyophilized	Roche
Dispase® II (neutral protease, grade II)	≥0.8 units/mg protein (37 °C, casein as substrate, pH 7.5)	Roche
iQ™ SYBR® Green Supermix	50 U/ml	Bio-Rad
KAPA2G Fast ReadyMix with Dye	20 U/ml	Peq Lab
PrimeTaq DNA polymerase	5 U/μl	Primetech

3.5 Oligonucleotides

3.5.1 Primers

All primers used for qRT-PCR, genotyping and sequencing were purchased from Eurofins or Invitrogen/Thermo Fisher Scientific and are listed in Table 3.6. Melting temperature (T_m) of each primer was calculated by T_m calculator provided by Thermo Fisher Scientific (<https://www.thermofisher.com/de/de/home/brands/thermo-scientific/molecular-biology/molecular-biology-learning-center/molecular-biology-resource-library/thermo-scientific-web-tools/tm-calculator.html>).

Table 3.6. Primers

Name	Primer 5'-3' Sequence	T_m (°C)	Application
Tgif1 fwd-new	GTC TAT CAA AGT CCA ACT GGC	54.9	genotyping
Tgif1 rev 1	GCC CTC ACA ACC TTG TCT TT	55.5	genotyping
Tgif1 rev 2	TGG GCC CTT CTG AAA TAC AC	55.9	genotyping
m Tbp fwd	GCT CTG GAA TTG TAC CGC AGC	61.0	qRT-PCR
m Tbp rev	CTC TTG GCT CCT GTG CAC AC	60.5	qRT-PCR
m OC-STAMP fwd	CTG AGC TGT CTC CTA AGG CTG	59.0	qRT-PCR
m OC-STAMP rev	GAA GAG GAT GAA GTC CAG AAC C	56.8	qRT-PCR
m Trap fwd	GGT TCC AGG AGA CCT TTG AGG	59.6	qRT-PCR
m Trap rev	AGC GCA AAC GGT AGT AAG GG	59.3	qRT-PCR
m Cathepsin K fwd	CAG TTT TAC AGC AGA GGT GTG T	56.1	qRT-PCR
m Cathepsin K rev	TGG CTG GAA TCA CAT CTT GGG	59.1	qRT-PCR
m Car1 fwd	ACT GGG GCA ACT CAA ACG AC	59.7	qRT-PCR
m Car1 rev	TGG GGC TCG TTT TCC CTT AG	59.2	qRT-PCR
m Car2 fwd	GCA CAA CGG ACC AGA GAA CTG	60.3	qRT-PCR
m Car2 rev	GAG GGG TCC TCC TTT CAG CA	61.5	qRT-PCR

Materials and Methods

m Atp6vOd2 fwd	ACA TTG CAG AGA CCC CCT CA	60.1	qRT-PCR
m Atp6vOd2 rev	CGG CCT CAA ACT CAA GAA TGG	58.1	qRT-PCR
m Nhedc2 fwd	GAA ACG GTT GGC CTT TGT GTT	58.1	qRT-PCR
m Nhedc2 rev	GAT CTT GCC GTG TCC AGA GC	60.7	qRT-PCR
m DC-STAMP fwd	TCC TCC ATG AAC AAA CAG TTC CAA	57.9	qRT-PCR
m DC-STAMP rev	AGA CGT GGT TTA GGA ATG CAG CTC	61.0	qRT-PCR
m NFATc1 fwd	CCT TCG GAA GGG TGC CTT TTG	61.1	qRT-PCR
m NFATc1 rev	CCG TCT CAT AGT GAG CCC TG	59.1	qRT-PCR
m RANK fwd	CTA CAG CAT GGG CTT TCC CAG	60.2	qRT-PCR
m RANK rev	CCA CGA TGA TGT CAC CCT TG	57.3	qRT-PCR
m Tgif1 fwd	GCA GAC ACA CCT GTC CAC ACT A	60.5	qRT-PCR
m Tgif1 rev	GGA ATG AAA TGG GCT CTC TTC T	56.4	qRT-PCR
Cre-C fwd	ACT GGG ATC TTC GAA CTC TTT GGA C	60.4	genotyping
Cre-C rev	GAT GTT GGG GCA CTG CTC ATT CAC C	64.8	genotyping
Cre-Cre fwd	CCA TCT GCC ACC AGC CAG	62.2	genotyping
Cre-Cre rev	TCG CCA TCT TCC AGC AGG	60.9	genotyping
m Pai1 fwd	ACG TTG TGG AAC TGC CCT AC	59.1	qRT-PCR
m Pai1 rev	GCC AGG GTT GCA CTA AAC AT	57.2	qRT-PCR
CtsK Primer #1N fwd	CCT AAT TAT TCC TTC CGC CAG GAT G	59.3	genotyping
CtsK Primer #2N rev	CCA GGT TAT GGG CAG AGA TTT GCT T	61.1	genotyping
CtsK Primer #3N rev	CAC CGG CAT CAA CGT TTT CTT TTC G	61.2	genotyping
m c-fms fwd	CTA CTG GAC CTT GGA CCC TG	58.8	qRT-PCR
m c-fms rev	GAT CAG ACA GGG CAG CAC AGC	63.2	qRT-PCR
S1P WT	TGG TGT GCG GCT GTC TAG TCA A	62.2	genotyping
S1P com	CAC AGC AAG CAG ACC TCC AGA	61.0	genotyping
S1P KO	ATC GAT ACC GTC GAT CGA CCT	58.8	genotyping
m c-Src fwd	GAA GCC ATG GAG TAC CTG GAG	59.2	qRT-PCR
m c-Src rev	CTC CAC ACA TCA GAC TTG GTG	56.7	qRT-PCR
m TRAF6 fwd	GCT GTG TCC ATG GCA TAT GAA G	57.7	qRT-PCR
m TRAF6 rev	GTG CCA AGT GAT TCC TCT GCA T	59.3	qRT-PCR
m PP2A-A α fwd	ATT GCC CAG CTT CTG CCA CAG	62.5	qRT-PCR
m PP2A-A α rev	ACC TCG GCC TCA CAG TCC TTC	63.6	qRT-PCR
m PP2A-B56 δ fwd	GCA TCC TCC CCA TCA TGT TTC C	60.5	qRT-PCR
m PP2A-B56 δ rev	CGA TCT TCT GCC ACA TCT CCT C	59.3	qRT-PCR
m Ppp2r1b fwd	GGT TTT AAT CGA CGA GCT CCG C	60.9	qRT-PCR
m Ppp2r1b rev	GAA ATT TCC CAG CTG CTC GGC	61.9	qRT-PCR
m Ppp2ca fwd	CTT CCT CTC ACT GCC TTG GTG	59.6	qRT-PCR
m Ppp2ca rev	GTA TAA CCA GCT CCC CGA GG	59.3	qRT-PCR
m Ppp2cb fwd	GAA CCA AGT GCG GAC GCT GTG	63.7	qRT-PCR
m Ppp2cb rev	GTA CCC TCT GTC TAC ATA GTC C	55.0	qRT-PCR
m Ppp2r2a fwd	GGT GGG AGA GTT GTC ATC TTT C	57.2	qRT-PCR

m Ppp2r2a rev	CAG CAT TTT TCT GGG GTA ACC ACC	60.4	qRT-PCR
m Ppp2r2b fwd	CTG TGT GAC AGG CAC ACC AAG	60.1	qRT-PCR
m Ppp2r2b rev	CTT GCT GCG GAG GTA GTC ATG	59.9	qRT-PCR
m Ppp2r2c fwd	GGA CCA CAG CTA TGT GAC AGA AG	59.0	qRT-PCR
m Ppp2r2c rev	GTA GTC AAA CTC CGG CTC GTG	59.9	qRT-PCR
m Ppp2r2d fwd	GTG CTT CTC GCA GGT GAA GG	60.7	qRT-PCR
m Ppp2r2d rev	CAT TGT ACT CTC CCC TAG AGT G	55.3	qRT-PCR
m Ppp2r5a fwd	GCA AGT TCC TTG GCC TGA GAG	60.5	qRT-PCR
m Ppp2r5a rev	GTG CGT GAA ACA AGG CCA ATC C	61.7	qRT-PCR
m Ppp2r5b fwd	GTC TAC CCA GAC ATC ATC CGC	59.5	qRT-PCR
m Ppp2r5b rev	CAC GTA TCT CTT GGC CAC AGA G	59.1	qRT-PCR
m Ppp2r5c fwd	GGC CTG CGT GCT TAC ATC AG	61.0	qRT-PCR
m Ppp2r5c rev	GGT AGA CAC TCA GGG ACT TCA C	58.6	qRT-PCR
m Ppp2r5e fwd	GAA GAT GAA CCT ACC CTC GAG G	58.7	qRT-PCR
m Ppp2r5e rev	CCG TTC TCG AGG GTC TTC AC	59.7	qRT-PCR
m Ppp2r3a1 fwd	GAT TCA GCA GAC GCC AGA AGT G	60.3	qRT-PCR
m Ppp2r3a1 rev	CAG GTG TCT GGG AGT CCT TC	59.2	qRT-PCR
m Ppp2r3a2 fwd	CTA GCA AGG GGC TGC GAT TTT G	61.0	qRT-PCR
m Ppp2r3a2 rev	GGA CAA CGG TGT ATT CAC GAC ATC	59.6	qRT-PCR
m Ppp2r3c fwd	GCC AAG GAT ACC TTC GGG AAT C	60.1	qRT-PCR
m Ppp2r3c rev	CTT CCC TGT TCT TAG AGG GTC C	58.8	qRT-PCR
m Ppp2r3d fwd	GAT TGA CCG CAT CTT CTC AGG G	59.9	qRT-PCR
m Ppp2r3d rev	GGC CTG CTC CTC ATA GAA GAA C	59.6	qRT-PCR
m Stern fwd	GAG CTC AGT AGG GCA GAT GAA G	59.1	qRT-PCR
m Stern rev	CTT AGG GTT CCA CGT CTT CCT C	59.1	qRT-PCR
m Stern3 fwd	GGC CTT GGA GAC CTT GCA GAC	63.2	qRT-PCR
m Stern3 rev	GTC CTC AGA GGC AGT AAC GAG	59.0	qRT-PCR
m Stern4 fwd	CTG TGG AAC CTG CAG AAG GC	60.8	qRT-PCR
m Stern4 rev	GGT CAT AGC CAT CAT ATG GGT CC	59.1	qRT-PCR
m Ppp2r4 fwd	GAC GAC CAG GTG GCT ATT GTC	59.9	qRT-PCR
m Ppp2r4 rev	CAT CCA CGA AAT GTC TGG GCT C	60.2	qRT-PCR
PP2A-C β _Primer #1	CCC GGG CCT AAC AGA CTA TAA CTT C	60.8	sequencing
PP2A-C β _Primer #2	CCC GGG CTG TTG AGC ACT TG	63.8	sequencing
PP2A-C β _Primer #3	CTC GAG TCT TCC CTC CCT CC	61.6	sequencing

T_m; melting temperature, fwd; forward, rev; reverse.

3.5.2 GapmeR oligonucleotides

GapmeR oligonucleotide sequences were designed based on Exiqon algorithm and purchased from QIAGEN. GapmeRs were used for silencing targeting genes.

Table 3.7. GapmeRs

Name	5'- Sequence -3'	MW, calculated (Da)
Tgif1-targeting #1	CTAGCGAAGAGTGCAT	5325.3
Tgif1-targeting #2	GAGGGCGTCTAAAGTA	5351.3
Tgif1-targeting #3	ACGAGAGAGGTGTCTG	5395.3
Tgif1-targeting #4	ACAGTCTTGGAACATA	5284.2
PP2A-C β -targeting #1	CGGACCTCTTGCACAT	5226.2
PP2A-C β -targeting #2	TGAGACCGTTGGCATG	5318.2
PP2A-C β -targeting #3	TAGCGCACCTTTAATG	5237.2
PP2A-C β -targeting #4	TCAACATCCAACAGT	4883.9
PP2A-C β -targeting #5	CACGACGAGGTGCTGG	5314.2
Negative control A	AACACGTCTATACGC	4928

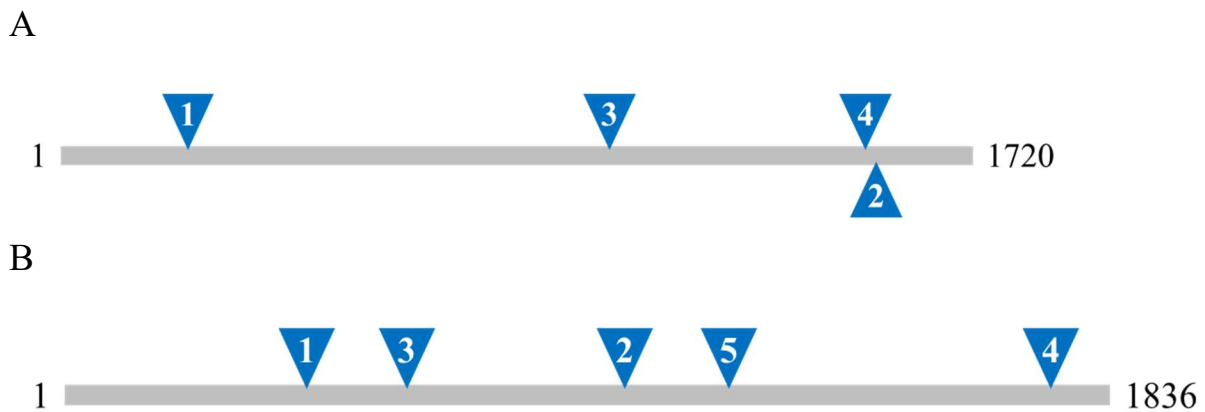


Fig. 3.1. Schematic GapmeR designs by Exiqon algorithm. (A) *In silico* design of top 4 Tgif1-targeting GapmeRs in the Exiqon design score rank. #1 is designed close to 5'-terminus, #3 is in the middle, and #2 and #4 are close to 3'-terminus of the Tgif1 gene (1720 bp). (B) *In silico* design of top 5 PP2A-C β -targeting GapmeRs in the Exiqon design score rank. #1 and 3 are designed in the right-half region, #2 is in the middle, #5 is in the left-half region, and #4 is in the 3'-terminus in the Ppp2cb gene (1836 bp).

3.6 Antibodies

Primary and secondary antibodies used for western blot analyses, immunofluorescence microscopy and FACS are listed in Table 3.8 and Table 3.9.

Table 3.8. Primary antibodies

Antibody	Host	Dilution	Company
Actin	Mouse, mono	1:4000	Millipore
Akt, pan	Rabbit, mono	1:1000	Cell Signaling
alpha-Tubulin	Mouse, mono	1:2000	Calbiochem
alpha-Tubulin	Mouse, mono	1:1000	Sigma

Materials and Methods

Arp2	Mouse, mono	1:2000	Abcam
Bcl-2	Rabbit, poly	1:200	Santa Cruz
Bim	Rabbit, poly	1:200	Santa Cruz
Cathepsin K	Mouse, mono	1:1000	Millipore
CD115, c-fms	Mouse, mono	1:50	Affymetric eBioscience
CD11b	Rat, mono	1:1000	Abcam
c-Fos	Rabbit, poly	1:1000	Cell Signaling
DCST1	Rabbit, poly	1:4000	Abcam
IEX-1	Goat, poly	1:200	Santa Cruz
Integrin α V, CD-51	Mouse, mono	1:500	BD Biosciences
Lamin A/C	Rabbit, poly	1:1000	Cell Signaling
MEK1/2	Rabbit, poly	1:1000	Cell Signaling
Mouse IgG2a	Mouse, mono	1:1000	Abcam
NFAT2	Rabbit, mono	1:1000	Cell Signaling
NF- κ B2 p100/p52	Rabbit, poly	1:1000	Cell Signaling
p38 MAPK	Rabbit, poly	1:1000	Cell Signaling
p44/42 MAPK	Mouse, mono	1:2000	Cell Signaling
PAI-1	Goat, poly	1:200	Santa Cruz
phospho p38	Rabbit, poly	1:1000	Cell Signaling
phospho p44/42	Rabbit, mono	1:2000	Cell Signaling
Phospho PP2A-C α / β	Mouse, mono	1:100	Santa Cruz
Phospho-Akt (Ser473)	Rabbit, mono	1:2000	Cell signaling
Phospho-MEK1/2 (Se217/221)	Rabbit, poly	1:1000	Cell Signaling
Phospho-NF- κ B2 p100 (Ser866/870)	Rabbit, poly	1:1000	Cell Signaling
Phospho-Smad2 (Ser465/467)	Rabbit, mono	1:1000	Cell Signaling
Phospho-Src Family (Tyr416)	Rabbit, mono	1:1000	Cell Signaling
PP2A-B56 alpha	Goat, poly	1:200	Santa Cruz
PP2A-B56 alpha	Goat, poly	1:200	Santa Cruz
PP2A-B56 beta	Goat, poly	1:200	Santa Cruz
PP2A-B56 delta	Mouse, mono	1:1000	Millipore
PP2A-C α	Rabbit, poly	1:1000	Thermo Fisher
PP2A-C α / β	Mouse, mono	1:200	Santa Cruz
PP2A-C α / β	Goat, poly	1:200	Santa Cruz
PP2A-C α / β	Mouse, mono	1:200	Santa Cruz
PP2A-C β	Rabbit, poly	1:500	Thermo Fisher
RANK	Mouse, mono	1:100-250	Abcam
Rat IgG	Rat, poly	1:2000	Abcam
SET	Rabbit, poly	1:1000	Bethyl
Smad2	Mouse, mono	1:1000	Cell Signaling
Src	Mouse, mono	1:1000	Millipore
TGIF1	Rabbit, mono	1:500	Abcam
TRAF6	Rabbit, mono	1:1000	Cell Signaling

TRAP5	Rabbit, mono	1:1000	Abcam
-------	--------------	--------	-------

Mono: monoclonal antibody, poly: polyclonal antibody.

Table 3.9. Secondary antibodies

Antibody	Application Dilution	Company
Goat anti-Rabbit IgG	WB 1:10 000	Promega
Goat anti-Mouse IgG	WB 1:10 000	Promega
Donkey anti-Goat IgG	WB 1:10 000	Promega
Alexa Fluor® 488 goat anti-rat IgG	IF 1:2000	Life Technologies
Alexa Fluor® 488 donkey anti-mouse IgG	IF 1:2000	Life Technologies
Alexa Fluor® 546 donkey anti-mouse IgG	IF 1:2000	Life Technologies

WB: western blot, IF: immunofluorescence

For WB Precision Protein™ Strep Tactin/HRP Conjugate, 5,000x [BIO-RAD #161-0380]

3.7 Live cell imaging

Vybrant™ Cell-Labeling Solutions were purchased from Molecular Probes and listed in

Table 3.10.

Table 3.10. Vybrant™ Cell-Labeling Solutions

Product #	Tracer	Absorption (nm)	Emmission (nm)
V-22886	DiO	484	501
V-22888	CM-DiI	553	570

3.8 Electronic data processing

Table 3.11. Softwares

Software	Company
cellSens Entry 1.6	Olympus Corp.
CFX Manager 3.1	Bio-Rad Laboratories
GraphPad Prism 5	GraphPad Software, Inc.
Image J 1.48, public domain	National Institutes of Health (NIH)
Image Lab™ 4.1	Bio-Rad Laboratories
Mendeley	Mendeley Ltd.
Microsoft Office Professional Plus 2010	Microsoft Corp.
Nanodrop 1.4.2	Thermo Fisher Scientific
OsteoMeasure™	OsteoMetrics
SCANCO Finite Element	SCANCO Medical AG
Serial Cloner 2.6.1	Serial Basics

Vision64 Map	BRUKER
WorkOut 2.5	Dazdaq Solutions Ltd.
ZEN 2012 (blue edition)	Zeiss

Table 3.12. Online programs and databases

Online programs /Databases	Website
ALGGEN-PROMO	http://algggen.lsi.upc.es/cgi-bin/promo_v3/promo/promoinit.cgi?dirDB=TF_8.3
addgene	https://www.addgene.org/
Blast	http://www.ncbi.nlm.nih.gov/blast/Blast.cgi
NCBI Database	http://www.ncbi.nlm.nih.gov
PubMed	https://www.ncbi.nlm.nih.gov/pubmed/
Tm Calculator	https://www.thermofisher.com/de/de/home/brands/thermo-scientific/molecular-biology/molecular-biology-learning-center/molecular-biology-resource-library/thermo-scientific-web-tools/tm-calculator.html

3.9 Mice

3.9.1 $Tgif1^{+/-}$ and $Tgif1^{loxP/+}$ mice

Hemizygous $Tgif1^{+/-}$ and $Tgif1^{loxP/+}$ mice were kindly provided by Dr. Christopher A. Walsh, Harvard University, Boston, USA²⁶⁶. The established $Tgif1^{+/-}$ mice were mated with $Tgif1^{+/+}$ mice to generate $Tgif1^{+/+}$ mice and $Tgif1^{+/-}$ mice. The hemizygous $Tgif1^{+/-}$ mice were mated to generate $Tgif1^{+/+}$, $Tgif1^{+/-}$ and $Tgif1^{-/-}$ mice. Mice with a germ-line deletion of $Tgif1$ ($Tgif1^{-/-}$) were used in the experiments and compared to littermate control ($Tgif1^{+/+}$) mice.

The established $Tgif1^{loxP/+}$ mice were mated with $Tgif1^{+/+}$ mice to generate $Tgif1^{+/+}$ mice and $Tgif1^{loxP/+}$ mice. The hemizygous $Tgif1^{loxP/+}$ mice were mated to generate $Tgif1^{+/+}$, $Tgif1^{loxP/+}$ and $Tgif1^{loxP/loxP}$ mice. $Tgif1^{loxP/loxP}$ mice were used for establishing $LysM-Cre^{+};Tgif1^{loxP/loxP}$ mice (3.9.2) and $Ctsk-Cre^{+};Tgif1^{loxP/loxP}$ mice (3.9.3).

3.9.2 LysM-Cre;Tgif1^{loxP/loxP} mice

LysM-Cre⁺ mice were kindly provided by Dr. Thorsten Schinke, UKE, Hamburg, Germany. LysM-Cre mice were originally generated by B.E. Clausen and I. Förster *et al*²⁶⁷. To delete Tgif1 specifically in the myeloid lineage, LysM-Cre⁺ mice were mated with Tgif1^{loxP/+} mice to generate LysM-Cre⁺;Tgif1^{loxP/+} mice and LysM-Cre⁻;Tgif1^{loxP/+} mice (First generation). LysM-Cre⁺;Tgif1^{loxP/+} mice and LysM-Cre⁻;Tgif1^{loxP/+} mice were then mated to obtain LysM-Cre⁺;Tgif1^{loxP/loxP} mice and LysM-Cre⁻;Tgif1^{loxP/loxP} mice (Second generation) which were used for our experiments.

3.9.3 Ctsk-Cre;Tgif1^{loxP/loxP} mice

Mice expressing the Cre recombinase downstream of the cathepsin K (Ctsk) promoter (Ctsk-Cre⁺) were kindly provided by Dr. Shigeaki Kato, the University of Tokyo, Japan²⁶⁸. To investigate the role of Tgif1 in mature osteoclasts, Ctsk-Cre⁺ mice were mated with Tgif1^{loxP/+} mice to generate Ctsk-Cre⁺;Tgif1^{loxP/+} mice and Ctsk-Cre⁻;Tgif1^{loxP/+} mice (First generation). Ctsk-Cre⁺;Tgif1^{loxP/+} mice and Ctsk-Cre⁻;Tgif1^{loxP/+} mice were then mated to obtain Ctsk-Cre⁺;Tgif1^{loxP/loxP} mice and Ctsk-Cre⁻;Tgif1^{loxP/loxP} mice (Second generation) which were used for our experiments.

3.10 Cell biology methods

3.10.1 Medium and solutions for cell culture

Alpha-modified minimum essential medium (alpha-MEM), trypsin/EDTA, Penicillin/Streptomycin (P/S; 10,000 U/ml Penicillin and 10 mg/ml Streptomycin) and phosphate-buffered saline (PBS) were obtained from Gibco Life Technologies. Fetal bovine serum (FBS) was evaluated to be suitable for osteoclast cultures and purchased from Gibco Life Technologies (Lot. #41F0120K).

3.10.2 Cell culture

Cultures of fresh bone marrow cells, bone marrow macrophages (BMMs) and osteoclasts were performed at 37°C and 5% CO₂ in pre-warmed alpha-MEM supplemented with 10% FBS and 1% P/S (complete medium).

3.10.3 Trypsinization

Adherent cells were washed twice with pre-warmed PBS and incubated for maximum 5 min with trypsin/EDTA solution at 37°C. The protease activity of trypsin was inactivated with culture medium containing 10% FBS. The detached cells in suspension were centrifuged at 900 rpm at room temperature for 5 min. The cell pellets were re-suspended in complete medium, counted and seeded for experiments.

3.10.4 Cell counting

For automatic cell counting, 10 µl of cell suspension was mixed with 10 µl of Trypan blue solution. The cell suspension was pipetted on a cell counting slide (Bio-Rad) and counted using the TC-20 cell counting device (Bio-Rad). Occasionally, the stained cell suspension was counted manually using a hemocytometer under the microscope.

3.10.5 Bone marrow isolation and BMM culture

Lower extremities were harvested from mice and placed in PBS with 5% P/S. Bones were washed once with fresh PBS with 5% P/S and periosteum was cleaned using a scalpel. Bones were replaced in fresh plain alpha-MEM and both epiphyses were cut. Bone marrow cells (BMs) were flushed from diaphyses with plain alpha-MEM using a 25G needle. BMs were centrifuged at 900 rpm for 5 min, and the supernatant was removed. BMs pellet was re-suspended in complete medium and incubated in a 35 mm or 60 mm dish at 37°C for 3-4 hours. Non-adherent cells were collected and expanded with 100 ng/ml M-CSF (PeproTech) at 37°C for 3-4 days.

3.10.6 Colony Forming Unit (CFU) assay

BM cell suspension was prepared in 6.0×10^4 cells/ml. The cell suspension (400 μ l) was mixed with 4 ml of MethoCult (STEMCELL) and 1.2 ml of the mixture was plated in a 35 mm dish in triplicate (6.6×10^3 cells/plate). Cells were incubated at 37°C for 7 days and the number of granuloma macrophage (GM)-CFU was counted manually. These experiments were performed 3 times.

3.10.7 Primary osteoblast isolation from the long bones

Long bone osteoblasts were isolated using collagenase digestion. For this purpose, Collagenase A (50 mg) was mixed with 50 ml alpha-MEM and prepared freshly before digestion. The digestion solution was sterilized with a filter flip. Lower extremities were harvested from mice in PBS with 5% P/S. Bones were washed with fresh PBS with 5% P/S and periosteum was cleaned using a scalpel. Bones were replaced in fresh plain alpha-MEM and epiphyses were cut. Bone marrow was flushed from diaphyses with alpha-MEM using a 25G needle and the bone envelope was washed in HBSS. Bones were cut and minced into small pieces using a scalpel. Bone pieces were distributed over several 1.5 ml Eppendorf tubes (e.g. 3 tubes per 1 sample) and digested with 1 ml of pre-warmed collagenase solution for 1 hour at 37°C in a shaking incubator at 1000 rpm. After one hour, tubes were mixed vigorously and collagenase digestion was continued for one more hour. The digestion solution was aspirated and bone pieces were washed twice with complete alpha-MEM (1 ml per tube). Bone pieces were transferred into a 35 mm dish filled with 3 ml complete alpha-MEM and minced with a scalpel into fine pieces. Fine bone pieces were transferred into a 60 mm dish and incubated in 5 ml complete alpha-MEM with 10% FBS at 37°C for 7 days.

3.10.8 Primary osteoblast isolation from calvariae

Calvarial osteoblasts were isolated using a sequential digestion. For this purpose, digestion solution was freshly prepared by mixing Dispase II (100 mg) and Collagenase A (50 mg) in 50

ml alpha-MEM. The digestion solution was sterilized with a filter flip. A head of a 3-day old mouse was cut off and washed shortly in a beaker containing 70% ethanol. In addition, tails were cut off and placed in an Eppendorf tube for genotyping. A scalp of a mouse was peeled off from hind head towards the nose and the whole calvaria was exposed. Calvaria was removed using a scissor and cleaned up by removing the soft tissue around the calvaria. Cleaned calvaria was kept in alpha-MEM in a 12 well-plate while collecting calvaria from the remaining mice. Calvariae were digested in a digestion solution in a shaking incubator at 37°C for 10 min and the first fraction was discarded. Calvariae were digested with fresh digestion solution in a shaking incubator at 37°C for 25 min for 4 times and fractions 2 to 5 were collected in 15 ml Falcon tubes containing 2 ml FBS. Collected digestion solution was centrifuged at 900 rpm for 5 min and supernatant was discarded. Cell pellet was re-suspended in 10 ml alpha-MEM with 10% FBS and 1% P/S and plated on a 10 mm culture dish. Cells were incubated at 37°C until 90% confluency.

3.10.9 Osteoblast differentiation and mineralization

Osteoblast precursor cells from long bone and/or calvaria were seeded at 300,000 cells/well into 6 well-plate with differentiation medium containing 50 µg/ml Ascorbic acid and 5 mM β-Glycerophosphate. Alkaline phosphatase (ALP) -positive cells (osteoblasts) were observed on culture day 14 by ALP staining as described in 3.11.1.2. Mineralization was observed on culture day 21 by alizarin red staining as described in section 3.11.1.3.

3.10.10 Osteoclast differentiation

After trypsinization and cell counting, BMMs were plated at a density of 15,000 cells/well, 150,000 cells/well and 300,000 cells/well into 96 well-plate, 12 well-plate and 6 well-plate, respectively, with 25 ng/ml M-CSF (PeproTech) and 100 ng/ml RANKL (PeproTech). TRAP-

positive (staining will be described in section 3.11.1.1) multi-nucleated cells (MNCs) were observed after 3 to 5 days of culture.

3.10.11 Pit formation assay

BMMs were trypsinized and seeded on dentin slices (4 mm x 4 mm) at a density of 15,000 cells/well in 96 well-plate and cultured at 37°C for 7 days. Dentin slices were removed from the culture plate and cleaned with 1% NaOH solution by sonication to remove all cells. Dentin slices were stained with toluidine blue and resorption pits were determined by optical microscopy, confocal microscopy and scanning electron microscopy (SEM).

3.10.12 Pit volume analysis

Resorptive activity of osteoclasts was determined by analyzing the volume of resorption pits. Dentine slices from pit formation assay were scanned on their surface using an optical profiler, Contour GT-K (BRUKER) and analyzed by Vision64®. "Statistic Filter (Median)" was used to smoothen sample data excluding noise. "Data Restore" was used to fill in small areas of inappropriate pixels, which were different from the surrounding area (using the height data surrounding the drop-out area) (Method: Legacy, Iterations: 5, Restore Edge: On). "Terms Removal (F-Operator)" was used to remove surface tilt (Tilt Only; Plane Fit, Zero Mean). "Basic Stats" was used for processing image of dentine surface in 3D. "Gaussian Regression Filter (Robust)" was used to flatten the sample surface (Short Wavelength Cutoff; S-Filter: 0.08 mm). The negative volume statistic contains the volume above the sample surface and below the zero level, namely, pit volume. Total scanned Surface Area (approximately 16 mm²) was calculated and used to divide total pit volume for normalization.

To see individual osteoclast resorption activity, total area, total volume and total depth of 1 dentin slice were divided by the number of osteoclast.

3.10.13 Osteoclast differentiation with Okadaic acid

Okadaic acid (OKA) is a naturally occurring C38 polyether fatty acid toxin that was originally derived from a black sponge *Halichondria okadai*²⁶⁹. OKA is reversible, potent and selective inhibitor of two serine/threonine protein phosphatases PP2A-C (PP2A) and PP1. Due to different hydrophilic affinities to OKA, PP2A is inhibited completely at 1 nM while PP1 requires higher concentrations (IC₅₀= 10-15 nM) for a complete inhibition.

BMMs were cultured in complete alpha-MEM with 25 ng/ml M-CSF in 6 well-plate. After 24 hours, BMMs were pre-treated with 1 nM OKA for 30 min and stimulated with 100 ng/ml RANKL. Cells were collected for protein isolation 0, 5, 15 and 30 min after RANKL stimulation.

3.11 Biochemical methods

3.11.1 Staining of cell culture

3.11.1.1 TRAP staining

TRAP staining solution consists of two separate solutions and was prepared freshly immediately before staining using the following protocol.

TRAP staining solution:

TRAP solution A (0.1 M Sodium Acetate buffer, pH 5)	70 ml
TRAP solution B (0.6% Acetic Acid buffer)	30 ml
Sodium L-tartrate dibasic dehydrate	1.15 g
Naphthol AS-MX phosphate	5 mg
<i>N,N</i> - Dimethylformamide	500 µl
Fast Red Violet LB salt	30 mg

To prepare a working solution, 70 ml of TRAP solution A and 30 ml of TRAP solution B was mixed and 1.15 g sodium L-tartrate dibasic dehydrate was added in TRAP A+B solution. Naphthol AS-MX phosphate was dissolved with *N,N*-Dimethylformamide and added to TRAP A+B solution. Fast Red Violet LB salt was added to TRAP A+B solution and mixed well by vortex. Mixed solution was filtered through a filter paper with a funnel before used.

Cells were fixed with 3.7% Formaldehyde/PBS and rinsed twice with PBS. Cells were permeabilized with 0.1% Triton X-100 for 1 min and washed twice with PBS. Cells were completely covered with TRAP staining solution and incubated for 5-10 min at 37°C. During incubation, cells were observed carefully under optical microscope. Stained cells were washed 3 times with distilled water and air dried. Cells were imaged using an optical microscope BX50 (Olympus), and quantified osteoclast parameters such as osteoclast number, osteoclast size, the number of nuclei (unstained) using the OsteoMeasure™ system.

3.11.1.2 Alkaline Phosphatase (ALP) staining

ALP staining solution:

1 M Tris-HCl (pH 8.4)	5 ml
Distilled water	45 ml
Naphthol AS-MX phosphate	5 mg
<i>N,N</i> -Dimethylformamide	200 µl
Fast Blue RR salt	30 mg

Tris-HCl (1 M) was diluted 10 times with water. Naphthol AS-MX was dissolved with *N,N*-Dimethylformamide and added to Tris-HCl (0.1 M) solution. Fast Blue RR salt was added to the solution and mixed well by vortex. The solution was filtered through a filter paper with funnel before used. ALP staining solution was prepared freshly and used as soon as possible.

Cells were fixed with 3.7% Formaldehyde/PBS and rinsed twice with PBS. Cells were covered with ALP staining solution and incubated for 15 min in the dark at room temperature. Blue-stained cells were washed with distilled water and air dried. The plate was scanned using EPSON Perfection V700 PHOTO scanner for macro imaging. ALP staining was used for the indicator of osteoblast differentiation.

3.11.1.3 Alizarin Red staining

Alizarin Red S (2 g) was dissolved in distilled water (final 100 ml) and pH was adjusted to 4.2 with HCl. Alizarin Red staining solution was filtered through a filter paper with funnel before use. Cells were fixed with 3.7% Formaldehyde/PBS and rinsed twice with PBS. Cells were

covered by Alizarin Red staining solution and incubated for 20 min at room temperature. Red-stained cells were washed with distilled water to reduce the background of staining using a shaker and air dried. The stained cells in the plate were scanned by EPSON Perfection V700 PHOTO scanner for macro imaging. Alizarin Red staining was utilized for the indicator of osteoblast mineralization.

3.11.2 Immunocytochemistry

3.11.2.1 Actin staining

Cells were cultured on Falcon™ Chambered Cell Culture Slides. Before staining, cells were washed twice with PBS (pH 7.4) and fixed with 3.7% formaldehyde/PBS for 10 min at room temperature. Cells were incubated with 0.1% Triton X-100/PBS for 3-5 min and washed two or more times with PBS. The fixed cells were pre-incubated for 10 min with PBS containing 1% BSA. Actin staining solution was prepared by mixing 5 µl of Alexa Flour™ 488 Phalloidin solution with 200 µl of 1% BSA/PBS. Cells were stained for 20 min at room temperature. To avoid evaporation, slides were incubated inside a covered container during the incubation.

After staining, the plastic chamber was removed from culture slide. One drop of Fluoromount-G was dropped on each sample and the slide was covered by microscope cover glass. The slides were kept in the dark at 2-6 °C.

3.11.3 Flow cytometry

The expression of osteoclast precursor markers CD11b, RANK and c-fms in the BM was evaluated by flow cytometry. A total amount of 3×10^5 BM cells was used for each experimental condition. Cells were incubated for 30 min with the primary antibodies diluted as described in section 2.1.6, Table 2.8. After washing with ice cold 3% BSA/PBS, cells were incubated with a secondary antibody; Alexa Fluor 488 Goat anti-Rat IgG (Invitrogen, Thermo Fisher Scientific) for the detection of CD11b and Alexa Fluor 488 anti-Mouse IgG (Invitrogen,

Thermo Fisher Scientific) for the detection of RANK and c-fms. Cells were washed 3 times with ice cold 3% BSA/PBS. To determine the background fluorescence for each antibody, both unstained samples and immunoglobulin-matched isotype samples were included in each analysis. Samples were acquired immediately with fluorescence-activated cell sorting (FACS, BD Biosciences) and analyzed using FACSDiva software version 6.2 (BD Biosciences). Forward scatter area versus forward scatter-height properties were used to exclude cell aggregates and live cells were separated from dead cells. The cells were first gated for CD11b and then for c-fms and RANK expression and positive populations were calculated.

3.11.4 Protein extraction (Total cell lysate preparation)

Proteins were extracted using a low salt Radio-Immunoprecipitation Assay (RIPA) buffer.

Low salt RIPA buffer:

- 50 mM Tris base
- 150 mM NaCl
- 0.5% Nonidet P-40 (NP-40)
- 0.25% Sodium-Desoxycholate
- Adjust pH to 7.5 with HCl

Immediately before use, Roche Complete protease inhibitor (from 25x stock) and Roche Complete phosphatase inhibitor (from 10x stock) were added into the low salt RIPA buffer. Tubes and tools were kept on ice to prevent protein degradation. Cells grown in 6 well-plates were washed twice with PBS and harvested with 100 μ l low salt RIPA buffer on ice using a cell lifter. In case of cell suspension, cells were centrifuged at 10,000 rpm for 1 min in 1.5 ml Eppendorf tube, or at 900 rpm for 5 min in 15 or 50 ml tube, washed twice with PBS and lysed with low salt RIPA buffer. After 10 min incubation on ice, lysates were centrifuged at 14,000 rpm for 10 min. The supernatants (total cell lysates) were transferred to new Eppendorf tubes and kept at -80°C until use.

3.11.5 Nuclear/Cytoplasmic Fractionation

Buffer A:	Final	Stock	for 50 ml
	10 mM HEPES (pH7.6)	1 M (pH 7.6)	500 μ l
	1.5 mM MgCl ₂	1 M	75 μ l
	10 mM KCl	1 M	500 μ l
	0.1 mM EDTA	0.5 M	10 μ l
	Add Roche Complete Protease and Phosphatase Inhibitors.		

Buffer C:	Final	Stock	for 50 ml
	20 mM HEPES (pH 7.6)	1 M (pH 7.6)	1 ml
	25% Glycerol	100%	12.5 ml
	420 mM NaCl	5 M	4.2 ml
	1.5 mM MgCl ₂	1 M	75 μ l
	0.2 mM EDTA	0.5 M	20 μ l
	Add Roche Complete Protease and Phosphatase Inhibitors.		

Cells were washed twice with PBS and scraped off from the 15 cm culture plate with 400 μ l of buffer A. The cell suspension was incubated on ice for 15 min. One sixteenth volume of 10% NP-40 in water (25 μ l) was added to the tubes and mixed by vortex for exact 10 sec. After centrifuging at 13,000 rpm for 1 min at room temperature, the supernatant was kept as a cytosol fraction. The pellet was re-suspended in 200 μ l of buffer C (half volume of the buffer A), incubated on ice for 30 min and mixed briefly by vortex every 5 min. After centrifuging at 14,000 rpm for 5 min at 4°C, the supernatant was kept as a nuclear fraction. Purity of fractions was determined by western blot against Tubulin (only detectable in cytosolic fraction) and Lamin A/C (only detectable in nuclear fraction).

3.11.6 Measurement of protein concentration

To determine protein concentration, Bio-Rad (Bradford) Protein Assay -kit or Thermo Scientific™ Pierce™ BCA (bicinchoninic acid) Assay -kit was used. For the Bradford Protein Assay, bovine serum albumin (BSA) standards were prepared at 0, 0.18, 0.37, 0.55, 0.73, 0.91, 1.1 mg/ml. Following manufacturer's protocol, Protein Assay Dye Reagent Concentrate was diluted with water at a ratio of 1:5 and filtered. Ten μ l of the BSA standards and of each unknown sample was pipetted into a 96 well-plate as triplicate and duplicate, respectively.

Diluted dye reagent (200 µl) was added to each well and the plate was mixed thoroughly on a shaker for 30 seconds. The 96 well-plate was covered and incubated at room temperature for 5 minutes. Absorbance was measured at 595 nm (near 562 nm) using a VICTOR™ X5 (Perkin Elmer).

For the BCA Assay, BSA standards were prepared at 0, 25, 125, 250, 500, 750, 1000, 1500, 2000 µg/ml. Following manufacturer's protocol, working reagent was prepared by mixing 50 parts of BCA Reagent A with 1 part of BCA Reagent B and filtered. Ten µl of BSA standards and each unknown sample was pipetted into a 96 well-plate. BCA reagent was added to each well and mixed thoroughly on a plate shaker for 30 seconds. The 96 well-plate was covered and incubated at 37°C for 30 minutes. Absorbance was measured at 595 nm (near 562 nm) using a VICTOR™ X5 (Perkin Elmer).

3.11.7 Sodium Dodecyl Sulfate (SDS)- Poly-Acrylamide Gel Electrophoresis (PAGE)

SDS-PAGE was used to separate proteins by their molecular mass.

Reagents:

- Separation gel buffer: 1.5 M Tris/HCl pH 8.8 (45.43 g Tris Base for 250 ml)
- Stacking gel buffer: 0.5 M Tris/HCl pH 6.8 (15.14 g Tris Base for 250 ml)
- 10% SDS solution in water
- 10% ammonium persulfate (APS) solution in water
- Acrylamide/Bisacrylamide (Rotiphorese Gel 30, 30% Acrylamid/Bisacrylamide 37.5:1)
- Tetramethylethylenediamine (TEMED)

Preparation of gels for two small gels:

Separation gel (12%):

Water	3.5 ml
Separation gel buffer	2.5 ml
10% SDS solution	100 µl
30% Acrylamide/Bisacrylamide	4 ml
TEMED	5 µl
10% APS solution	50 µl

Stacking gel (4%):

Water	3 ml
Stacking gel buffer	1.25 ml
10% SDS solution	50 µl
30% Acrylamide/Bisacrylamide	650 µl

TEMED	5 μ l
10% APS solution	25 μ l

10x electrode (running) buffer, pH 8.3 (makes 1 L):

Tris base	30.3 g
Glycine	144.0 g
SDS	10.0 g
Dilute 1:10 before use	

Before use, glass plates were soaked in cleaning solution (diluted of 50x Cleaning Concentrate, Bio-Rad, Cat. #161-0722) overnight. The glass plates were washed well with water, rinsed with dH₂O and dried.

After separation gel solution was mixed, the solution was poured into the gel chambers, overlaid carefully with water and let to polymerize for approximately 20 min before the stacking gel solution was poured. SDS-PAGE samples were prepared by adding 4x sample buffer supplemented with 10% β -mercaptoethanol and boiled for 5 min at 95°C. Gels were run at a constant voltage of a range 100-200 V.

3.11.8 Transferring

Reagents:

10x Transfer buffer:

Tris base	30.3 g
Glycine	144.0 g
dH ₂ O	up to 1 L

1x Transfer buffer (20% Methanol):

10x Transfer buffer	200 ml
Methanol	400 ml
dH ₂ O	up to 2 L
Store at 4°C.	

Filter paper, nitrocellulose membrane and Poly-Vinylidene Di-Fluoride (PVDF) membrane were cut in approximately 9 cm x 7.5 cm pieces. PVDF membrane was soaked in absolute Methanol for 5 min prior use. Blotting pads, filter papers and transfer membranes were soaked well in 1x transfer buffer. SDS-PAGE gel and transfer membrane were bond by filter papers,

and further bond by 2 of blotting pads as shown in the figure below. Transferring was performed in the cold room (4°C) at 15 V overnight using the XCell II™ Blot Module (Invitrogen).

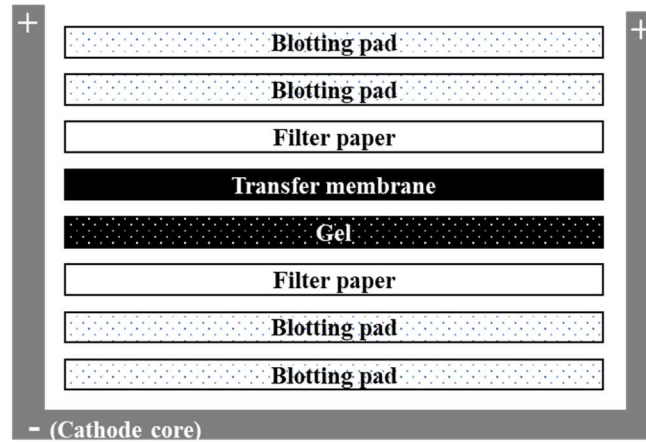


Fig. 3.2. Transferring membrane in order. Electricity flows + to -. Negative-charged proteins in the gel run from - to +, thereby put a transfer membrane on top of the gel. A gel and a transfer membrane are enclosed with a filter paper and further 2 blotting pads on the both side. Modified from the XCell II™ Blot Module (Invitrogen) User Manual, page 12, Transferring One Gel.

3.11.9 Immunoblotting

Reagents:

10x Tris-buffered saline (TBS):

Tris base	12.0 g
NaCl	87.6 g
dH ₂ O	up to 1 L

1x TBS with Tween 20 (TBS-T):

10x TBS	200 ml
dH ₂ O	1798 ml
Tween 20	2 ml

After transferring, the membranes were incubated in Ponceau S Red staining solution for 1 min on a shaker and washed with water to observe the transferred proteins on the membrane. If the membrane was used for the blotting against several antibodies, the membrane was cut using a scalpel according to the protein size. Membranes were soaked in 5% milk/TBS-T or 5% BSA/TBS-T for 30 min to block non-specific binding. The membrane was incubated with a primary antibody diluted in the blocking solution as described in section 2.1.6, Table 2.8 Primary antibodies. The membranes were washed 3 times with TBS-T for 10 min and incubated with secondary antibodies in 5% milk/TBS-T for 2 hours at room temperature (RT) with a

dilution described in section 2.1.6, Table 2.9 Secondary antibodies. The membranes were washed 3 times with TBS-T for 10 min and developed using Clarity™ Western ECL Substrate (Bio-Rad) or SuperSignal® West Femto Maximum Sensitivity Substrate (Thermo Fisher Scientific). The membrane was imaged using the ChemiDoc™ MP Imaging System (Bio-Rad) and Image Lab™ 4.1 (Bio-Rad) software.

3.11.10 Mild retrieving of western blot membrane

Mild re-probing buffer (1 L):

Glycine	15 g
SDS	1 g
Tween20	10 ml
dH ₂ O	up to 1 L
Adjust pH to 2.2	

To remove the primary and secondary antibodies from the membrane for re-probing the membrane with another antibody of interest, membranes were incubated twice with a mild stripping buffer for 5-10 min. Next, the membranes were incubated twice with PBS for 10 min and twice with TBS-T for 5 min. Afterwards, the membranes were processed for blocking.

3.12 Molecular biology methods

3.12.1 Alkaline digestion for the isolation of genomic DNA

Alkaline digestion solution A (25 mM NaOH, 0.2 mM EDTA, pH 12), 100 ml

1M NaOH	2.5 ml
0.5 M EDTA	40 µl
dH ₂ O	97.46 ml

Alkaline digestion solution B (40 mM Tris-HCl, pH 5), 100 ml

Tris-HCl	0.63 g
dH ₂ O	up tp 100 ml

*test solution A+B (1:1) should be at pH 8.

Tip of tails from mouse pups were digested in 50 µl of solution A at 95°C in a heat block for 2 hours. During the digestion, tubes were shaken down once by hand. After the tails were

digested, 50 µl of alkaline digestion solution B (equal volume of solution A) was added to neutralize alkaline condition and stop digestion. Sample tubes were mixed well by vortex, centrifuged shortly and kept at 4°C. Solution volume was adjusted depending on the sample size.

3.12.2 Genotyping

3.12.2.1 Preparation

50x Tris base/Acetate/EDTA (TAE) buffer (2 M Tris, 1 M Acetate, 50 mM EDTA), 1 L

Tris base	242 g
Acetic acid	57.1 ml
EDTA solution (0.5 M, pH 8.0)	100 ml
dH ₂ O	up to 1 L

1x TAE buffer (40 mM Tris, 20 mM Acetate, 1 mM EDTA, pH app. 8.6), 1 L

50x TAE buffer	200 ml
dH ₂ O	9800 ml

2% 1x TAE agarose gel, 100 ml

1x TAE buffer	100 ml
LE Agarose	2 g
Ethidium bromide drop (0.025%)	1 drop

LE agarose and 1x TAE buffer were mixed and boiled up by a microwave. One drop of Ethidium bromide (0.025%) was added and mixed before the mixture started to solidify. The mixture was cooled down (app. 65°C) and poured into a mold (a making-gel chamber). Immediately, a comb was inserted into the mold. The gel was solidified at room temperature. The comb was removed from the gel as wells remain. After making the gel, the gel was replaced into an electrophoresis chamber and 1x TAE buffer was added to cover the gel. The wells were orientated at the negative electrode end.

3.12.2.2 Tgif1 genotyping

Per reaction:

dH ₂ O up to 25 µl	15.19-17.19 µl
10x Dream Green Mix	2.5 µl
Primer Tgif 1f-new, 10 µM	1.25 µl
Primer Tgif 1r, 10 µM	0.44 µl
Primer Tgif 2r, 10µM	0.82 µl
dNTPs, 10 mM each	0.5 µl
DreamTaq, 5 U/µl	0.3 µl
Genomic DNA solution	1.0-3.0 µl

Cycling program:

94°C	5 min	
94°C	30 sec	
56.5°C	1 min	x 35 cycles
72°C	1 min	
72°C	10 min	
12°C	Hold	

PCR products were separated on a 2% 1x TAE agarose gel (Fig. 3.3).

Expected amplicons:

- Wild type (+): 356 bp
- LoxP (p): 418 bp
- Tgif (-): 557 bp

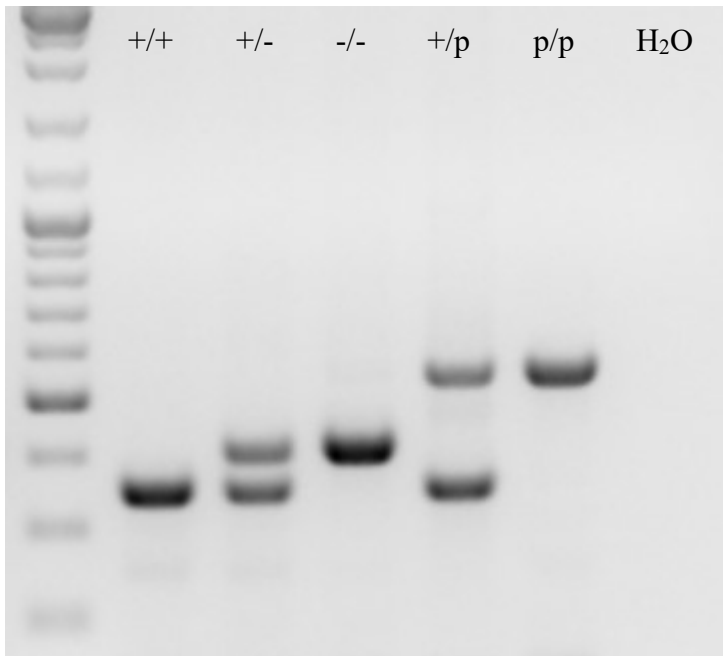


Fig. 3.3. Agarose gel electrophoresis for Tgif1 genotyping. The PCR products were electrophoresed on a 2% agarose gel by 150 V. From left to right, lane 1; DNA ladder marker, lane 2; +/+; Tgif1^{+/+}, lane 3; +/-; Tgif1^{+/-}, lane 4; -/-; Tgif1^{-/-}, lane 5; +/p; Tgif1^{+/loxP}, lane 6; p/p; Tgif1^{loxP/loxP}, lane 7; H₂O as a negative control.

3.12.2.3 Ctsk-Cre genotyping

Per reaction:

dH ₂ O up to 25 µl	13.7 µl
10x Dream Green Mix	2.5 µl
Primer Ctsk P1N, 10 µM	1.25 µl
Primer Ctsk P2N, 10 µM	1.25 µl
Primer Ctsk P3N, 10 µM	1.25 µl
dNTPs, 10 mM each	0.5 µl
DreamTaq, 5 U/µl	0.3 µl
Genomic DNA solution	3.0 µl

Cycling program:

95°C	3 min	
95°C	45 sec	x 40 cycles
58°C	45 sec	
72°C	1 min	
72°C	10 min	
12°C	Hold	

PCR products were separated on a 2% 1x TAE agarose gel (Fig. 3.4).

Expected amplicons:

Wild type (Cre⁻): 600 bp
 Knock-in (Cre⁺): 427 bp + (600 bp)

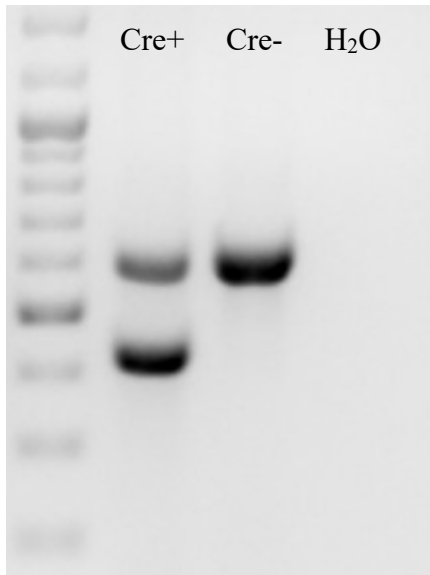


Fig. 3.4. Agarose gel electrophoresis for Ctsk-Cre genotyping. The PCR products were electrophoresed on a 2% agarose gel by 150 V. From left to right, lane 1; DNA ladder marker, lane 2; Cre⁺; Ctsk-Cre⁺, lane 3; Cre⁻; Ctsk-Cre⁻, lane 4; H₂O as a negative control.

3.12.2.4 LysM-Cre genotyping

Per reaction:

dH ₂ O up to 25 µl	13.7-15.7 µl
10x DreamTaq buffer with loading dye	2.5 µl
DMSO	0.5 µl
Primer Cre-Cf, 10 µM	1.25 µl

Primer Cre-Cr, 10 μ M	1.25 μ l
Primer Cre-Cref, 10 μ M	1.25 μ l
Primer Cre-Crer, 10 μ M	1.25 μ l
dNTPs, 10 mM each	0.5 μ l
DreamTaq, 5 U/ μ l	0.3 μ l
Genomic DNA solution	1.0-3.0 μ l

Cycling program:

94°C	3 min	
94°C	30 sec	x 35 cycles
62°C	30 sec	
72°C	1 min	
72°C	7 min	
12°C	Hold	

PCR products were separated on a 2% 1x TAE agarose gel (Fig. 3.5).

Expected amplicons:

- Wild type (Cre-): 420 bp
- Knock-in (Cre+): 281 bp (+ 420 bp)



Fig. 3.5. Agarose gel electrophoresis for LysM genotyping. The PCR products were electrophoresed on a 2% agarose gel by 150 V. From left to right, lane 1; DNA Ladder marker, lane 2; Cre+; LysM-Cre⁺, lane 3; Cre-; LysM-Cre⁻, lane 4; H₂O as a negative control.

3.12.3 RNA extraction

RNA was extracted from BMMs and osteoclasts using the RNeasy kit (QIAGEN) according to manufacturer's instructions. The RNA quality and quantity were measured by NanoDrop and the RNA was stored at -80°C.

3.12.4 Synthesis of complementary DNA (cDNA)

Complementary DNA was synthesized from maximum of 1 μg of RNA using the High-Capacity cDNA reverse transcription kit according to manufacturer's instructions.

Per reaction:

10x RT-Buffer	2 μl
25x dNTP-Mix (100 mM)	0.8 μl
10x RT random primers	2 μl
MultiScribe™ reverse transcriptase	1 μl
RNA	1 μg
Nuclease-free water (20 μl final volume)	x μl

Program:

25°C	10 min
37°C	120 min
85°C	5 min

3.12.5 Quantitative real-time polymerase chain reaction (qRT-PCR)

Complementary DNA acquired from 1 μg RNA was diluted 20 times with dH₂O. Three μl of the diluted cDNA was used for one reaction of qRT-PCR. For one reaction, the following components were mixed:

dH ₂ O	3 μl	
Forward Primer	0.75 μl	Master Mix
Reverse Primer	0.75 μl	
SYBR® Select Master Mix for CFX	7.5 μl	
cDNA	3 μl	
total	15 $\mu\text{l}/\text{tube}$	

Quantitative RT-PCR was performed using the following protocol: an initial step of 2 min at 50°C and 10 min at 95°C followed by 40 cycles of 15 seconds at 95°C and 1 min at 60°C. Glyceraldehyde-3-phosphate dehydrogenase (Gapdh) or TATA-binding protein (Tbp) was used as endogenous controls. Gene expression levels were quantified using the comparative threshold cycle (Ct) method. First, the amount of target mRNA in each sample was normalized to the amount of the housekeeping mRNA (Gapdh or Tbp), designated as a calibrator, to give ΔCt (Ct target - Ct Gapdh or Tbp). Second, the amounts of target mRNA in the samples were expressed using the formula: Amount of target mRNA = $2^{-\Delta\Delta\text{Ct}}$, where $\Delta\Delta\text{Ct} = \Delta\text{Ct}(\text{sample1})$

- Δ Ct (untreated sample). Technical duplicates were performed for each experimental point and experiments were repeated several times with cells obtained from different mice.

3.12.6 Inhibition of mRNA function by GapmeR

GapmeR are antisense oligonucleotides that have several properties to allow silencing of targeted RNA stably, specifically and efficiently. First advantage is the structure of Locked Nucleic Acid (LNATM). The ribose ring is connected by a methylene bridge between the 2'-O and 4'-C atoms thus "locking" the ribose ring in the 3'-endo (North) conformation, ideal for Watson-Crick base-pairing. When incorporated into DNA oligonucleotide, LNATM leads to a dramatic increase in affinity (melting temperature) for complementary RNA targets, without loss of sequence specificity. The higher binding affinity of LNATM results in exceptionally potent antisense oligonucleotides. Second advantage is the structure of the phosphorothioate (PS) bond. The non-bridging oxygen atom of oligonucleotide's phosphodiester backbone is replaced with a sulphur atom. This modification renders the nucleotide bond highly resistant to nucleases. The third benefit is the unique short single-stranded design of GapmeR. Antisense LNATM GapmeRs contain a central DNA part flanked by LNATM. The LNATM parts increase the affinity for the target RNA and confer nuclease resistance. RNase H1 is activated by the DNA part of the antisense oligonucleotide, resulting in endonucleolytic cleavage of the target RNA.

RNase H is a ubiquitous enzyme found both in the nucleus and the cytoplasm of all cells. RNase H specifically recognizes the A form of the RNA strand and the B form of the DNA strand. The enzyme hydrolyzes the RNA of the RNA-DNA heteroduplexes formed after sequence-specific binding of antisense oligonucleotides to their target mRNA or long non-coding RNA (lncRNA). Therefore, targeted RNA will be degraded in the nucleus and the cytoplasm and not be translated into the corresponding proteins, leading to a reduced abundance of the target protein.

The advantage of GapmeR is the feasibility to silence RNA in cells that are difficult to transfect using conventional methods (Lipofectamine® and PromoFectin), such as primary osteoclasts and primary T lymphocytes. GapmeR can be applied (/transfected) to osteoclasts and other cells without any transfection reagents via “Gymnosis”.

Lipofectamine® reagent contains lipid subunits that can form cationic liposomes which complexes with negatively charged nucleic acid molecules to allow them to overcome the electrostatic repulsion of the cell membrane. Comparing to endocytotic Lipofectamine® transfection, gymnotic application of GapmeR is taken up by the cells by macropinocytosis²⁷⁰, resulting in less cytotoxicity.

3.12.7 *In silico* analysis

Tgif binding sites were searched in the promoter region of the PP2A-C β gene (Ppp2cb) using the online program PROMO 3.0 (http://alggen.lsi.upc.es/cgi-bin/promo_v3/promo/promoinit.cgi?dirDB=TF_8.3) which is designed to study transcription factor binding sites in DNA sequences.

Select Species:

Considering factors: All factors

Considering sites: All sites

Select Factors:

TGIF [T04076]

Search Promoter Sites:

Ppp2cb

```
GCCGTCAGGACAGCAGAGGATGCTATGCTAATGACTTATACAGGGCCCAGTTTCCCCGGAAC
CTACTGATGCTCAGTTCTTGGGGATGCTTTCCCTTTCCTAACAGACTATAACTTCTTCCCTG
ACCTCTGAACATTCTTTTTTCTACTCTCTACTCCTCGCACCTTGTAGCTCCACTATGGAACAT
GCCTGCTTTCTGAGGCCTTACCTCAAAGGTGTGATTTCTCTCTTCTTCTTCTTCTTCTTCTCC
CTCTTGGTCAAATTTGCCAAGATCTGCAGCCCTGCCTGTTGTTCTCTTAAACTCTGACAAAC
GGGTCCTTGAGCTTTCCTTCTATTTACCAAAGCTTTTCGTTAATAAGACAGAGAACGCCTCAA
GGGAATCCTGAGTTCCCCAGGCATAGCCACACTTCACAGAGAAGGCATTTAGATGTGGAGGG
GCATGCTGCTAACCTCAGCAACTCACAAAGCTGAGGCAAGACACTGCAGGTACCAGTGCAGC
TTGTGGCACACAGTGAAAACTGCCTCGGGGTGGCAAGTGTGGGGGACCAAATTCCTGCCTCC
TCTATAGCACTACTTAGTAAACACTTTAGTCTCTCTTACTTACTGCCGATATTCCTCATA
ACTTATAAAGTCAGCTCCCAACCCTTGCACTGTAGTAGTGTGCTGTACCACTGGGCAGCTG
```

CTTTTCCCCTCCATCGTTGAGAGAGGTGTGGTAGGTAGCAGTGCCTGTAATCCCAGAATTT
GGAAAGTGGAGACAGGAGGATTAGGAGTTCAAGGTCATCCTCAACTCCAGAGCAGGGAGCCA
GCCTGGAATAAAAAGAAACCTTGTCTTAAAATAAACAAGGTCTGCAGAGATGGCTGGGGGGCA
GCGTACTTTGCCTACAAGCCTGAGTGTGATGCCAGAGCCCACCTAAAACCTGGAGATCATCT
ACTTCACAAAGTCCATGTACTCACACAACCTGACAAGATTTTGTGCTTACTTATTTCAACTAA
TGACAAATCTGCAGCTAGAGGCAGTTTGGGGATTGCTTCAAGCTGAGAAATTGACAAAACCA
ACTCAGGAACCATGACGCTGTTGAGCACTTGCGAACAGCAGAAGCAGCCGTACATGTTTCAG
ACCCAGGAAATAGGGTCTGTGAGCACAGCTTTAAAGGTCTCGGTATCTAGCCCCCTGTTATAT
AAAGATCACTAATTACAGCCAAGGCATCATAGTAGTCACAACAAAGAATGATAAGATGGAAT
GGCCACAGAAAAATTTAAAAATCATTTTCATGGTTTAAAGAGATTAGCTGAGGTTAGGATAAA
CACAGCTTGGTGGTAGTGGTGCACACCTTTAACCCAGCAGTTGGGAGGCAGAGGCAAGTGG
ATCTCTGAGTTCGAAGTCAGCCTGGTCAACAGAATGAGTTCCAGGACAGCCAAGGCTACACT
GAGAAACCCTGTGTTGAAAAAACCAAGAGAAGAAGAAAGAAGAAAGAAGGAAGAGGGGG
AAGGAGAGGGGGAGGGGGGGGGGGAGGAGGAGGAGGAGGAGGAGGAGGAGGAGGAGGAGGAG
GAGGAGGAGGAGAAGAAGAAGAAGAAGAAGAAGAAGAAGAAGAAGAAGAAGAAGAAGAAGA
GAAGA
AGAAAGAAAGAAGAATGAAGAATGTGTGCTACTCTTACAGATGCCCTAAATTTGGTTTCTA
GCACCATATACCACCAACTCCAGCTCCTGGAGAGCCAATACTCTCTTCTGTCCTCCCAAGGC
ACCTGTACACACGTGACATAAACGTAAATACATCCTTTGTTAAAAGTTATCTTTCTGATATA
GACAGAAAGGGTCTGAGATTCAAGGCTACGCAATGAATTACTGCTAAGAGTAGAAATTTACT
CAATAAATATTTAGTGCATGCTCTAGGGTAGTGAAAGGTTGAGGGAAAAGCCCAACAGTCTC
AATGCCCTGTGCGGAGAGAGGTCCAAGGCGAGAACCGGATTCCCCAAGGGCAGAGTGGGCAG
GAGGACCGGGGAAGGATGCAAGGGGACCGTTTCTCCGCCGGCCGCGCGAGGGCGCTGCTC
CCCTCCTCGTGCGCCGGGCCCGGCGGCGCCGCCCCTCGCCTTTTCCCGGCGGAAATGCCCG
GGCGATGACGGAACCCGGAGGGAGGGAAGA

3.13 *In vivo* analysis

3.13.1 *In vivo* sample collection

Seven days and two days before sacrificing mice, Calcein (4 mg/ml) and Demeclocycline (4 mg/ml) were injected into mice (10 µl/g body weight) intraperitoneally (i.p.), respectively. Before sacrifice, mice were anesthetized by injecting Ketamine (120 mg/kg) and Rompun® (xylazine base equivalent) (16 mg/kg). Mice were sacrificed using cervical dislocation and the lower extremities and vertebrae were collected in tubes with 3.7% formaldehyde/PBS.

3.13.2 Dehydration of bone samples

Fixed bones were replaced into histology embedding cassette labeled sample number by a pencil. The cassettes were replaced into the basket of a tissue processor (BAVIMED) and bones were processed through the program described below.

Program:

70% Ethanol	1 h	x2
80% Ethanol	1 h	x2
96% Ethanol	1 h	x3
Abs. Ethanol	1 h	x5

3.13.3 Infiltration of bone samples

Methyl methacrylate (MMA) solution was destabilized via aluminum oxide 60 (active basic 0.063-0.200 mm) before use.

Infiltration solution (I, II):

MMA solution	900 ml
Benzoyl peroxide (BPO), dried	3.3 g
Nonylphenyl-polyethyleneglycol acetate	100 ml

Bone samples were processed in the infiltration solution 2 times (I and II) for over 24 hours at 4°C.

3.13.4 MMA embedding

Embedding solution:

MMA solution	900 ml
Benzoyl peroxide (BPO), dried	6.6 g
Nonylphenyl-polyethyleneglycol acetate	100 ml

Active embedding solution:

Embedding solution	200 ml
<i>N,N</i> -dimethyl- <i>p</i> -toluidine (starter)	500 µl

After the starter was added in the embedding solution, the solution started polymerization. The solution was poured into the glass vials and bone samples were orientated in the vials as desired.

The vials were replaced in a water bath at 4°C and polymerized overnight.

3.13.5 Staining of tissue sections

MMA-embedded bone sections were processed through several treatments including deplastination, dehydration, staining, hydration and mounting.

3.13.5.1 von Kossa/van Giesson staining

Solutions:

3% Silver nitrate solution

Materials and Methods

Silver nitrate	3g
dH ₂ O	100 ml
Soda formal solution	
Sodium carbonate	12.5 g
dH ₂ O	187 ml
37% Formardehyde	62.5 ml
5% Sodium thiosulfate solution	
Sodium thiosulfate	5 g
dH ₂ O	100 ml
van Gieson-stain mixture	
Acid Fuchsin	2.5 g
Picric acid, saturated	900 ml
Glycerol	100 ml
Nitric acid, concentrated	5 ml

Process:

2-Methoxyethyl acetate	5-10 min	x3
Abs. Ethanol	2-5 min	x2
96% Ethanol	2-5 min	
80% Ethanol	2-5 min	
70% Ethanol	2-5 min	
50% Ethanol	2-5 min	
dH ₂ O	dip 3-5 times	x2
3% Silver nitrate solution	5 min	
dH ₂ O	5 min	x2
Soda formol solution	5 min	
Running tap water	10 min	
dH ₂ O	rinse	
5% Sodium thiosulfate solution	5 min	
Running tap water	10 min	
dH ₂ O	rinse	
van Gieson-stain mixture	20 min	
Tap water	dip	
80% Ethanol	dip	
96% Ethanol	dip	
Abs. Ethanol	2-5 min	x2
Xylol	5 min	x3
DPX	cover	

Mineralized bones were turned into black, collagen and collective tissue were stained with red, and muscles and erythrocytes were stained with yellow. Von Kossa/van Giesson staining was utilized for measuring structural parameters such as bone volume/total volume, trabecular number, trabecular separation and trabecular thickness in histomorphometry.

3.13.5.2 Toluidine blue staining

Solutions:

1% Toluidine blue solution		
Toluidine blue O	1 g	
dH ₂ O	100 ml	
adjust pH 4.5		

Process:

2-Methoxyethyl acetate	5-10 min	x3
Abs. Ethanol	2-5 min	x2
96% Ethanol	2-5 min	
80% Ethanol	2-5 min	
70% Ethanol	2-5 min	
50% Ethanol	2-5 min	
dH ₂ O	dip	x3-5
1% Toluidine blue solution (pH 4.5)	30 min	
dH ₂ O	rinse	
50% Ethanol	rinse	
70% Ethanol	2 min	
80% Ethanol	2 min	
96% Ethanol	2 min	
Abs. Ethanol	5 min	
Abs. Ethanol	rinse	
Xylol	5 min	x3
DPX	cover	

Toluidine blue staining was employed for measuring cellular parameters including osteoclasts and osteoblasts in histomorphometry. Osteoclasts were stained with turquoise color, osteoblasts were stained with blue, nuclei were stained with dark blue. Mineralized bones were stained with light blue and cartilage was stained with violet.

3.13.5.3 TRAP staining

TRAP staining solution for tissue sections was made as same as that for cell culture staining.

TRAP staining solution:

TRAP solution A (0.1 M Sodium Acetate buffer, pH 5)	70 ml
TRAP solution B (0.6% Acetic Acid buffer)	30 ml
Sodium L-tartrate dibasic dehydrate	1.15 g
Naphthol AS-MX phosphate	5 mg
<i>N,N</i> - Dimethylformamide	500 μ l
Fast Red Violet LB salt	30 mg

To prepare a working solution, 70 ml of TRAP solution A and 30 ml of TRAP solution B was mixed and 1.15 g sodium L-tartrate dibasic dehydrate was added in TRAP A+B solution.

Naphthol AS-MX phosphate was dissolved with *N,N*-Dimethylformamide and added to TRAP A+B solution. Fast Red Violet LB salt was added to TRAP A+B solution and mixed well by vortex. Mixed solution was filtered through a filter paper with a funnel before used.

Process:

2-Methoxyethyl acetate	5-10 min	x3
Abs. Ethanol	2-5 min	x2
96% Ethanol	2-5 min	
80% Ethanol	2-5 min	
70% Ethanol	2-5 min	
50% Ethanol	2-5 min	
dH ₂ O	rinse	
TRAP staining solution	1-2 h, 37°C, shaking	
dH ₂ O	dip	
Aqua-Poly/Mount®	cover	

If counter stain was required after TRAP staining, it was continued below.

0.1% light green (counter stain)	1-5 min
dH ₂ O	rinse
Air	dry
Permout	cover

Sections were imaged using an optical microscope BX50 (Olympus) and quantified using the OsteoMeasure™ system for measuring osteoclast parameters in histomorphometry.

3.13.6 Histomorphometry

MMA-embedded bones were cut into 4 µm sections by a microtome, which were stained with von Kossa/van Giesson, Toluidine blue or TRAP staining. Histomorphometric analyses were performed according to ASBMR standards^{271,272} using the OsteoMeasure™ system.

3.13.7 Micro-computed tomography (µCT) scan

3.13.7.1 *In vivo* scan

Mice were anaesthetized by an inhalation of 2.5% isoflurane and placed on the *in-vivo*-sample-holder connecting narcotic supply. Mice were straightened and the tibia was fixed in the sample-holder. The sample-holder was inserted in the µCT device (VivaCT 80, SCANCO).

After performing a scout view, reference line was adjusted for the bone area to be scanned. Scanning protocol was 70 kV, HR (high resolution), 200 m/s.

3.13.7.2 *Ex vivo* scan

Plastic embedded tibia samples were used for *ex vivo* scanning. Maximum 5 samples were scanned in one *ex vivo* scan. Samples were fixed on *ex-vivo*-sample-holder to ensure that no movements occur during the scan. Sample holder was inserted in the μ CT device. After performing a Scout view, multiple reference lines were adjusted for each bone area of interest to be scanned. Scan protocol was 70 kV, HR (high resolution), 400 m/s.

3.13.8 μ CT analysis

μ CT analysis was performed using the VivaCT 80 scanner with a threshold of 326 mgHA/ccm. Trabecular bone area of interest was contoured counter-clockwise to manually distinguish trabecular bone from the cortical bone. Below the growth plate of the proximal tibiae, 121 slices of the region of interest (ROI) were analyzed using Morphometry and Density Measurements and Visualization in 2D and 3D. Tomographic image reconstruction was automatically conducted.

3.14 Ethics

Animal study was carried out in strict accordance with the guidelines and recommendations in the Federation of European Laboratory Animal Science Associations (FELASA). The protocol was approved by the Animal Studies Committee of the local authority (Behörde für Gesundheit und Verbraucherschutz (BGV); Protocol number: G15-105). All experimentalists involved in this study either have been permitted by the Hamburg local authority to be responsible for animal experiments and/or have finished the education and training of Category B course in FELASA.

3.15 Statistics

Statistical analysis was performed by means of the statistical package Prism version 5.00, (GraphPad Software, San Diego, CA, USA). Statistically significant differences were determined using a two-tailed student's t-test for unpaired samples with equal variances or the nonparametric ANOVA test.

Independent experiments were completed and reproduced for minimum three times. Within one experiment biological and technical duplicates were conducted, if not otherwise specified. Images or graphs from representative replicates are shown. Error bars indicate \pm standard deviation. Significance level was * $p < 0.05$, ** $p < 0.01$ or *** $p < 0.001$.

4 Results

4.1 RANKL and M-CSF stimulation increases Tgif1 expression in osteoclasts

A previous study from our laboratory has demonstrated that mice carrying a germline deletion of *Tgif1* display a low bone turnover phenotype with a significant reduction of osteoblast-mediated anabolic activity as well as osteoclast-mediated resorptive activity (manuscript under review)²⁶⁵. The goal of this thesis project was to determine whether the decreased osteoclast activity in *Tgif1*^{-/-} mice is cell autonomous. To determine the expression of *Tgif1* in osteoclasts, bone marrow macrophages (BMMs) were isolated from wild type (WT) mice and stimulated with osteoclast-promoting cytokines, RANKL and M-CSF. Interestingly, *Tgif1* expression was up-regulated during osteoclast differentiation stimulated by RANKL (100 ng/ml) or M-CSF (25 ng/ml) (Fig. 4.1.A). Since RANKL and M-CSF stimulation are essential for osteoclastogenesis²⁷³, regulation of *Tgif1* expression in BMMs was further evaluated after short term stimulation with RANKL or M-CSF. For this purpose, BMMs were expanded with M-CSF (100 ng/ml), re-plated with M-CSF (25 ng/ml) and allowed to adhere for 9 hours. BMMs were treated with RANKL and cell lysates were collected 0, 0.5, 2, 4, 8, 12, 24 hours after stimulation. Western blot analysis revealed that *Tgif1* expression in BMMs is gradually increasing for 24 hours after RANKL stimulation, resembling the expression pattern of the osteoclast-related transcription factor NFATc1 (Fig. 4.1.B). To determine *Tgif1* expression in BMMs after M-CSF stimulation, confluent BMMs were cultured without serum for 4 hours. BMMs were stimulated with M-CSF and cell lysates were collected 0, 0.5, 2, 4 hours after stimulation. Western blot analysis showed an increased expression of *Tgif1* in BMMs between 30 min and 4 hours of M-CSF stimulation (Fig. 4.1.C). Furthermore, *Tgif1* mRNA expression has a tendency to increase in BMMs 30 minutes stimulated by both RANKL and M-CSF (Fig. 4.1.D, 4.1.E). These results suggest that *Tgif1* has a role downstream of RANKL and M-CSF signaling in BMMs, implicating that *Tgif1* might play a role in osteoclast differentiation.

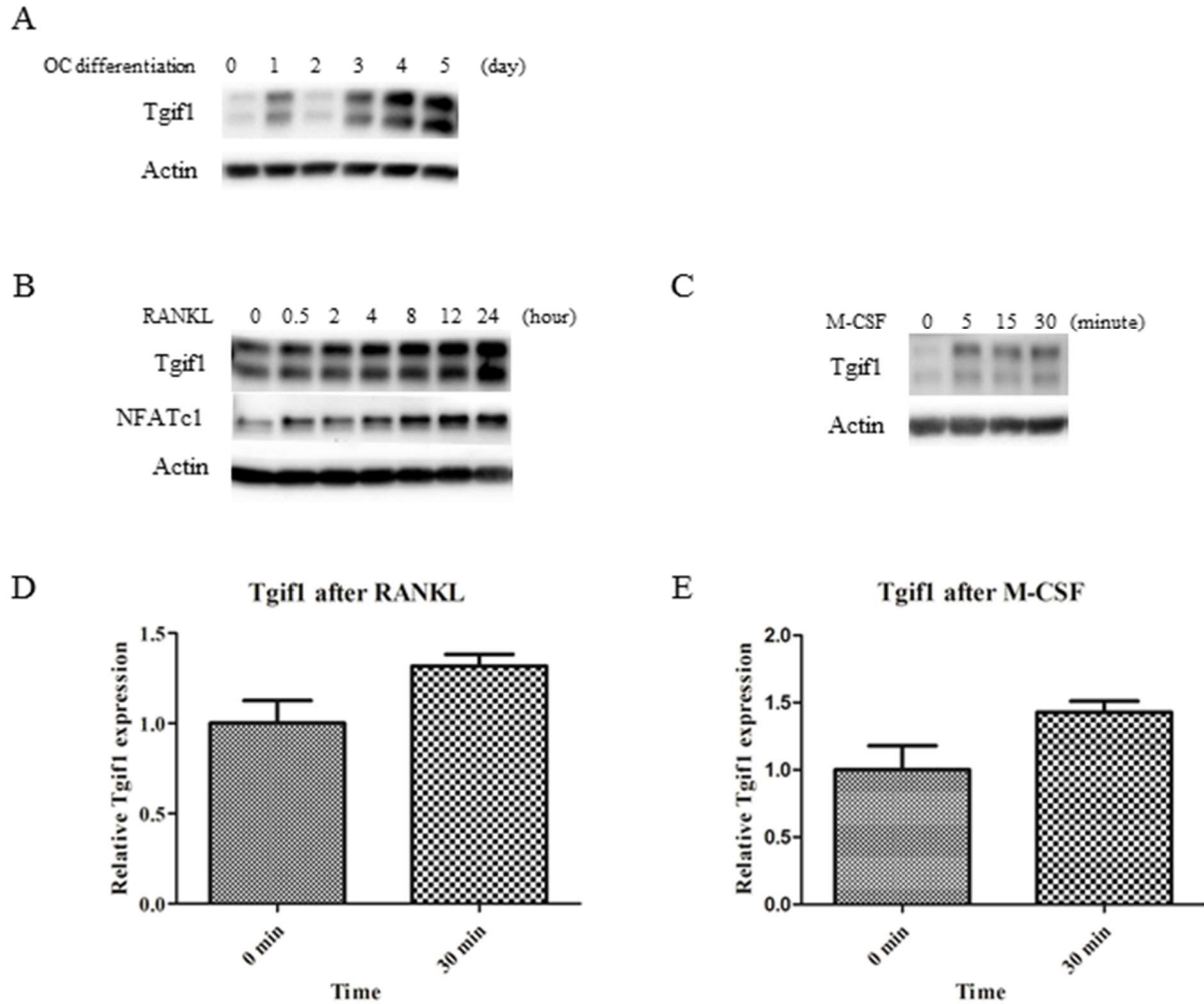


Fig. 4.1. Tgif1 expression increases in osteoclasts during differentiation and in response to RANKL and M-CSF stimulation. (A) Western blot analysis of Tgif1 expression during osteoclast (OC) differentiation stimulated by M-CSF (25 ng/ml) and RANKL (100 ng/ml). (B) Western blot analysis of Tgif1 and NFATc1 expression in BMMs 0, 0.5, 2, 4, 8, 12, 24 hours after stimulation with RANKL. (C) Western blot analysis of Tgif1 expression in BMMs 0, 5, 15 and 30 minutes after stimulation by M-CSF. n=2. (D) qRT-PCR analysis of Tgif1 expression in BMMs 30 mins after stimulation by RANKL. n=2, duplicate. (E) qRT-PCR analysis of Tgif1 expression in BMMs 30 mins after stimulation by M-CSF. n=2, duplicate.

4.2 Osteoclast-targeted deletion of Tgif1

To examine the function of Tgif1 in osteoclasts *in vivo*, we generated osteoclast-targeted Tgif1 conditional knockout mice, in which the Tgif1 gene was specifically deleted in cells of the myeloid cell lineage or the osteoclast lineage using the *Lyz2* (LysM) or *Ctsk* Cre-loxP system, respectively, and analyzed their skeletal phenotypes.

4.3 Analysis of LysM-Cre⁺;Tgifl^{loxP/loxP} mice

4.3.1 *In vitro* phenotype

4.3.1.1 Tgifl expression in osteoclasts

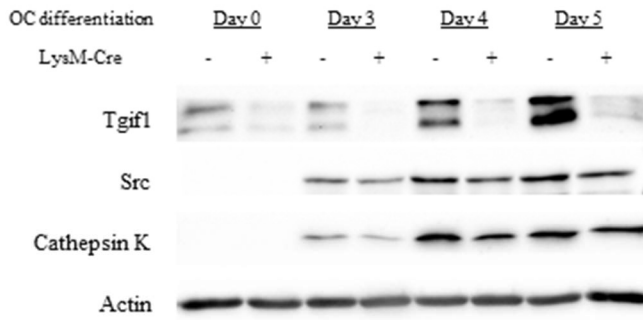
To confirm that Tgifl is deleted in the osteoclast lineage in LysM-Cre⁺;Tgifl^{loxP/loxP} mice, bone marrow cells were isolated from LysM-Cre⁺;Tgifl^{loxP/loxP} mice and their respective LysM-Cre⁻;Tgifl^{loxP/loxP} control animals and Tgifl expression was analyzed during osteoclast differentiation. Western blot revealed a reduced Tgifl protein expression in LysM-Cre⁺;Tgifl^{loxP/loxP} osteoclasts at each time point during differentiation compared to LysM-Cre⁻;Tgifl^{loxP/loxP} osteoclasts (Fig. 4.2.A, 4.2.B). In addition, expression of osteoclast markers such as Src and Cathepsin K was decreased in LysM-Cre⁺;Tgifl^{loxP/loxP} osteoclasts at each time point during differentiation compared to LysM-Cre⁻;Tgifl^{loxP/loxP} osteoclasts (Fig. 4.2.B).

4.3.1.2 Differentiation of osteoclasts from LysM-Cre⁺;Tgifl^{loxP/loxP} mice

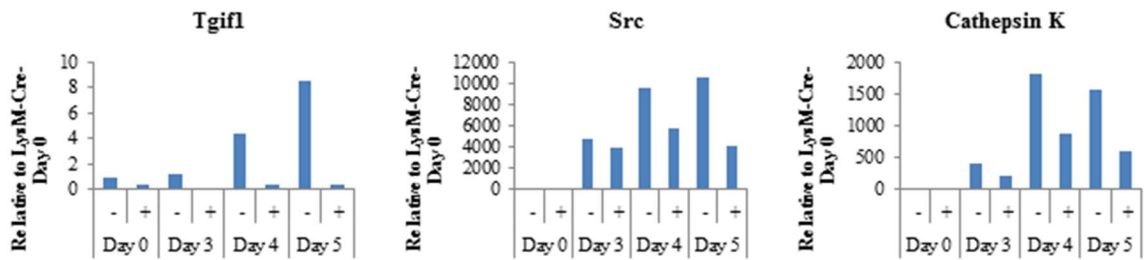
To determine the role of Tgifl during osteoclast differentiation, osteoclast differentiation was performed using LysM-Cre⁺;Tgifl^{loxP/loxP} BMMs. TRAP staining revealed an impaired differentiation of LysM-Cre⁺;Tgifl^{loxP/loxP} osteoclasts compared to control (Fig. 4.2.C). Quantification of TRAP-positive multinucleated cells showed that osteoclast size, the number of osteoclasts and the number of nuclei were significantly decreased in LysM-Cre⁺;Tgifl^{loxP/loxP} osteoclasts compared to LysM-Cre⁻;Tgifl^{loxP/loxP} osteoclasts (Fig. 4.2.D). These data confirmed that Tgifl expression is reduced in osteoclasts of LysM-Cre⁺;Tgifl^{loxP/loxP} mice, causing an impaired osteoclast differentiation. This result confirms that Tgifl plays a role in osteoclast differentiation.

Results

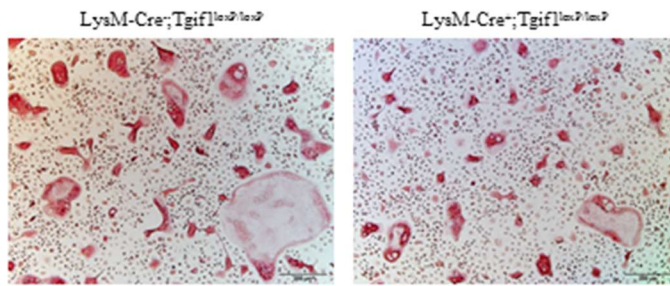
A



B



C



D

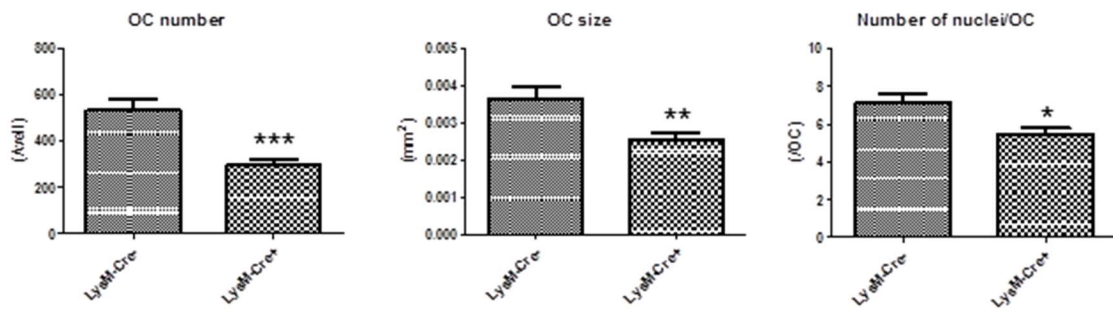


Fig. 4.2. Osteoclast differentiation is impaired in LysM-Cre⁺;Tgif1^{loxP/loxP} osteoclasts *in vitro*. (A) Western blot of Tgif1 expression in LysM-Cre⁺;Tgif1^{loxP/loxP} osteoclasts on culture day 0, 3, 4 and 5. (B) Quantification of Panel A. (C) TRAP staining of LysM-Cre⁻;Tgif1^{loxP/loxP} and LysM-Cre⁺;Tgif1^{loxP/loxP} osteoclasts on culture day 4. Scale bar; 200 μ m. (D) Quantification of Panel C. OC; osteoclast. * $p < 0.05$, ** $p < 0.01$, *** $p < 0.001$, vs LysM-Cre⁻;Tgif1^{loxP/loxP}. n=3 vs 3.

4.3.2 *In vivo* phenotype

4.3.2.1 Bone phenotype of young LysM-Cre⁺;Tgif1^{loxP/loxP} mice

Bone histomorphometric analysis of 8-week old mice showed no change in bone mass of LysM-Cre⁺;Tgif1^{loxP/loxP} mice compared to LysM-Cre⁻;Tgif1^{loxP/loxP} control mice (Fig. 4.3.A, 4.3.B). Furthermore, bone formation was unchanged in LysM-Cre⁺;Tgif1^{loxP/loxP} mice compared to control mice with a tendency towards a decreased osteoblast number but a significant decrease of the osteoblast surface in LysM-Cre⁺;Tgif1^{loxP/loxP} mice. Osteoclast surface was slightly increased, while the number of osteoclasts was significantly increased in LysM-Cre⁺;Tgif1^{loxP/loxP} mice. In 8-week old LysM-Cre⁺;Tgif1^{loxP/loxP} mice, there were certain trends in bone parameters with some significant alterations. However, this did not cause a major bone phenotype.

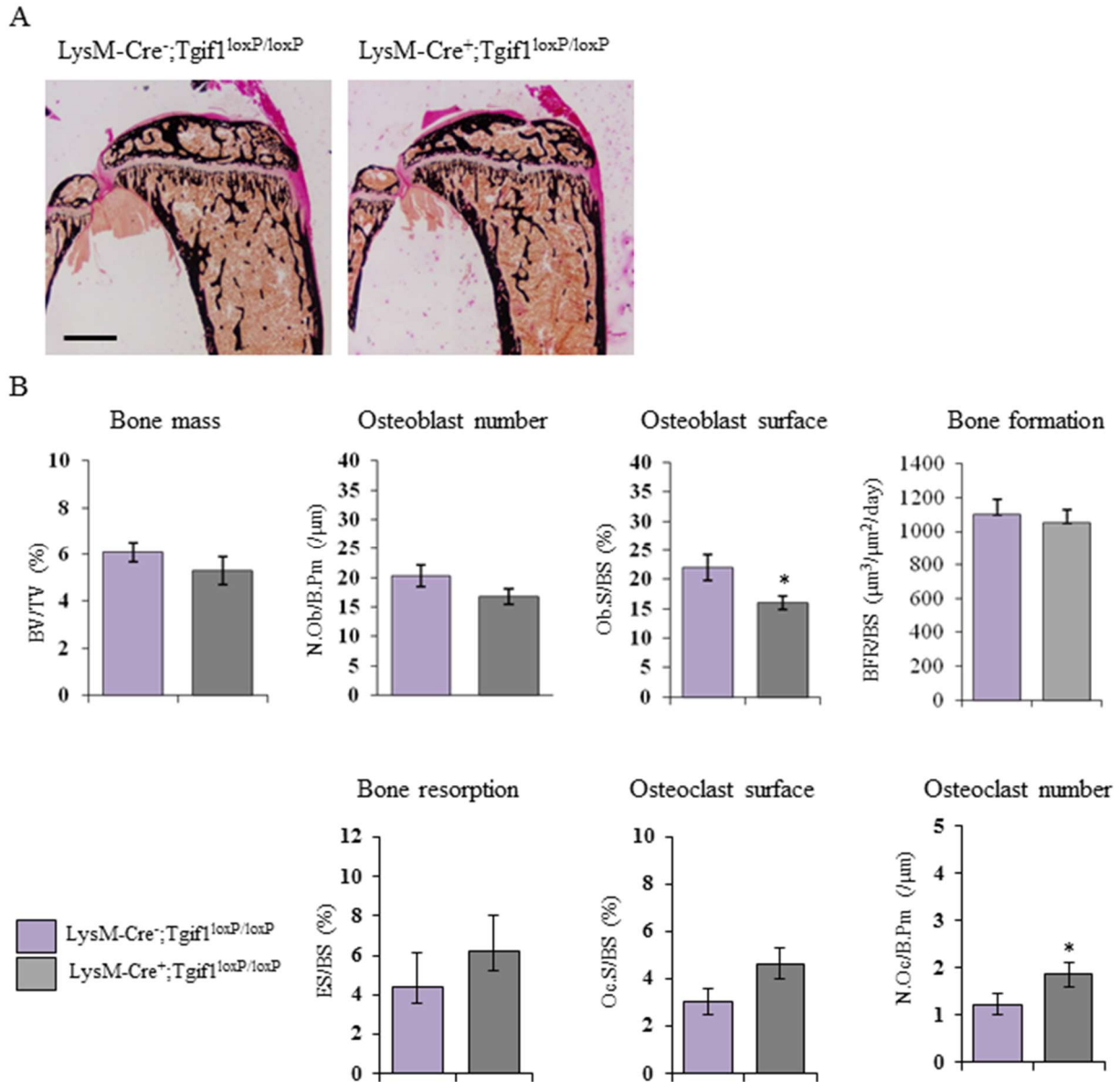


Fig. 4.3. LysM-Cre⁺;Tgif1^{loxP/loxP} mice have no striking phenotype at 8 weeks of age. (A) Von Kossa/van Gieson staining of tibia from LysM-Cre⁺;Tgif1^{loxP/loxP} male mouse at 8 weeks of age. Scale bar; 1 mm. (B) Histomorphometry of Panel A. BV/TV; bone volume/total volume, N.Ob./B.Pm; number of osteoblasts/bone perimeter, Ob.S/BS; osteoblast surface/bone surface, BFR/BS; bone formation rate/bone surface, ES/BS; eroded surface/bone surface, Oc.S/BS; osteoclast surface/bone surface, N.Oc./B.Pm; number of osteoclasts/bone perimeter. *p<0.05, vs LysM-Cre⁻;Tgif1^{loxP/loxP}. n=11 vs 10.

4.3.2.2 Bone phenotype of aged LysM-Cre⁺;Tgif1^{loxP/loxP} mice

To determine the function of Tgif1 in osteoclasts *in vivo* in aged mice, bone mass of 36-week old LysM-Cre⁺;Tgif1^{loxP/loxP} mice was quantified by *ex vivo* μ CT. *Ex vivo* μ CT revealed a slight increase in bone mass of LysM-Cre⁺;Tgif1^{loxP/loxP} mice compared to control littermates of both genders (Fig. 4.4.A, 4.4.B). However, this did not reach significance (Male: p=0.320, Female:

p=0.087). These data indicate that $\text{LysM-Cre}^+;\text{Tgif1}^{\text{loxP/loxP}}$ mice have a trend of an attenuated aging-related bone loss.

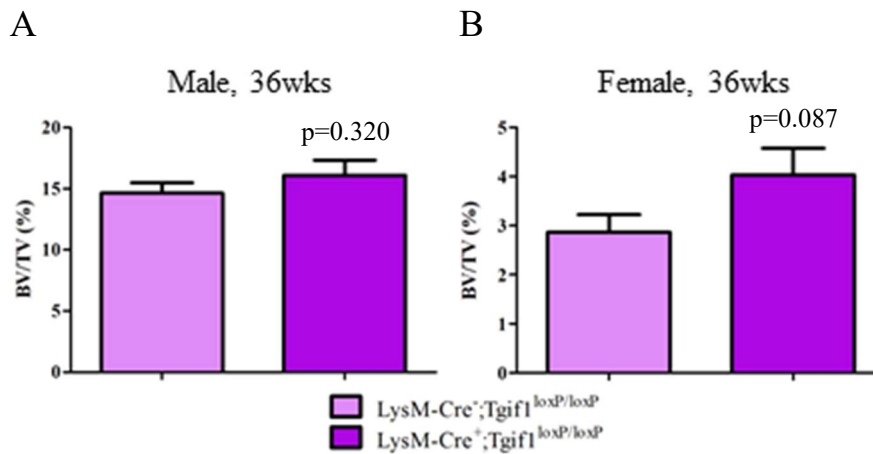


Fig. 4.4. $\text{LysM-Cre}^+;\text{Tgif1}^{\text{loxP/loxP}}$ mice have a tendency towards an increased bone mass compared to control mice at 36 weeks of age. BV/TV of 36-week old $\text{LysM-Cre}^+;\text{Tgif1}^{\text{loxP/loxP}}$ mice by *ex vivo* μCT in male (A) and in female mice (B). Male: n=17 vs 12. Female: n=10 vs 17. BV/TV; bone volume/total volume.

4.4 Analysis of $\text{Ctsk-Cre}^+;\text{Tgif1}^{\text{loxP/loxP}}$ mice

4.4.1 *In vitro* phenotype

4.4.1.1 *Tgif1* expression in osteoclasts

To target *Tgif1* deletion to mature osteoclasts, $\text{Tgif1}^{\text{loxP/loxP}}$ mice were mated with Ctsk-Cre^+ mice. Bone marrow cells were isolated from $\text{Ctsk-Cre}^+;\text{Tgif1}^{\text{loxP/loxP}}$ mice and their respective $\text{Ctsk-Cre}^-;\text{Tgif1}^{\text{loxP/loxP}}$ controls. Osteoclast differentiation was induced and cell lysates were collected 0, 1, 2, 3, 4 and 5 days of culture. Determination of *Tgif1* expression by western blot analysis revealed a decreased expression of *Tgif1* in $\text{Ctsk-Cre}^+;\text{Tgif1}^{\text{loxP/loxP}}$ osteoclasts during differentiation (Fig. 4.5.A, 4.5.B).

4.4.1.2 Osteoclast differentiation of $\text{Ctsk-Cre}^+;\text{Tgif1}^{\text{loxP/loxP}}$ BMMs

To determine the effect of *Tgif1* ablation in Cathepsin K-Cre-positive cells, BMMs were isolated from $\text{Ctsk-Cre}^+;\text{Tgif1}^{\text{loxP/loxP}}$ and $\text{Ctsk-Cre}^-;\text{Tgif1}^{\text{loxP/loxP}}$ mice and differentiated into osteoclasts. TRAP staining revealed an impaired osteoclast differentiation of Ctsk-

$Cre^+;Tgfl^{loxP/loxP}$ BMMs compared to controls (Fig. 4.5.C). Detailed analyses of osteoclast parameters showed that the osteoclast size, the number of nuclei and the number of nuclei per osteoclast were significantly decreased in $Ctsk-Cre^+;Tgfl^{loxP/loxP}$ osteoclasts compared to controls. However, the osteoclast number was not changed in the absence of $Tgfl$ in the osteoclast lineage (Fig. 4.5.D). These data indicate that $Tgfl$ expression is reduced in osteoclasts from $Ctsk-Cre^+;Tgfl^{loxP/loxP}$ mice, leading to an impaired osteoclast differentiation.

Results

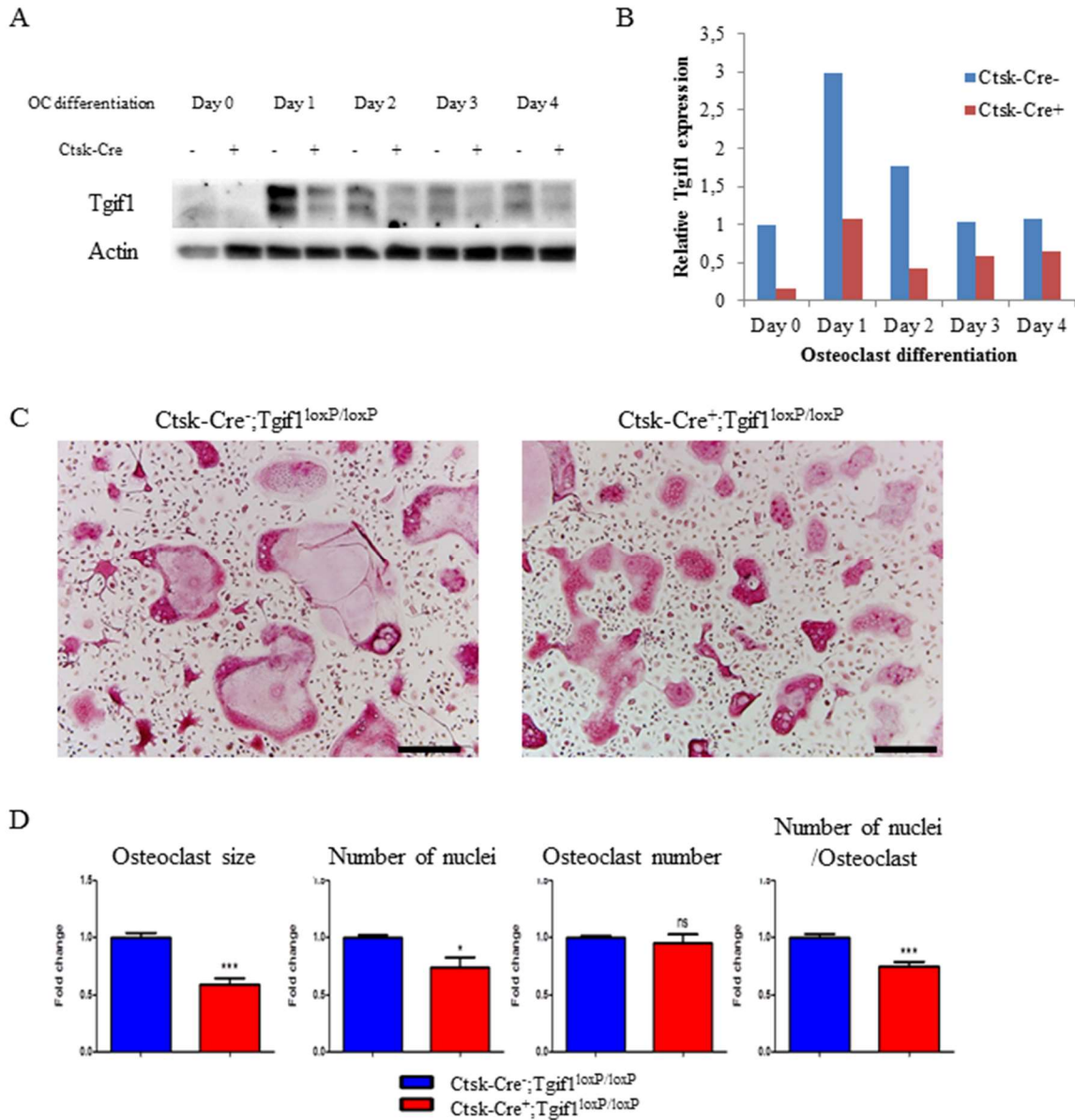


Fig. 4.5. Osteoclast differentiation is impaired in Ctsk-Cre⁺;Tgif1^{loxP/loxP} BMMs *in vitro*. (A) Western blot of Tgif1 expression in Ctsk-Cre⁻;Tgif1^{loxP/loxP} osteoclasts on culture day 0, 1, 2, 3, 4 and 5. “-” indicates Ctsk-Cre⁻;Tgif1^{loxP/loxP}, “+” indicates Ctsk-Cre⁺;Tgif1^{loxP/loxP}. OC; osteoclast. (B) Quantification of Panel A. Normalized to differentiation day 0 of Ctsk-Cre⁻ BMMs. (C) TRAP staining of Ctsk-Cre⁻;Tgif1^{loxP/loxP} and Ctsk-Cre⁺;Tgif1^{loxP/loxP} osteoclasts on culture day 4. Scale bar; 200 μ m. (D) Quantification of Panel C. * p <0.05, ** p <0.01, *** p <0.005, vs Ctsk-Cre⁻;Tgif1^{loxP/loxP}. n =3 vs 3.

4.4.1.3 Tgif1 expression and differentiation of osteoblasts isolated from Ctsk-Cre⁺;Tgif1^{loxP/loxP} mice

To clarify if the Ctsk-Cre driven Tgif1 knockout system works specifically in osteoclasts, Tgif1 expression was also analyzed in osteoblasts isolated from Ctsk-Cre⁺;Tgif1^{loxP/loxP} mice. For this purpose, mesenchymal stromal cells and calvarial osteoblasts were isolated from Ctsk-

Cre⁻;Tgif1^{loxP/loxP} and Ctsk-Cre⁺;Tgif1^{loxP/loxP} mice. Osteoblast differentiation was induced and cell lysates were collected after 0, 7, 14 and 21 days of culture. Western blot analysis showed that Tgif1 expression is decreased in Ctsk-Cre⁺;Tgif1^{loxP/loxP} osteoblasts during differentiation (Fig. 4.6.A). Furthermore, osteoblast differentiation and mineralization were impaired in Ctsk-Cre⁺;Tgif1^{loxP/loxP} osteoblasts (Fig. 4.6.B, 4.6.C).

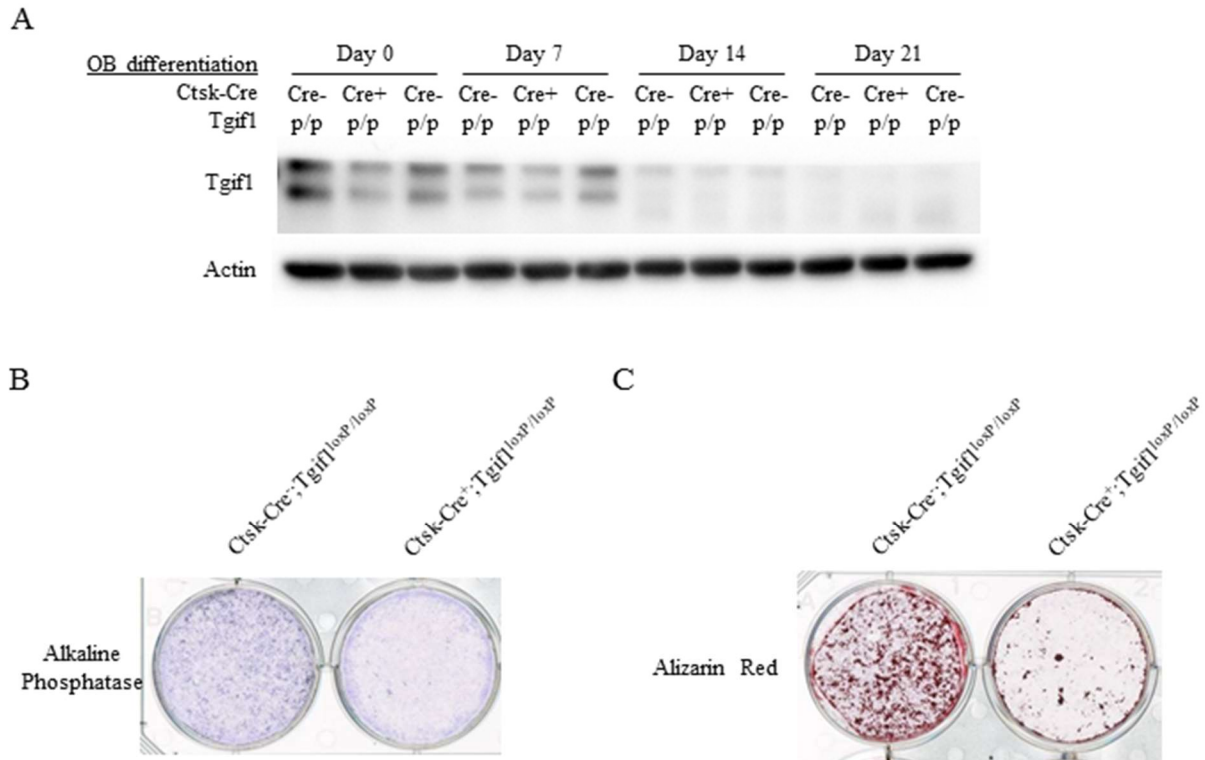


Fig. 4.6. Osteoblast differentiation is impaired in Ctsk-Cre⁺;Tgif1^{loxP/loxP} calvarial osteoblasts *in vitro*. (A) Western blot of Tgif1 expression in Ctsk-Cre⁻;Tgif1^{loxP/loxP} and Ctsk-Cre⁺;Tgif1^{loxP/loxP} osteoblast on culture day 0, 7, 14 and 21. p/p indicates Tgif1^{loxP/loxP}. OB; osteoblasts. (B) ALP staining of Ctsk-Cre⁻;Tgif1^{loxP/loxP} and Ctsk-Cre⁺;Tgif1^{loxP/loxP} osteoblasts on culture day 7. (C) Alizarin red staining of Ctsk-Cre⁻;Tgif1^{loxP/loxP} and Ctsk-Cre⁺;Tgif1^{loxP/loxP} osteoblasts on culture day 21.

4.4.2 Bone mass kinetics of Ctsk-Cre⁺;Tgif1^{loxP/loxP} mice

To analyze the bone mass during aging, bone mass of Ctsk-Cre⁺;Tgif1^{loxP/loxP} mice and their control Ctsk-Cre⁻;Tgif1^{loxP/loxP} littermates was measured by *in vivo* μ CT. According to μ CT analysis, there was no difference between Ctsk-Cre⁺;Tgif1^{loxP/loxP} mice and control mice in bone mass until the mice were 10 weeks old. After the peak bone mass was reached at 10 weeks of age, bone mass age-dependently decreased. Interestingly, bone mass was decreased less in

$Ctsk-Cre^+;Tgif1^{loxP/loxP}$ mice than in control mice. A significant difference in bone mass was observed in 24-week old and 32-week old male mice (Fig. 4.7.A). Similar results were obtained in 32-week old female mice (Fig. 4.7.B), indicating that the phenotype is gender independent. Together, these results suggest that targeted deletion of $Tgif1$ in osteoclasts protects from age-related bone loss.

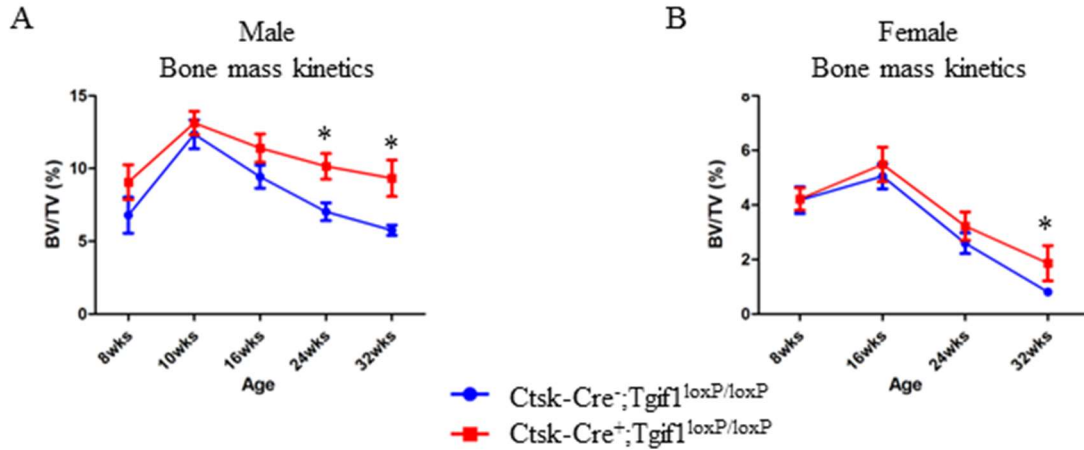


Fig. 4.7. Deletion of $Tgif1$ in osteoclasts protects from age-related bone loss. (A) Bone mass kinetics of male $CtsK-Cre^+;Tgif1^{loxP/loxP}$ mice compared to control littermates by *in vivo* μ CT analysis. (B) Bone mass kinetics of female $CtsK-Cre^+;Tgif1^{loxP/loxP}$ mice compared to control littermates by *in vivo* μ CT analysis. BV/TV; bone volume/total volume. * $p < 0.05$.

4.4.3 Bone phenotype of young $Ctsk-Cre^+;Tgif1^{loxP/loxP}$ mice

Histological sections of tibiae were stained by von Kossa/ van Gieson staining (Fig. 4.8.A). Histomorphometric analysis of structural bone parameters revealed an unchanged bone mass, trabecular thickness, trabecular separation and trabecular number in $Ctsk-Cre^+;Tgif1^{loxP/loxP}$ mice compared to controls in both genders (Fig. 4.8.B). However, bone formation parameters such as mineralizing surface, mineral apposition rate and bone formation rate were significantly decreased in $Ctsk-Cre^+;Tgif1^{loxP/loxP}$ mice compared to controls. Consistently, osteoblast parameters such as osteoid surface, osteoblast surface and osteoblast number were reduced in $Ctsk-Cre^+;Tgif1^{loxP/loxP}$ mice. Similarly, osteoclast parameters such as eroded surface indicating bone resorption as well as osteoclast surface and osteoclast number were significantly decreased

Results

in $Ctsk-Cre^+;Tgfl^{loxP/loxP}$ mice compared to $Ctsk-Cre^-;Tgfl^{loxP/loxP}$ controls. Together, these data suggest that 8-week old $Ctsk-Cre^+;Tgfl^{loxP/loxP}$ mice have a low turnover bone phenotype.

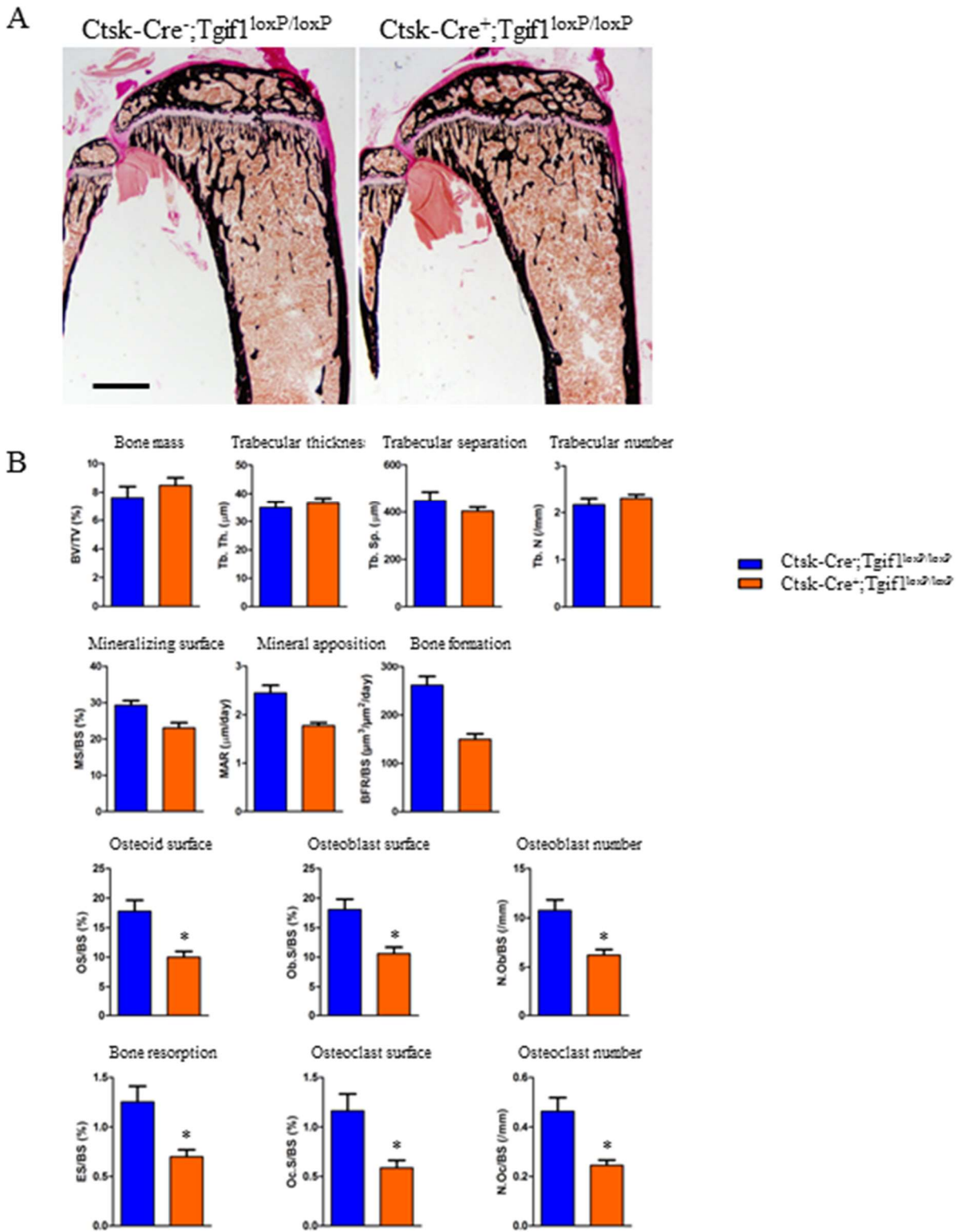


Fig. 4.8. $Ctsk-Cre^{+};Tgif1^{loxP/loxP}$ mice have a low turnover bone phenotype at 8 weeks of age. (A) Von Kossa/van Gieson staining of tibia from 8 weeks old $Ctsk-Cre^{-};Tgif1^{loxP/loxP}$ and $Ctsk-Cre^{+};Tgif1^{loxP/loxP}$ mice. Scale bar; 1 mm. (B) Histomorphometric analysis of Panel A. BV/TV; bone volume/total volume, Tb.Th.; trabecular thickness, Tb.Sp.; trabecular separation, Tb.N.; trabecular number, MS/BS; mineralized surface/bone surface, MAR; mineral apposition rate, BFR/BS; bone formation rate/bone surface, OS/BS; osteoid surface/bone surface, Ob.S/BS; osteoblast surface/bone surface, N.Ob/BS; number of osteoblasts/bone surface, ES/BS; eroded surface/bone surface, Oc.S/BS; osteoclast surface/bone surface, N.Oc/BS; number of osteoclasts/bone surface. * $p < 0.05$.

4.4.4 Bone phenotype of aged *Ctsk-Cre⁺;Tgif1^{loxP/loxP}* mice

Longitudinal histological sections of tibiae were stained by von Kossa/ van Gieson staining (Fig. 4.9.A). Detailed analysis of structural bone parameters revealed a higher bone mass, trabecular thickness and trabecular number in *Ctsk-Cre⁺;Tgif1^{loxP/loxP}* mice compared to controls in both male and female mice (Fig. 4.9.B). Interestingly, osteoclast parameters such as eroded (bone resorption) surface, osteoclast surface and osteoclast number were significantly decreased in *Ctsk-Cre⁺;Tgif1^{loxP/loxP}* mice while parameters reflecting bone formation and osteoblast function (mineralizing surface, mineral apposition rate, bone formation rate, osteoid surface, osteoblast surface and osteoblast number) were unchanged in *Ctsk-Cre⁺;Tgif1^{loxP/loxP}* mice. These data strongly suggest that osteoclast-targeted deletion of *Tgif1* results in osteopetrotic phenotype in 32-week old mice.

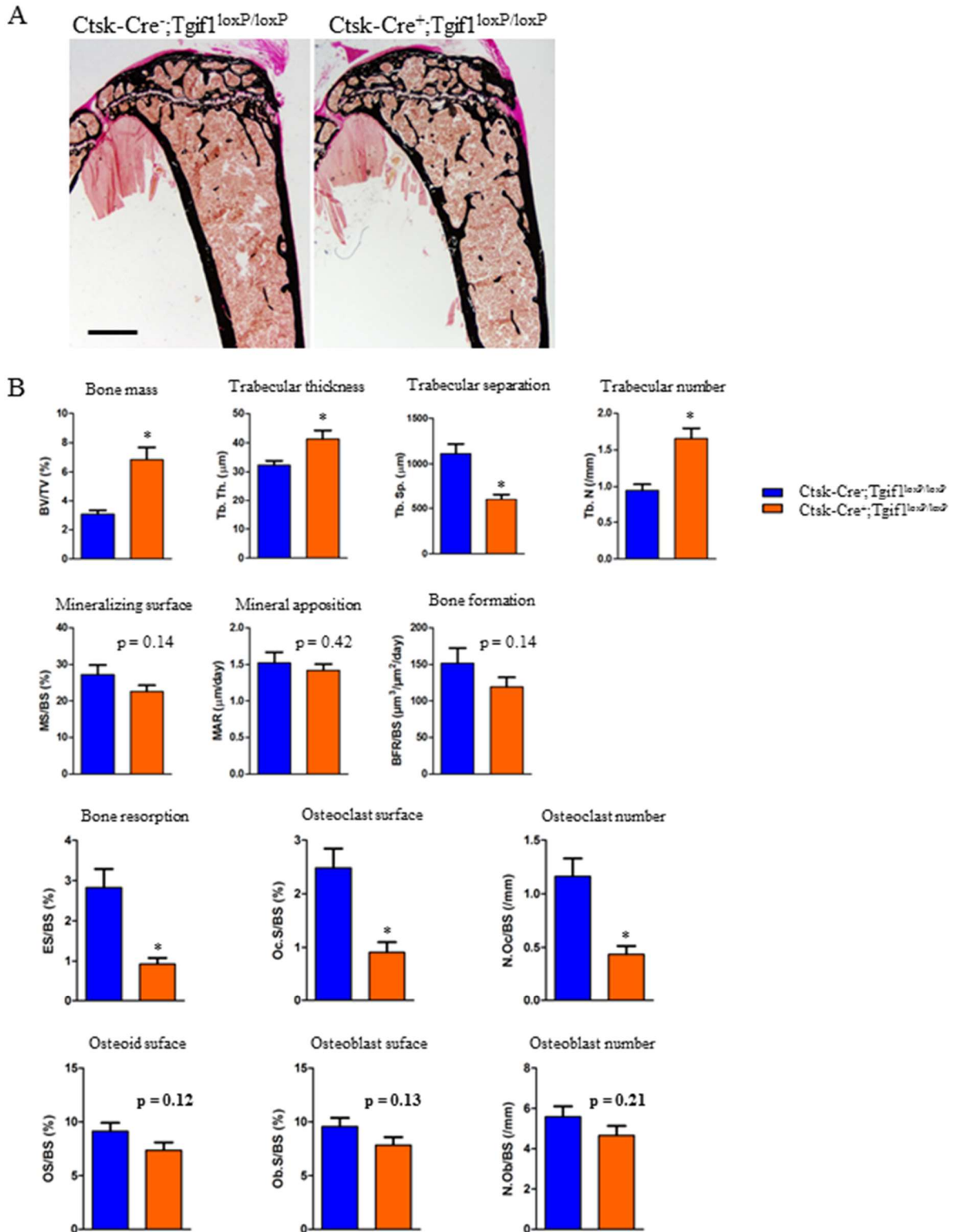


Fig. 4.9. Aged Ctsk-Cre⁺;Tgif1^{loxP/loxP} mice have a higher bone mass than controls due to a decreased osteoclast activity. (A) Von Kossa/van Gieson staining of tibia from 32 weeks old Ctsk-Cre;Tgif1^{loxP/loxP} mice. Scale bar; 1 mm. (B) Histomorphometric analysis of Panel A. BV/TV; bone volume/total volume, Tb.Th.; trabecular thickness, Tb.Sp.; trabecular separation, Tb.N.; trabecular number, MS/BS; mineralized surface/bone surface, MAR; mineral apposition rate, BFR/BS; bone formation rate/bone surface, ES/BS; eroded surface/bone surface, Oc.S/BS; osteoclast surface/bone surface, N.Oc./BS; number of osteoclasts/bone surface. OS/BS; osteoid surface/bone surface, Ob.S/BS; osteoblast surface/bone surface, N.Ob/BS; number of osteoblasts/bone surface. *p<0.05.

4.5 *In vitro* osteoclast phenotype of Tgif1-deficient BMMs

To assess the role of Tgif1 in osteoclasts *in vitro*, osteoclast precursors were isolated from mice with a germ-line deletion of Tgif1 (Tgif1^{-/-}) and littermate controls (Tgif1^{+/+}) and seeded in 96 well-plates with M-CSF and RANKL. TRAP-positive cells appeared on culture day 3 and TRAP-positive multinucleated cells were observed on culture day 4. On culture day 5, many apoptotic cells were observed. Interestingly, osteoclast differentiation was impaired in Tgif1^{-/-} osteoclasts compared to Tgif1^{+/+} osteoclasts (Fig. 4.10.A). Detailed analysis revealed a significantly decreased osteoclast size, number of osteoclasts, number of nuclei and number of nuclei per osteoclast on culture day 4 (Fig. 4.10.B).

To confirm the impaired osteoclast differentiation in Tgif1^{-/-} osteoclasts at the mRNA and protein level, qRT-PCR and western blot analysis of osteoclast markers such as NFATc1, Src and Cathepsin K was performed. The results show that the expression of various osteoclast markers is decreased in Tgif1^{-/-} osteoclasts during differentiation, consistent with the impaired osteoclast differentiation of Tgif1^{-/-} osteoclasts (Fig. 4.10.C, 4.10.D). Collectively, these results show that Tgif1 has an important role in osteoclast differentiation.

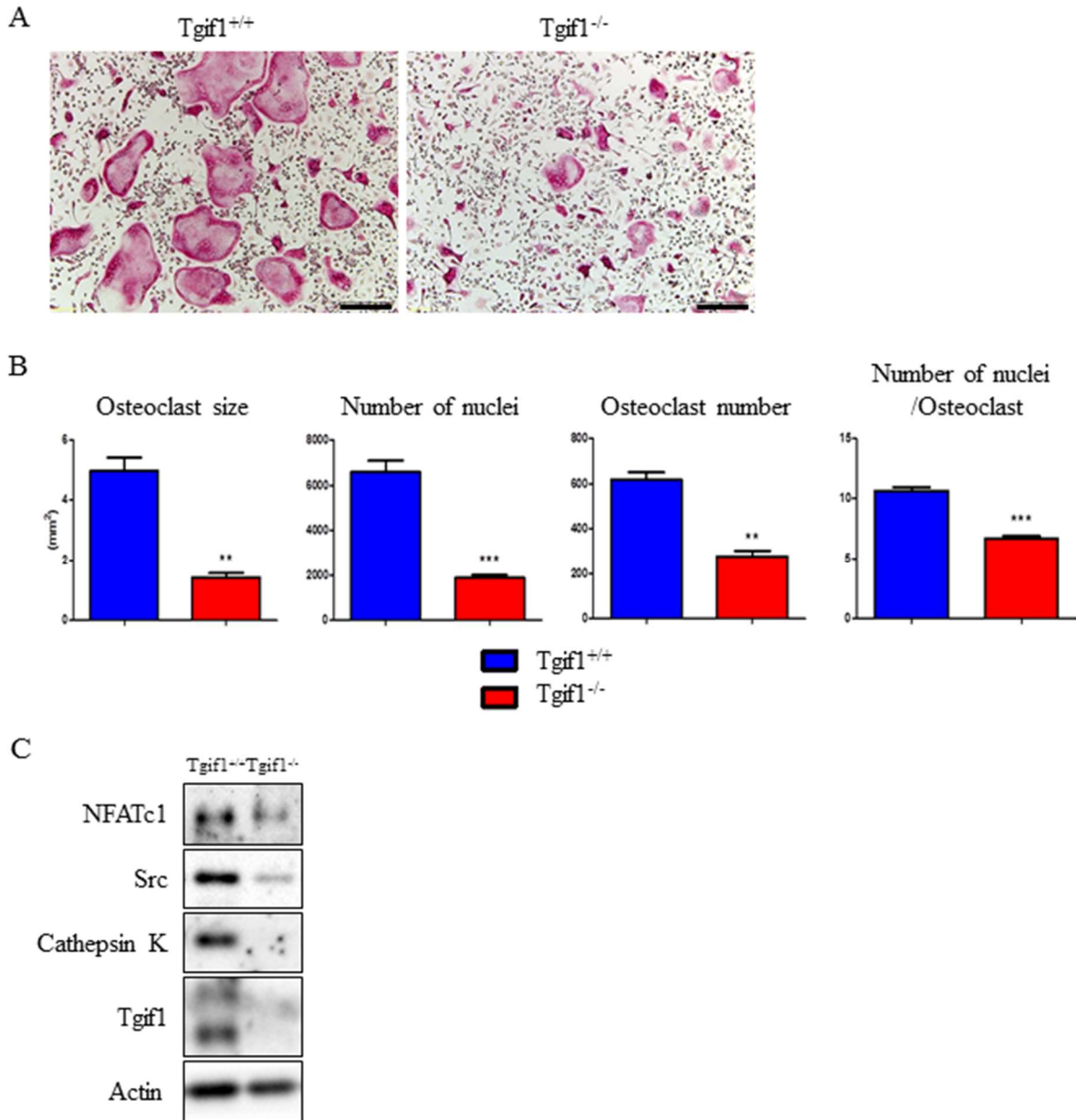


Fig. 4.10. Loss of Tgif1 impairs osteoclast differentiation. (A) TRAP staining of osteoclast culture day 4. Scale bar; 200 μ m. (B) Quantification of Panel A. ** $p < 0.01$, *** $p < 0.001$ vs Tgif1^{+/+}. (C) Western blot of osteoclast markers NFATc1, Src, Cathepsin K and Tgif1 in osteoclasts on culture day 4.

4.6 Osteoclast precursors

To determine a potential difference of osteoclast progenitor cells, bone marrow cells were flushed out from the tibiae of 8-12-week old Tgif1^{+/+} and Tgif1^{-/-} mice and the presence of CD11-positive cells was analyzed by FACS. As shown in Figure 4.11.A, the number of cells positive for the osteoclast precursor marker CD11 is comparable between Tgif1^{+/+} and Tgif1^{-/-}

mice (Fig. 4.11.A). This result suggests that deficiency of *Tgif1* does not alter the osteoclast precursor pool in the bone marrow.

In addition, to examine the number of functional HSCs in the bone marrow, GM-CFU assay was performed with MethoCult™ assay following the manufacturer's protocol. Consistent with the results obtained from FACS analysis, GM-CFU was unchanged in *Tgif1*^{-/-} bone marrow compared to *Tgif1*^{+/+} control littermates (Fig. 4.11.B). These results demonstrate that *Tgif1*-deficiency does not affect the population of osteoclast precursor cells.

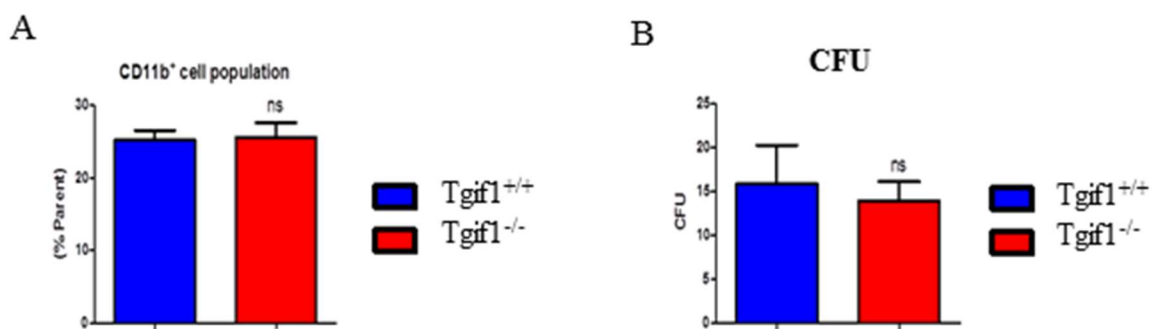


Fig. 4.11. The osteoclast progenitor cell population is unchanged in *Tgif1*^{-/-} mice. (A) CD11b⁺ cell population was quantified by FACS in the bone marrow of *Tgif1*^{-/-} mice and control littermates. (B) CFU assay was performed using the bone marrow of *Tgif1*^{-/-} mice and control littermates. ns; no significance.

4.7 Osteoclast fusion

To examine osteoclast fusion, the cell density for osteoclast differentiation was increased from the standard condition (15,000 cells/well) to 20,000 cells/well, 30,000 cells/well and 60,000 cells/wells. Analysis of TRAP-positive multinucleated cells revealed a significantly decreased osteoclast size, osteoclast number and number of nuclei and number of nuclei in *Tgif1*^{-/-} osteoclasts in each condition compared to littermate control culture (Fig. 4.12.A). Remarkably, osteoclast parameters were significantly increased in *Tgif1*^{+/+} osteoclast cultures when the cell density was increased from 15,000 cells/well to 20,000 cells/well. However, this increase did not occur in *Tgif1*^{-/-} osteoclast cultures, suggesting that *Tgif1* supports osteoclast fusion. Additionally, in *Tgif1*^{+/+} cultures with 30,000 cells/well apoptosis was observed already on

culture day 4. Furthermore, no osteoclast differentiation was observed when 60,000 cells were plated per well. This observation confirms that osteoclast precursors need a proper space to move/fuse for osteoclast differentiation *in vitro*⁵⁰. As an additional method to determine cell fusion, live imaging of osteoclasts was performed during fusion and differentiation and similar observations were made (videos not shown).

Since DC-STAMP has an essential role in osteoclast fusion¹⁴³, we next measured DC-STAMP mRNA expression by qRT-PCR. However, there was no difference in DC-STAMP expression between *Tgif1*^{+/+} and *Tgif1*^{-/-} osteoclasts during differentiation (Fig. 4.12.B). These data suggest that *Tgif1* has a role in cell-cell fusion during osteoclast differentiation, which is not related to DC-STAMP expression.

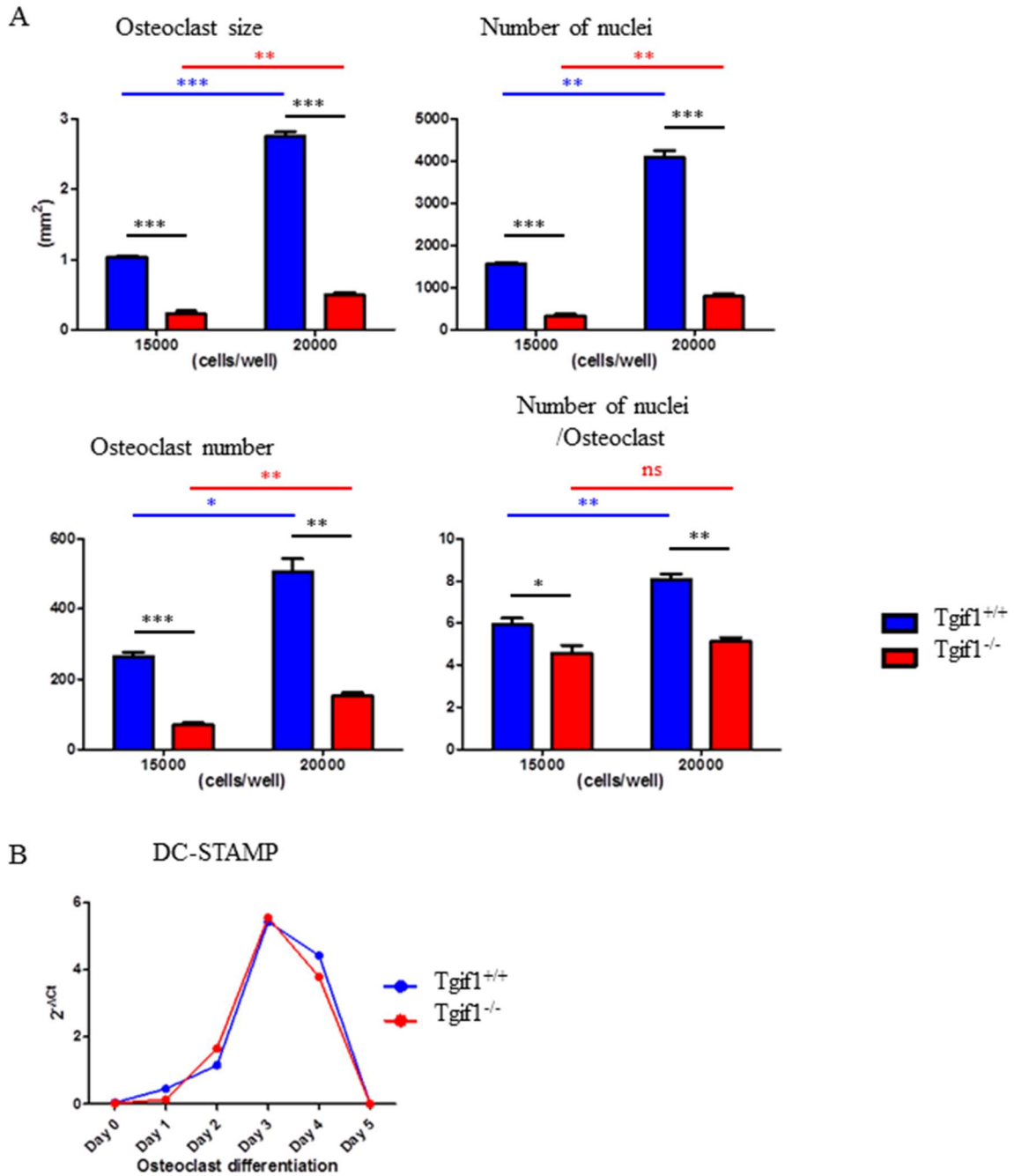


Fig. 4.12. Tgif1 supports osteoclast fusion. (A) Comparison of the effect of cell densities (15,000 cells/well and 20,000 cells/well) on osteoclast size, the number of nuclei, osteoclast number and the number of nuclei per osteoclast on culture day 4 after TRAP staining. * $p < 0.05$, ** $p < 0.01$, *** $p < 0.001$. ns; no significance. (B) DC-STAMP mRNA expression during osteoclast differentiation quantified by qRT-PCR.

4.8 Actin ring formation in osteoclasts

Since actin ring formation is important for osteoclast function^{274,275}, osteoclasts were stained with Alexa-Fluor 488 Phalloidine to visualize the actin and the actin ring formation during

osteoclast differentiation. Formation of a clear actin ring was observed in *Tgif1*^{+/+} osteoclasts on culture day 4 while no actin ring was observed in *Tgif1*^{-/-} osteoclasts at that time point (Fig. 4.13.A). However, on culture day 5, a distorted actin ring formation was also observed in *Tgif1*^{-/-} osteoclasts, suggesting that the *Tgif1*-deficient osteoclasts have a machinery to form an actin ring but the process is delayed and impaired.

Since Src is an important protein for cytoskeletal organization^{160,276}, Src expression was measured in undifferentiated BMMs and during osteoclast differentiation. The basal level of Src expression in BMMs was unchanged in the absence of *Tgif1* (Fig. 4.13.B). However, during osteoclast differentiation, Src expression was decreased in *Tgif1*^{-/-} osteoclasts reflecting the impaired differentiation process (Fig. 4.13.C). These results demonstrate that *Tgif1* is involved in early stage prior actin ring formation.

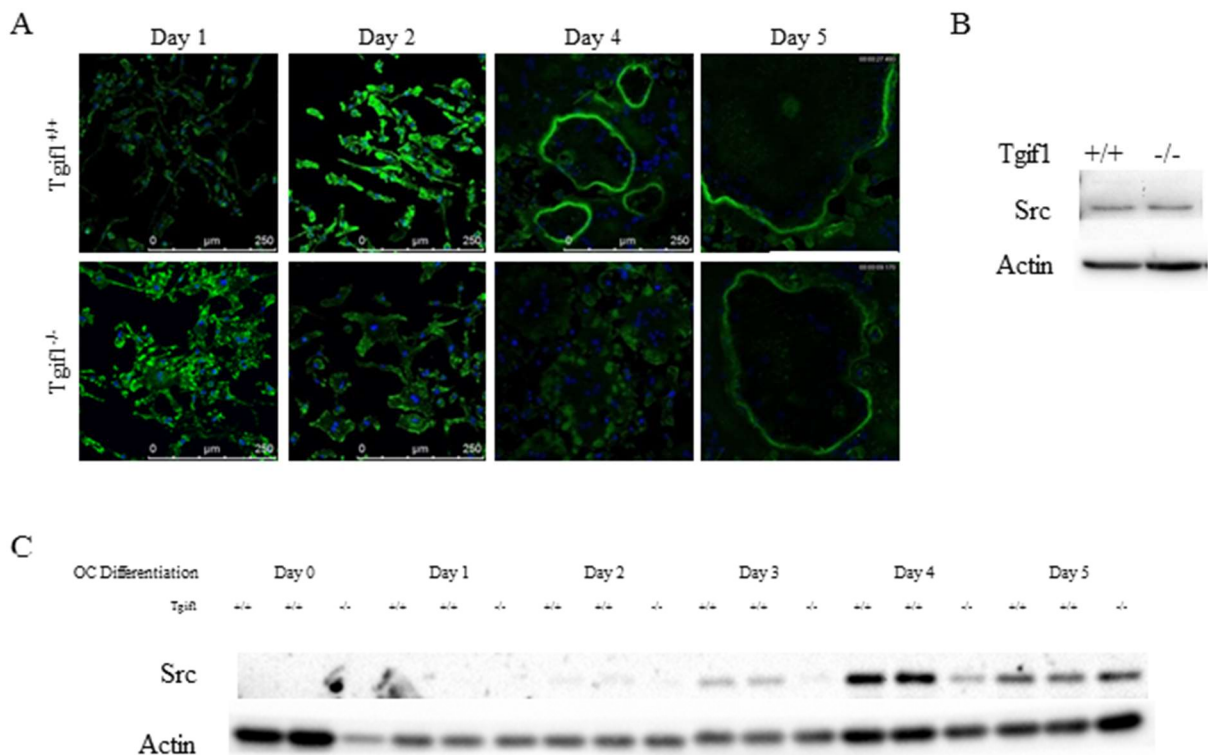


Fig. 4.13. Actin ring formation is delayed in *Tgif1*^{-/-} osteoclasts. (A) Phalloidine and DAPI staining of osteoclasts by culture day 0, 1, 2, 4 and 5. (B) Western blot analysis of Src expression in osteoclast precursors. (C) Western blot analysis of Src expression in osteoclasts during differentiation. OC; osteoclast.

4.9 Osteoclast resorption activity

To evaluate the resorption capacity of *Tgif1*-deficient osteoclasts, pit formation assays were performed. For this purpose, BMMs were seeded on dentin slices and cultured for 7 days. Afterwards, dentin slices were removed from the culture plate and analyzed. Light microscopy images of dentine slices after toluidine blue staining showed a reduced number and size of resorption pits formed by *Tgif1*^{-/-} osteoclasts compared to *Tgif1*^{+/+} control cells (Fig. 4.14.A). Scanning electron microscopy provided a more detailed picture of the dentin, showing less individual pits in *Tgif1*^{-/-} cultures (Fig. 4.14.B). To further analyze the resorption capacity, resonance scanning by confocal microscopy was performed and pit depth and volume was analyzed using Vision64 software (Fig. 4.14.C). Interestingly, pit volume was significantly reduced in the absence of *Tgif1* in osteoclasts (Fig. 4.14.D). To measure individual osteoclast resorption activity, the total pit area, total pit volume and total pit depth were divided by the osteoclast number. Consistent with previous results, the resorption activity of individual osteoclasts was decreased in *Tgif1*^{-/-} osteoclasts compared to control (Fig. 4.14.E). Collectively, these results strongly indicate that *Tgif1* has an important role in osteoclast function.

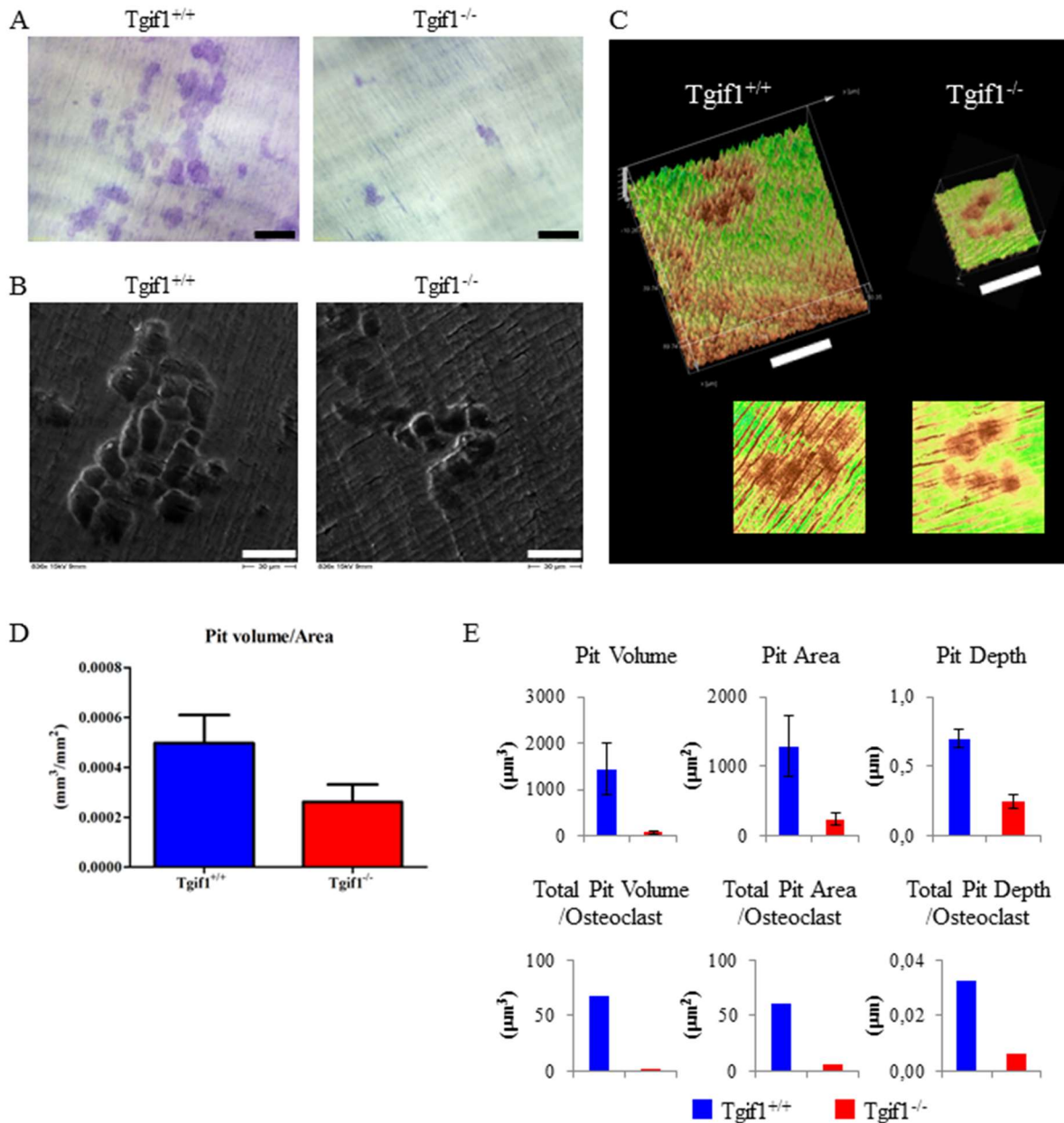


Fig. 4.14. Tgif1 deficiency reduces osteoclast function. (A) Optical microscope images of dentine slices from pit formation assay after toluidine blue staining. Scale bar; 100 µm. (B) SEM (Scanning Electron Microscopy) images of dentine slices from pit formation assay. Scale bar; 30 µm. (C) Resonance scanning images of dentine surface quantified by confocal microscope. Scale bar; 50 µm. (D) Quantification of pit volume on dentin slices. Mice: Tgif1^{+/+} n=4 vs Tgif1^{-/-} n=4. Dentin slices: n=10 vs 10. (E) The value of total pit volume, total pit area and total pit depth were divided by the average number of osteoclasts from the experiment (osteoclasts/well). Exp. n=1.

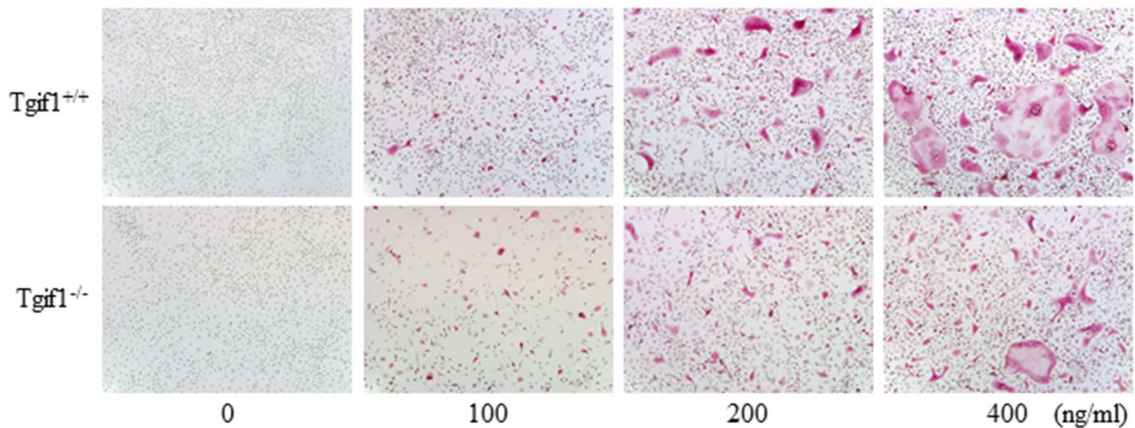
4.10 RANKL and M-CSF signaling pathways

To elucidate the molecular mechanisms by which Tgif1 promotes osteoclast differentiation and function, RANKL and M-CSF pathways were analyzed in the presence and absence of Tgif1.

To examine the potential impairment in RANKL signaling in Tgif1^{-/-} osteoclasts, the concentration of RANKL to stimulate osteoclast precursors was increased *in vitro*, to 100 ng/ml

(standard condition), 200 ng/ml and 400 ng/ml. TRAP staining revealed an impaired osteoclast differentiation of *Tgif1*^{-/-} cells, which was not restored by a high concentration of RANKL (Fig. 4.15.A, 4.15.B). This result supports the notion that *Tgif1* is required for RANKL signaling in osteoclasts and for osteoclast differentiation.

A



B

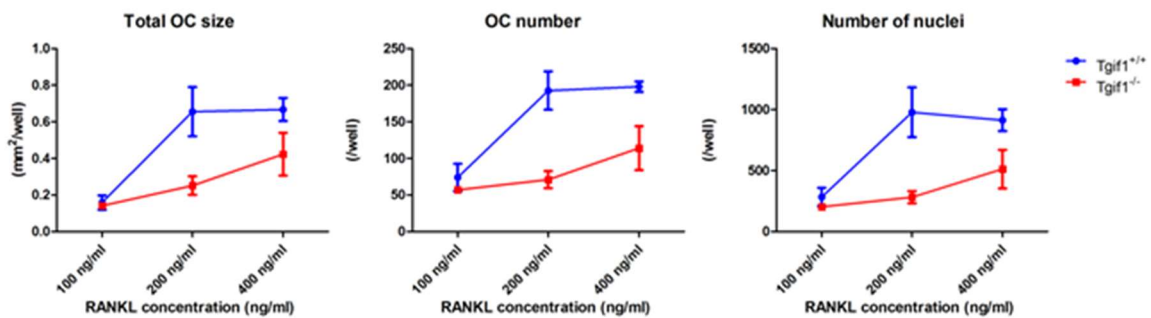


Fig. 4.15. High concentration of RANKL does not restore the impaired differentiation of *Tgif1*^{-/-} osteoclasts. (A) TRAP staining images of osteoclast differentiation with different concentrations (0, 100, 200 and 400 ng/ml) of RANKL on culture day 4. Scale bar; 200 μ m. Representative data from 3 independent experiments. (B) Quantification of Panel A. Technical triplicate. Exp. n=1.

4.11 RANK and c-fms receptors

M-CSF and RANKL signal go through c-fms and RANK receptors, respectively, to promote osteoclast differentiation. To analyze the abundance of c-fms and RANK in the bone marrow of *Tgif1*^{+/+} and *Tgif1*^{-/-} mice, FACS analysis was performed. Both c-fms and RANK-positive cell populations were comparable between *Tgif1*^{+/+} and *Tgif1*^{-/-} bone marrow cells (Fig. 4.16.A).

In addition, western blot analysis was performed to quantify RANK expression in osteoclast

precursors. In support of the FACS analysis, there was no difference in RANK expression between *Tgif1*^{-/-} and control osteoclast precursors (Fig. 4.16.B). Furthermore, the expression of *c-fms* as well as of RANK and its adaptor protein TRAF6 was quantified by qRT-PCR. Consistently, *c-fms*, RANK and TRAF6 expression were comparable between *Tgif1*^{+/+} and *Tgif1*^{-/-} osteoclast precursors (Fig. 4.16.C). These results show that the important receptors for osteoclastogenesis *c-fms*, RANK are not affected in *Tgif1*^{-/-} osteoclast precursors. Therefore, we hypothesize that *Tgif1* might be involved in a signaling cascade downstream of RANKL or M-CSF during osteoclast differentiation.

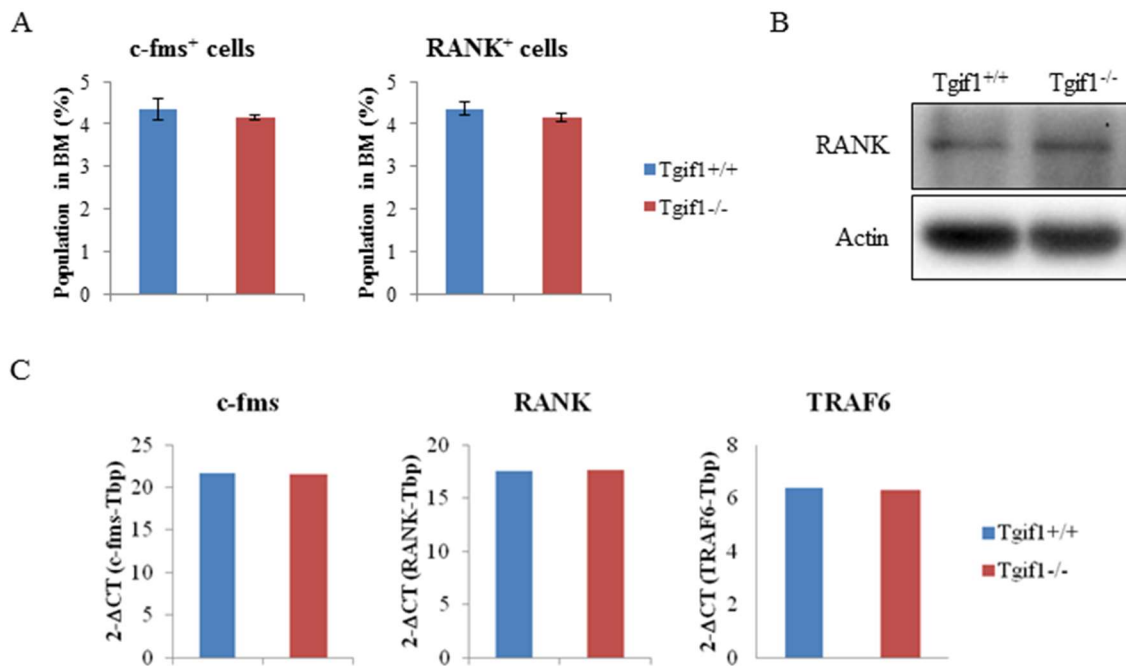


Fig. 4.16. RANK, *c-fms* and TRAF6 expressions are unchanged in *Tgif1*^{-/-} osteoclast precursors. (A) FACS analysis of *c-fms*⁺ and RANK⁺ cell populations in the bone marrow of *Tgif1*^{+/+} and *Tgif1*^{-/-} mice. (B) Western blot analysis of RANK expression in BMMs of *Tgif1*^{+/+} and *Tgif1*^{-/-} mice. (C) qRT-PCR analyses of *c-fms*, RANK and TRAF6 expression in *Tgif1*^{+/+} and *Tgif1*^{-/-} BMMs.

4.12 Signaling cascades

To test the hypothesis that the absence of *Tgif1* affects the downstream signaling cascades of M-CSF or RANKL, major cascades downstream of M-CSF or RANKL were analyzed in BMMs²⁷⁷. Among the signaling pathways analyzed, phosphorylated ERK1/2 was decreased in

Tgif1^{-/-} osteoclast precursors at 5, 15 and 30 minutes after M-CSF and RANKL stimulation (Fig. 4.17.A, 4.17.B). In contrast, phosphorylated AKT and phosphorylated p38 were unchanged in Tgif1^{-/-} osteoclast precursors compared to controls. Interestingly, the striking difference of phosphorylated ERK1/2 between wild type and Tgif1^{-/-} osteoclast precursors was observed after 15 and 30 minutes of stimulation. Since ERK1/2 is phosphorylated by MEK1/2^{278,279}, phosphorylated MEK1/2 was assessed after RANKL stimulation. However, phosphorylated MEK1/2 was not changed in Tgif1^{-/-} osteoclast precursors compared to controls (Fig. 4.17.C), suggesting that the phosphorylation of ERK1/2 is not affected in Tgif1^{-/-} osteoclasts. This result allowed us to hypothesize that Tgif1 might be involved in the dephosphorylation of ERK1/2.

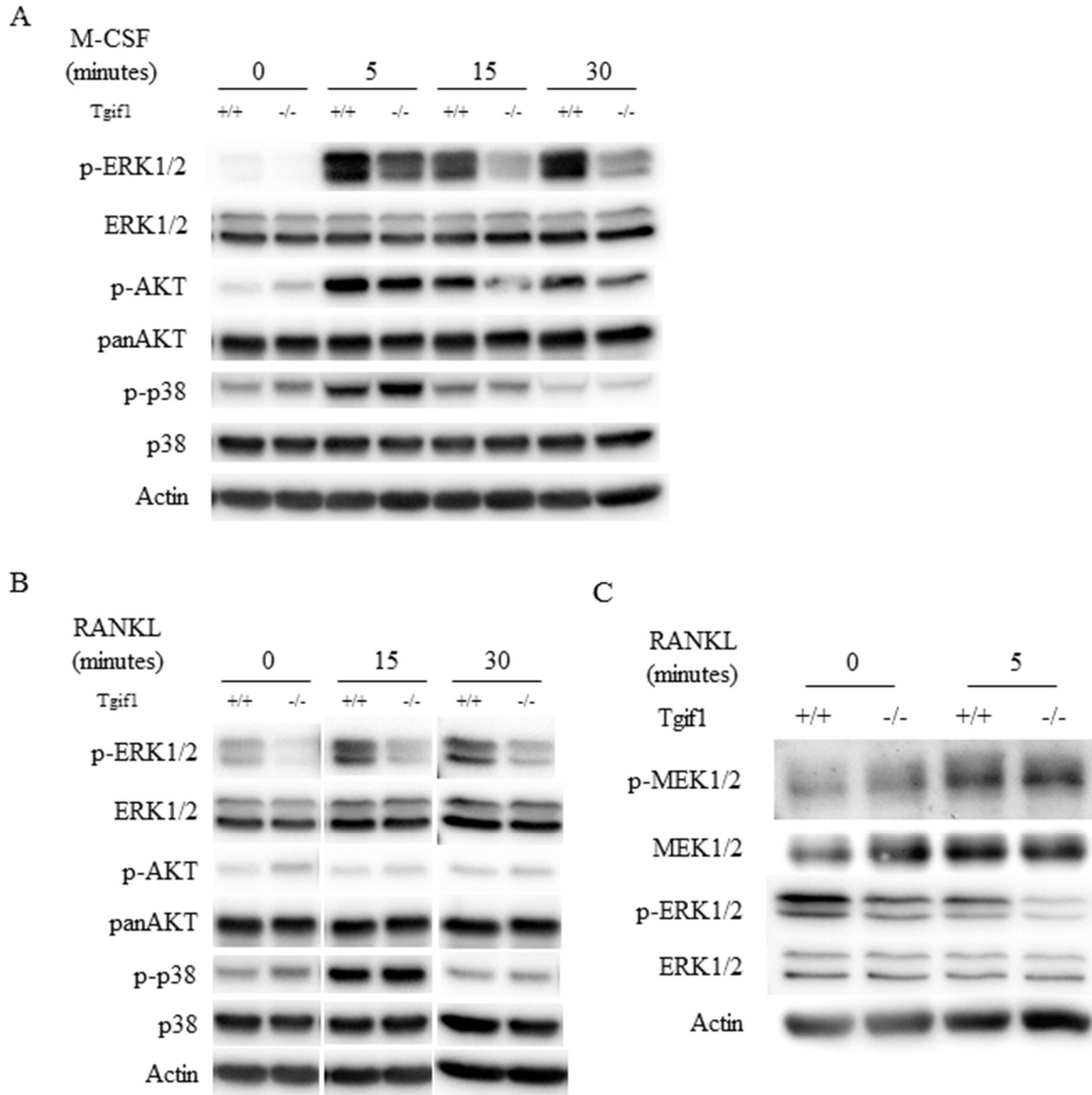


Fig. 4.17. Phosphorylated ERK1/2 is decreased in Tgif1^{-/-} BMMs. (A) Western blot analysis of phosphorylated ERK1/2, ERK1/2, phosphorylated AKT, panAKT, phosphorylated p38 and p38 expressions in osteoclast precursors after M-CSF stimulation for 0, 5, 15 and 30 minutes. (B) Western blot analysis of phosphorylated ERK1/2, ERK1/2, phosphorylated AKT, panAKT, phosphorylated p38 and p38 expressions in osteoclast precursors after RANKL stimulation for 0, 15 and 30 minutes. (C) Western blot analysis of phosphorylated MEK1/2, MEK1/2, phosphorylated ERK1/2 and ERK1/2 expression in osteoclast precursors after RANKL stimulation for 0 and 5 minutes.

4.13 Protein Phosphatase 2A (PP2A)

Since Protein Phosphatase 2A (PP2A) is an established phosphatase for ERK1/2, we next investigated the potential interaction between PP2A and Tgif1. PP2A is a holoenzyme, which consists of 3 subunits, the scaffold, the catalytic subunit and the regulatory subunit²⁸⁰ (Fig. 4.18.A). The scaffold has 2 isoforms, the catalytic subunit has 2 isoforms and the regulatory

subunit has 18 isoforms²⁸⁰. First, the expression of the PP2A isoforms was analyzed during osteoclast differentiation by qRT-PCR (Fig. 4.18.B). Next, the expression of 7 isoforms that highly expressed during osteoclast differentiation were compared between wild type and *Tgif1*^{-/-} osteoclast precursors by qRT-PCR. Intriguingly, the PP2A catalytic subunit isoform β (PP2A-C β) was expressed approximately 2.5 times higher in *Tgif1*^{-/-} than in wild type osteoclast precursors (Fig. 4.18.C). An increased PP2A-C β expression in *Tgif1*^{-/-} osteoclast precursors was confirmed by qRT-PCR repeatedly with 4 wild type mice vs 4 *Tgif1*^{-/-} mice (Fig. 4.18.D). In addition, to confirm the high expression of PP2A catalytic subunit (PP2A-C), immunoblot analysis was performed after nuclear/cytosol fractionation. Western blot analysis revealed approximately 9.4 times higher expression of PP2A-C in the cytosolic fraction of *Tgif1*^{-/-} osteoclast precursors compared to wild type cells (Fig. 18). Moreover, phosphorylated ERK1/2 was decreased in the nuclear fraction of *Tgif1*^{-/-} BMMs compared to controls (Fig. 4.19). This result suggests that the abundance of PP2A-C might interrupt ERK1/2 signaling activity downstream of RANKL or M-CSF stimulation. Since *Tgif1* often functions as a transcriptional repressor, these results led us to hypothesize that *Tgif1* regulates PP2A-C gene expression in osteoclasts.

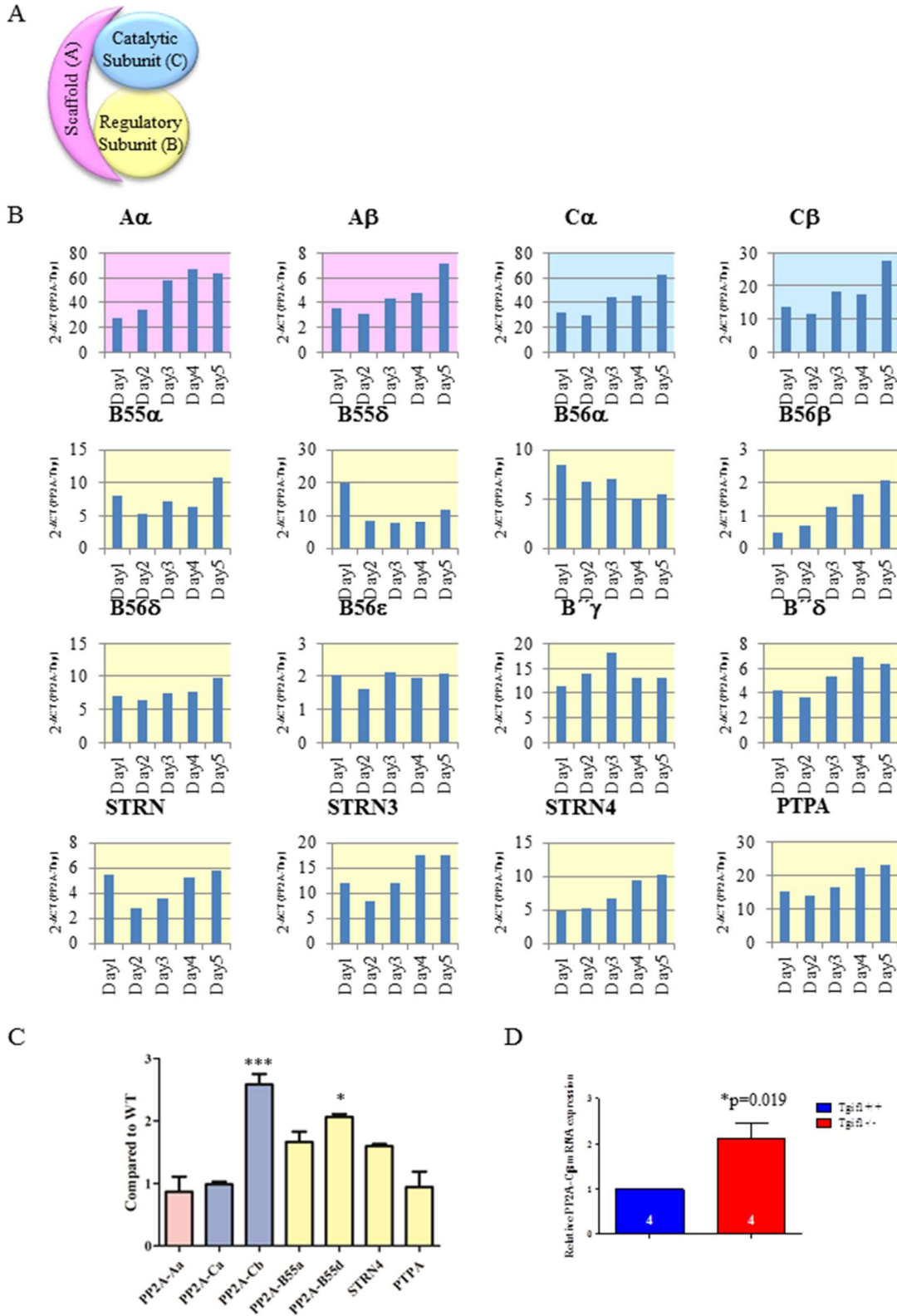


Fig. 4.18. PP2A catalytic subunit β expression is increased in $Tgfr1^{-/-}$ BMMs. (A) Schematic image of the holoenzyme Protein Phosphatase 2A (PP2A). (B) Screening of the expression of PP2A subunits expressions in $Tgfr1^{+/+}$ osteoclasts during differentiation quantified by qRT-PCR. PP2A-B55 β , PP2A-B55 γ , PP2A-B56 γ , PP2A-B α 1 and PP2A-B α 2 are not shown because of no or very low detection. (C) Comparison of PP2A subunit mRNA expression between $Tgfr1^{+/+}$ and $Tgfr1^{-/-}$ BMMs. * $p < 0.05$, *** $p < 0.001$ vs PP2A-A α . (D) PP2A-C β expression quantified by qRT-PCR in BMMs from $Tgfr1^{+/+}$ and $Tgfr1^{-/-}$ mice. * $p < 0.05$; vs $Tgfr1^{+/+}$. n=4 vs 4.

Results

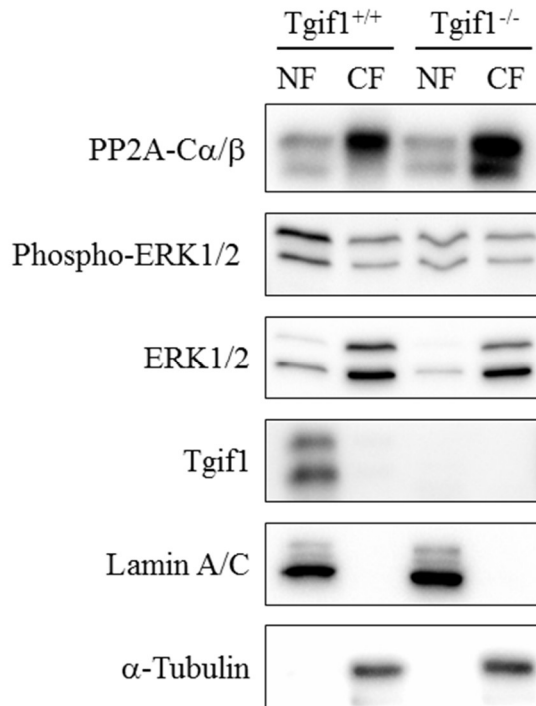


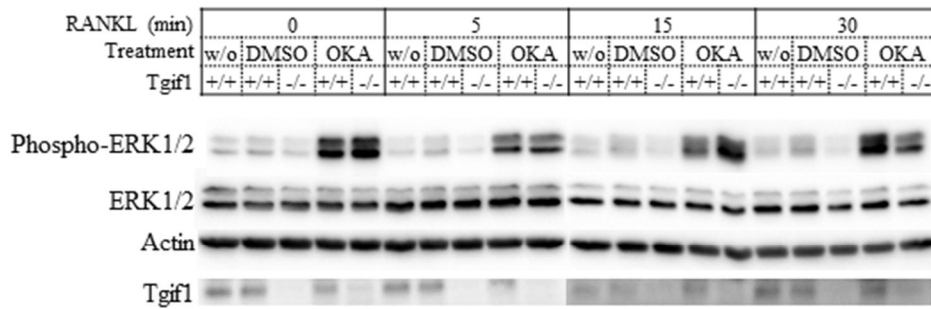
Fig. 4.19. PP2A catalytic subunit is increased in *Tgif1*^{-/-} osteoclast precursor cells. Western blot of PP2A catalytic subunit, phosphorylated ERK1/2 and ERK1/2 after nuclear/cytosol fractionation. Lamin A/C and α -tubulin is the control of a nuclear fraction and a cytosol fraction, respectively. NF; nuclear fraction, CF; cytosol fraction.

4.14 Okadaic acid (OKA)

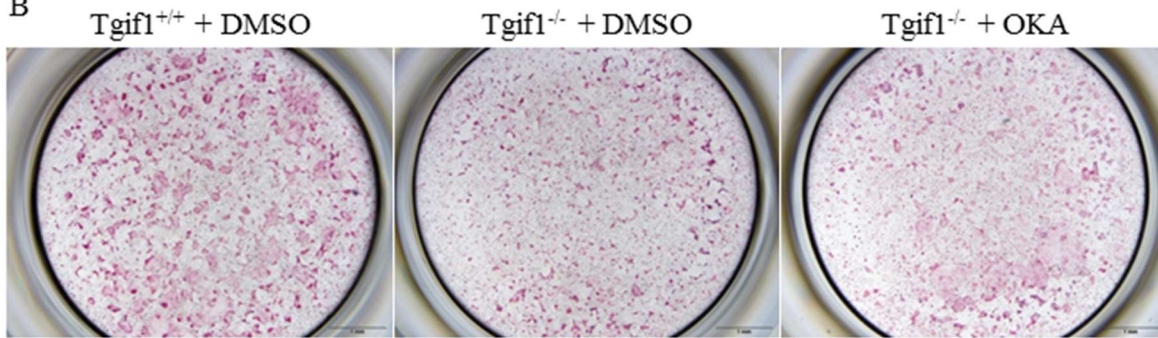
To investigate the functional interaction between *Tgif1* and PP2A in osteoclastogenesis, PP2A function was inhibited using okadaic acid (OKA), which is a well-known potent inhibitor of PP2A²⁸¹⁻²⁸⁴. Western blot analyses demonstrated that OKA increased the phosphorylation of ERK1/2 in both, wild type and *Tgif1*^{-/-} osteoclast precursors (Fig. 4.20.A). To address whether OKA treatment also restores the impaired differentiation of *Tgif1*^{-/-} osteoclasts, BMMs were treated with 1 μ M OKA for 30 minutes before RANKL stimulation was started and cultured up to 5 days for osteoclast differentiation. Images of TRAP staining were taken on culture day 4 to determine osteoclast differentiation (Fig. 4.20.B). Indeed, OKA treatment improved the impaired osteoclast differentiation of *Tgif1*-deficient osteoclasts on culture day 4. Osteoclast size, number of nuclei and number of nuclei per osteoclast were increased in *Tgif1*^{-/-} osteoclasts with OKA treatment compared to *Tgif1*^{-/-} osteoclasts without OKA treatment (Fig. 4.20.C). The

results demonstrate that inhibiting PP2A activity in *Tgif1*^{-/-} osteoclasts recovered the impaired osteoclast differentiation of *Tgif1*^{-/-} osteoclasts. This suggests that the abundance of PP2A-C causes a high PP2A activity downstream of RANKL or M-CSF stimulation, thereby impairing osteoclast differentiation in *Tgif1*-deficient osteoclasts.

A



B



C

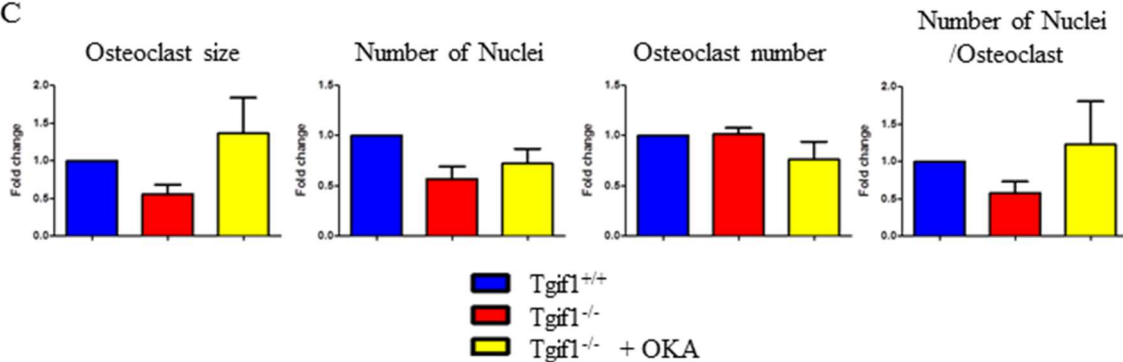


Fig. 4.20. PP2A inhibitor Okadaic acid restores the impaired ERK1/2 phosphorylation in *Tgif1*^{-/-} BMM and recovers the impaired differentiation of *Tgif1*^{-/-} osteoclasts. (A) Western blot of phosphorylated ERK1/2 and ERK1/2 after 1 μ M okadaic acid (OKA) treatment for 30 min. DMSO; Dimethylsulfoxid. w/o; no additives. (B) TRAP staining images of osteoclast differentiation on culture day 4 without OKA (DMSO only) or with 1 μ M OKA treatment before start differentiation. (C) Quantification of Panel B.

4.15 Silencing by GapmeR

In addition to the pharmacological rescue approach, we specifically silenced the PP2A catalytic subunit β using the GapmeR technology. Briefly, GapmeR is a stable short antisense oligonucleotide, which can bind to the targeted mRNA with high affinity and induce RNaseH to degrade the targeted mRNA thereby interrupting gene translation.

4.15.1 PP2A-C β -targeting GapmeR

Based on an EXIQON algorithm, PP2A-C β -targeting GapmeRs were designed (Fig. 4.21.A). Top 5 PP2A-C β -targeting GapmeRs (#1-#5) in the EXIQON design score rank were evaluated by qRT-PCR. Among the 5 tested PP2A-C β -targeting GapmeRs #1 and #2 strongly down-regulated PP2A-C β expression compared to other PP2A-C β -targeting GapmeRs (#3, #4 and #5) (Fig. 4.21.B). To test the specificity of the GapmeRs, the expression of PP2A-C α was analyzed by qRT-PCR. As shown in Figure 4.21.B (left), PP2A-C β -targeting GapmeR do affect the expression of PP2A-C α . After initial validation, GapmeR #2 was selected to be used in further experiments since it is efficient and relative specific.

To test the hypothesis that silencing PP2A-C β affects the amount of phosphorylated ERK1/2, osteoclast precursors were treated with PP2A-C β -targeting GapmeR for 72 hours, followed by western blot analysis. PP2A-C expression was decreased in the PP2A-C β -targeting GapmeR treatment group compared to non-targeting GapmeR (Fig. 4.21.C). In addition, phosphorylated ERK1/2 was increased in PP2A-C β -targeting GapmeR treatment group compared to non-targeting GapmeR treatment. This result suggests that PP2A-C β functions as a protein phosphatase in osteoclasts to regulate the abundance of phosphorylated ERK1/2.

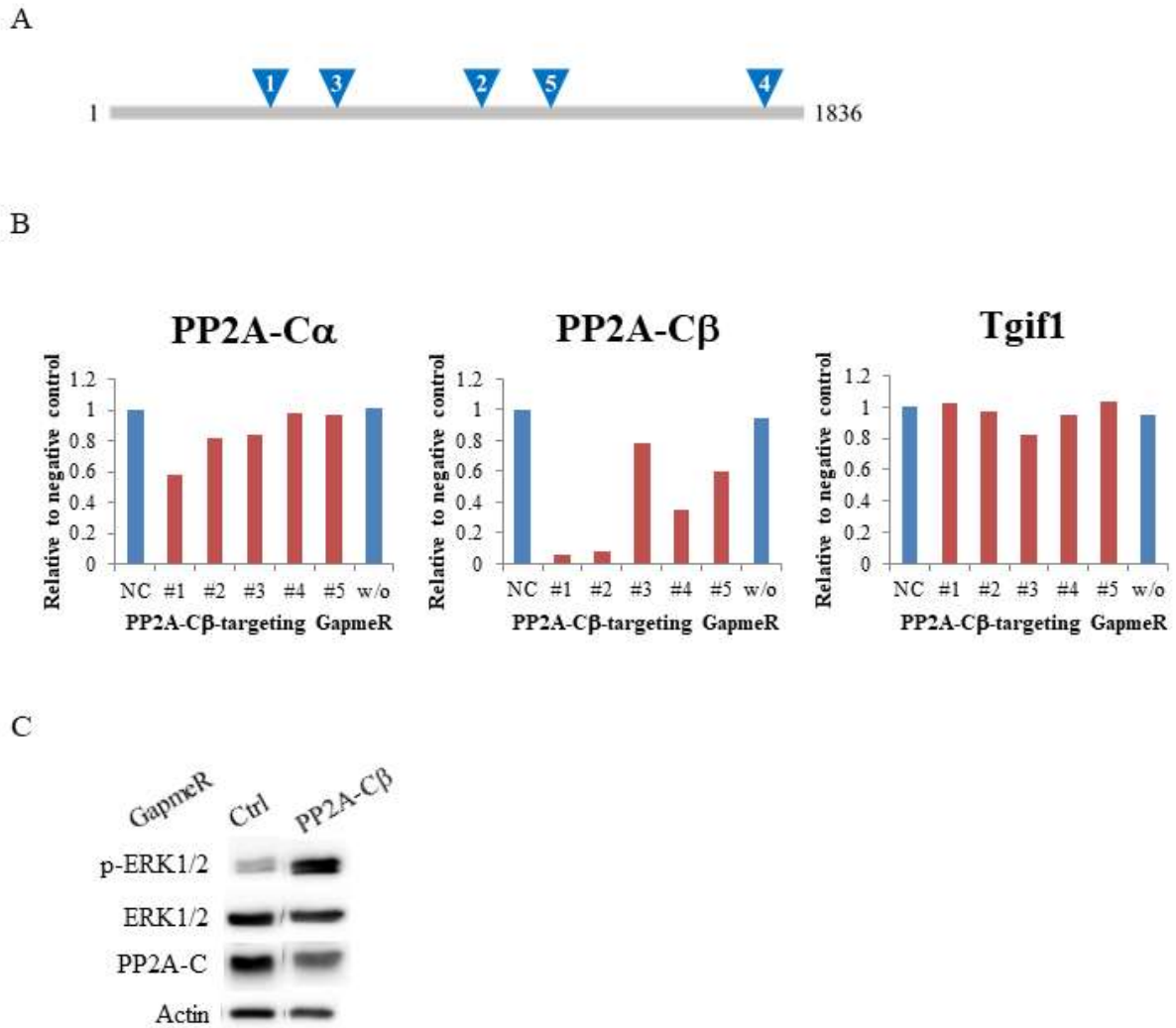


Fig. 4.21. Silencing of PP2A increases phosphorylated ERK1/2. (A) *In silico* GapmeR design (#1-5) for silencing of PP2A-C β . (B) PP2A-C α , PP2A-C β and Tgif1 mRNA expression quantified by qRT-PCR 35 hours after 1 μ M PP2A-C β -targeting GapmeR (#1-5) treatment. NC; negative control GapmeR. w/o; without GapmeRs. (C) Western blot of PP2A catalytic subunits (α and β), phosphorylated ERK1/2 and ERK1/2 expressions in osteoclast precursors for 72 hours with treatment of PP2A-C β -targeting GapmeR.

4.15.2 Tgif1-targeting GapmeR

To determine if targeted inhibition of PP2A-C β can restore the impaired osteoclast differentiation of Tgif1-deficiency, we next designed GapmeRs targeting Tgif1 using the EXIQON algorithm (Fig. 4.22.A). The efficiency of top 4 Tgif1-targeting GapmeRs (#1-#4) in the EXIQON design score rank was evaluated by qRT-PCR for Tgif1. To determine the specificity, expression of Tgif2 was also analyzed by qRT-PCR. Tgif1-targeting GapmeRs #3 and #4 were more efficient in down-regulating Tgif1 expression compared to the other Tgif1-

targeting GapmeRs (#1 and #2) (Fig. 4.22.B). Importantly, the results show that Tgif1-targeting GapmeRs are specific and do not target Tgif2. After validation of efficiency and specificity, we decided to pursue with Tgif1-targeting GapmeR #4.

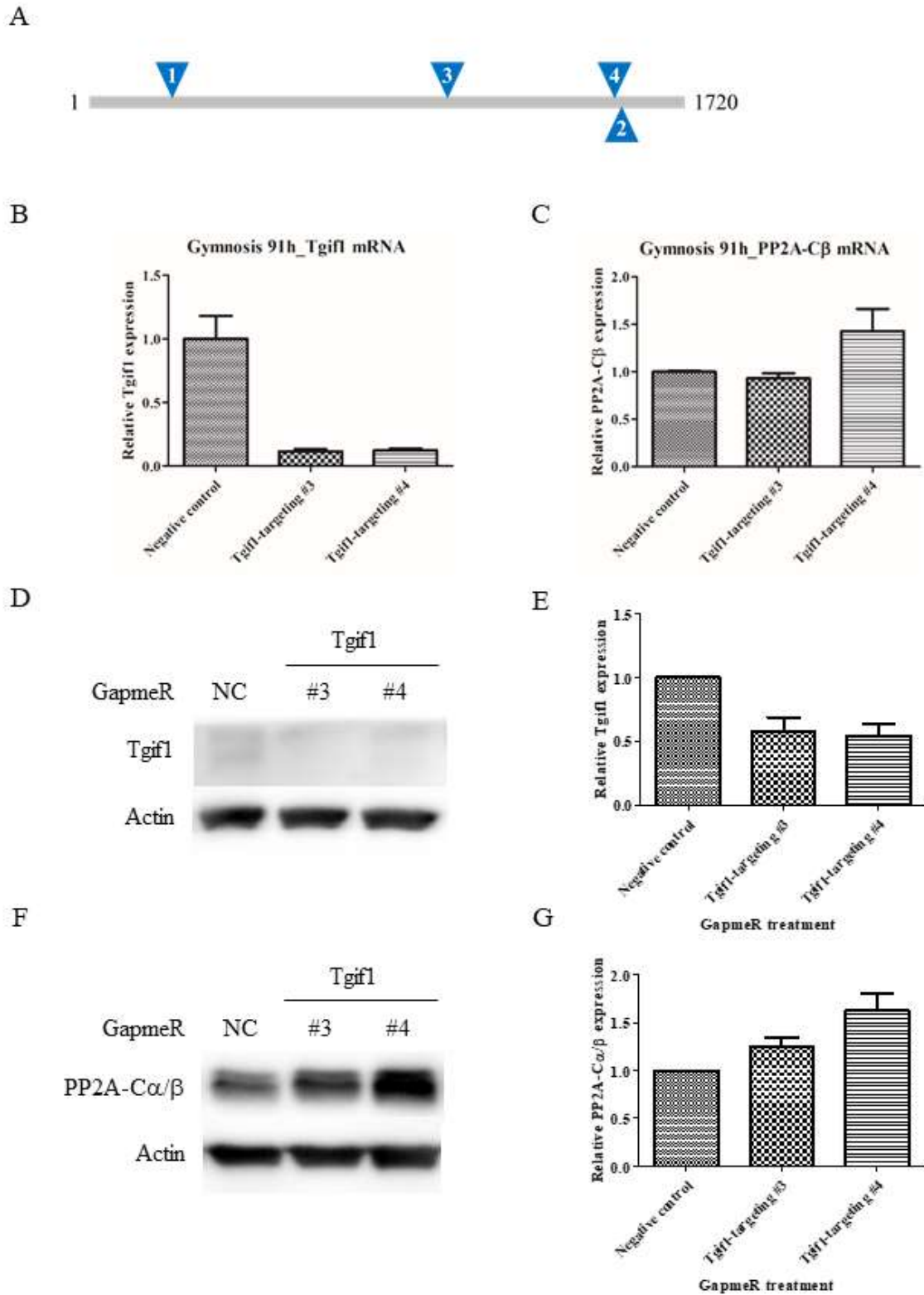


Fig. 4.22. Silencing of Tgfl increases the abundance of the catalytic subunit of PP2A. (A) *In silico* GapmeR design for silencing of Tgfl. (B) Tgfl mRNA expression 91 hours after Tgfl-targeting GapmeR quantified by qRT-PCR. Biological and technical duplicates. (C) PP2A-C β mRNA expression 91 hours after Tgfl-targeting GapmeR quantified by qRT-PCR. Biological and technical duplicates. (D) Western blot of Tgfl expression in osteoclast precursors for 72 hours with treatment of Tgfl-targeting GapmeR. (E) Quantification of Panel D. (F) Western blot of PP2A catalytic subunit (α and β) expression in osteoclast precursors for 72 hours with treatment of Tgfl-targeting GapmeR. (G) Quantification of Panel G. * $p < 0.05$.

4.15.3 Targeting Tgif1 and PP2A-C β using GapmeRs

To recapitulate the Tgif1 knockout osteoclast phenotype, osteoclast precursors were treated with Tgif1-targeting GapmeR. After 72 hours, Tgif1 expression in osteoclast precursors was decreased in Tgif1-targeting GapmeR treatment compared to non-targeting GapmeR treatment (Fig. 4.23.A). Moreover, PP2A-C expression was increased in Tgif1-targeting GapmeR treatment compared to non-targeting GapmeR treatment (Fig. 4.23.A). To test the effect of transient Tgif1 inhibition on osteoclast differentiation, osteoclasts were differentiated in the presence of Tgif1-targeting GapmeR for 4 days. Consistent with the results obtained from cells with germline deletion of Tgif1, osteoclast markers such as NFATc1, Src and Cathepsin K were decreased in Tgif1-targeting GapmeR treatment compared to non-targeting GapmeR (Fig. 4.23.B). Furthermore, Tgif1-targeting GapmeR led to an impaired osteoclast differentiation as determined by TRAP staining (Fig. 4.23.C). Interestingly, PP2A-C β -targeting GapmeR restored the impaired osteoclast differentiation of Tgif1-deficient osteoclasts (Tgif1-targeting GapmeR treatment) (Fig. 4.23.C). Quantification of the osteoclast parameters confirmed that the osteoclast size, the osteoclast number, the number of nuclei and the number of nuclei per osteoclast were significantly decreased in Tgif1-deficient osteoclasts (Tgif1-targeting GapmeR treatment) compared to non-targeting GapmeR treatment (Fig. 4.23.D). Interestingly, the osteoclast size, the number of nuclei and the number of nuclei per osteoclast were significantly increased by treating Tgif1-deficient osteoclasts with PP2A-C β -targeting GapmeRs. The osteoclast size and the number of nuclei were fully restored (Fig. 4.23.D). These specific gene silencing experiments confirm that Tgif1-deficiency increases the expression of PP2A-C β in osteoclasts, thereby impairing ERK1/2 activity and osteoclast differentiation.

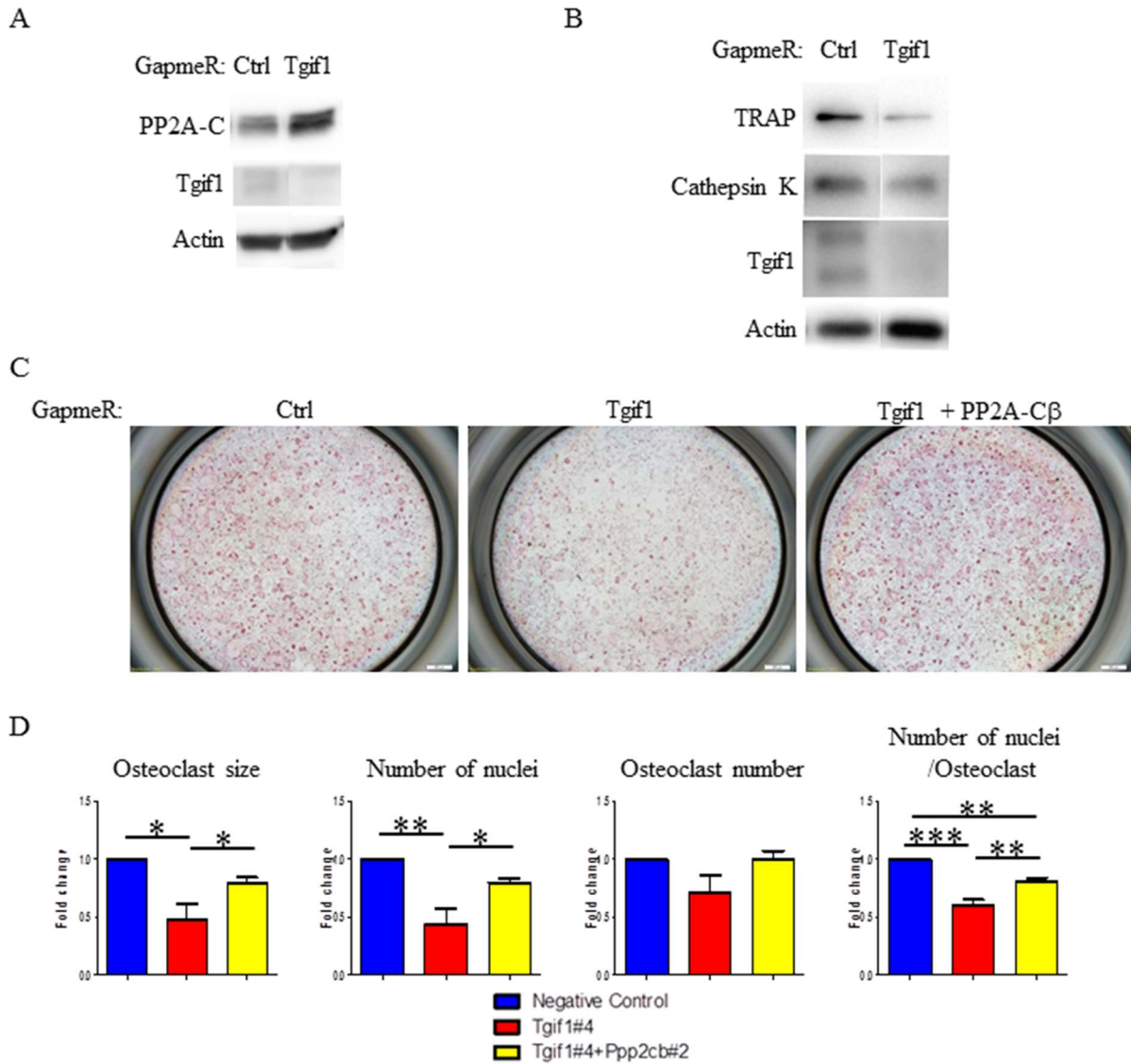


Fig. 4.23. Silencing of PP2A rescues the impaired differentiation of Tgfl-deficient osteoclasts. (A) Western blot of PP2A-C and Tgfl 72 hours after treatment with Tgfl-targeting GapmeR. (B) Western blot of osteoclast markers such as TRAP, Cathepsin K and Tgfl on osteoclast differentiation day 4 with treatment of Tgfl-targeting GapmeR. (C) TRAP staining of Tgfl^{+/+} osteoclasts with treatment of Tgfl-targeting GapmeR or with combination treatment of Tgfl-targeting GapmeR and PP2A-C β -targeting GapmeR on differentiation day 4. Scale bar; 200 μ m. (D) Quantification of Panel C. * $p < 0.05$, ** $p < 0.01$, *** $p < 0.001$.

4.16 *In silico* analysis of the PP2A-C β promoter

To examine if Tgfl interacts with the PP2A-C β promoter region to regulate its expression, *in silico* analysis was performed using the Promo3.0 software. The 2.1 kb upstream region of the transcription start site (TSS) of the PP2A-C β gene in chromosome 8 named Ppp2cb was

analyzed for the presence of TGIF binding sites. Five potential TGIF binding sites were found in the proximal promoter region of Ppp2cb as described in the table below (Table 4.1).

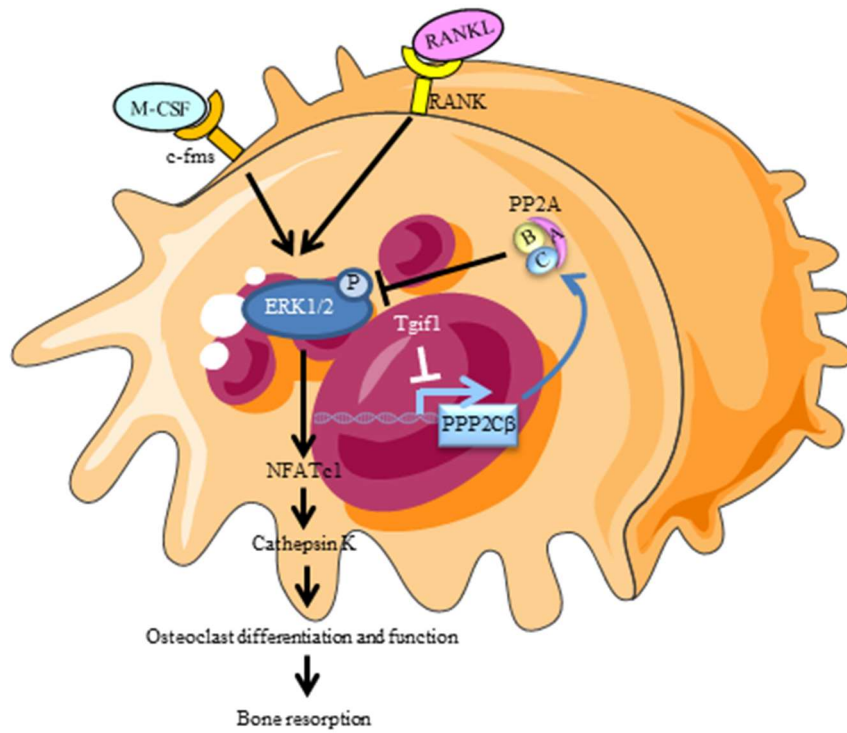
Table 4.1. Tgif1 potential binding sites on the promoter region of PP2A-C β gene (Ppp2cb)

5' - Sequence -3'		
-1899	TGACAAAC	-1892
-1242	TGACAAGA	-1235
-1209	TGACAAAT	-1202
-1158	TGACAAA	-1151
-390	TGACATAA	-383

This analysis revealed five potential TGIF binding sites in the promoter region of Ppp2cb. Three potential TGIF binding sites form one cluster -1.2 kb upstream of the TSS. One is -1.9 kb upstream and another one is -400 bp upstream of TSS. This result suggests that Tgif1 might bind to the promoter of Ppp2cb to regulate PP2A-C β expression.

In summary, Tgif1 regulates the expression of PP2A catalytic subunit β to sustain phosphorylated ERK1/2 in osteoclast precursors in response to RANKL or M-CSF stimulation, leading to osteoclast differentiation. Therefore, Tgif1-deficiency causes abundant PP2A-C β to dephosphorylate ERK1/2 upon RANKL or M-CSF stimulation, leading to an interruption of RANKL signaling and resulting in an impaired osteoclast differentiation. We propose that Tgif1 is a novel regulator of osteoclast differentiation, function and bone resorption (Fig. 4.24).

A



B

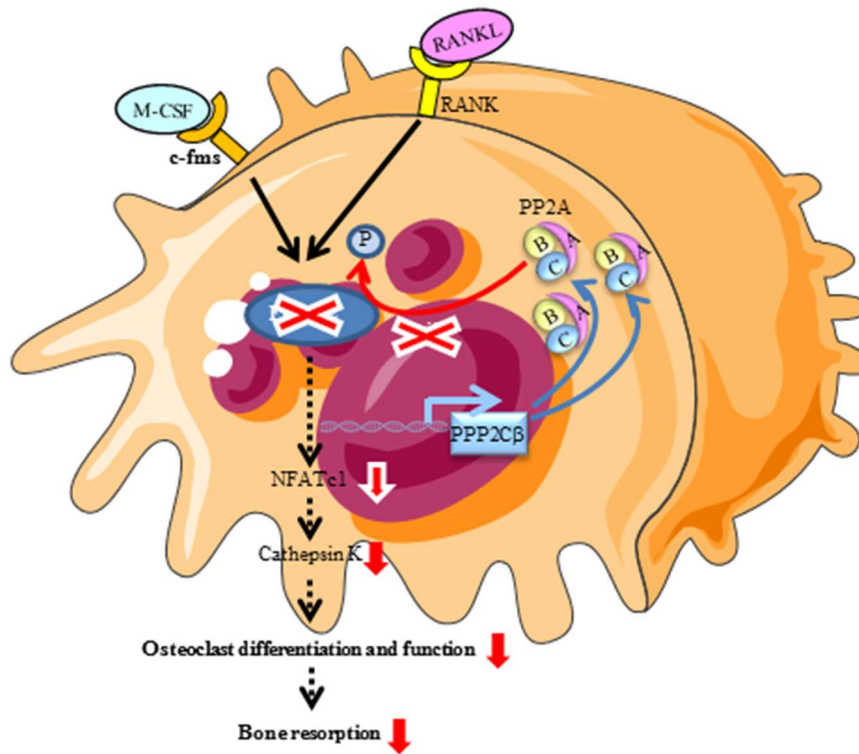


Fig. 4.24. Tgfb1 regulates PP2A-C β expression to sustain phosphorylated ERK1/2 downstream of RANKL and M-CSF stimulation. (A) Schematic image of the role of Tgfb1 in osteoclasts. In response to M-CSF or RANKL stimulation, Tgfb1 suppresses the expression of PP2A catalytic subunit to sustain phosphorylated ERK1/2, leading to osteoclast differentiation. (B) Schematic image of Tgfb1-deficiency model in osteoclasts. Deletion of Tgfb1 causes abundant PP2A catalytic subunit and promotes de-phosphorylation of ERK1/2, resulting in an interruption of signaling cascades downstream of M-CSF or RANKL, thereby impairing osteoclast differentiation.

5 Discussion

Aging-related bone loss is often caused by a decrease in osteoblast-mediated bone formation and an increase in osteoclast-dependent bone resorption. This unbalanced bone remodeling not only causes a decrease in bone mass but also impairs the bone micro-architecture. This condition is termed osteoporosis and may lead to fragility fractures, which are classically located at the wrist, the humerus, the spine and hip⁹. It has been estimated that 1 in 3 women and 1 in 5 men over 50 years of age will experience an osteoporotic fracture²⁸⁵. Furthermore, osteoporosis causes more than 8.9 million fractures each year worldwide, resulting in an osteoporotic fracture every 3 seconds. Once a fracture has occurred, the risk for subsequent fractures is greatly increased and each fracture is associated with a high morbidity and mortality³⁷. Thus, an early and sufficient treatment is of great importance for the patients. Treatment of osteoporosis includes a healthy life style with sports and exercise, sufficient calcium intake and an appropriate Vitamin D serum concentration⁹. If the fracture risk is deemed high for the next 10 years or if an osteoporotic fracture has occurred, specific osteoporosis drugs are needed for future fracture prevention. Specific treatment of osteoporosis includes anti-resorptive drugs that restrict the osteoclast activity like bisphosphonates or an anti-RANKL antibody (Denosumab). Alternatively, in severe cases of osteoporosis with prevalent fractures, augmenting the osteoblast activity in the context of an anabolic treatment the use of Teriparatide is another valuable approach²⁸⁶. Despite the available treatment options, the drugs that are used in the clinics have rare side effects like osteonecrosis of the jaw, atypical femoral fractures or other limitations and restrictions. Thus, more and better drugs are needed. In early 2019, it is expected that an anti-sclerostin antibody (Romosozumab; Evenity®, Amgen/UCB) will be available in the clinics. This antibody augments bone mass and decreases fractures due to the dual mechanism of increasing bone formation and decreasing bone resorption²⁵². Nevertheless, aging societies still need more treatment options beyond this innovation. To reach this goal, a better understanding of the mechanisms regulating bone

remodeling is needed as a base for future drug development. Basic research is necessary to provide these new insights into the underlying biological processes. This is why our laboratory is dedicated to unravel novel factors and mechanisms regulating bone turnover with the goal to better understand the biological principles that are behind the preservation of the function and integrity of the skeleton.

In this thesis, we identified an increased expression of the homeodomain protein TG-interacting factor 1 (Tgif1) during osteoclast differentiation and in response to RANKL and M-CSF stimulation, suggesting an important role of Tgif1 in osteoclast function and bone resorption. To test this hypothesis, we deleted Tgif1 in the germline (Tgif1^{-/-}) and in the osteoclast lineage (LysM-Cre⁺;Tgif1^{loxP/loxP} and Ctsk-Cre⁺;Tgif1^{loxP/loxP}). Interestingly, although young or aged LysM-Cre⁺;Tgif1^{loxP/loxP} mice did not demonstrate major changes in their bone phenotype, Ctsk-Cre⁺;Tgif1^{loxP/loxP} mice were protected from an aging-related decrease in bone mass due to a reduced osteoclast number and bone resorption. Furthermore, *in vitro* differentiation of bone marrow macrophages (BMMs) obtained from Tgif1^{-/-}, LysM-Cre⁺;Tgif1^{loxP/loxP} or Ctsk-Cre⁺;Tgif1^{loxP/loxP} mice demonstrated a decreased number and size of osteoclasts, fewer and more shallow resorption pits and a diminished expression of the osteoclast-related genes NFATc1, Src and Cathepsin K. These findings indicate that Tgif1 promotes osteoclast differentiation and function in a cell-autonomous manner and establish Tgif1 as a novel regulator of bone resorption. To elucidate the underlying molecular mechanism we performed signaling pathway analyses, which revealed less phosphorylated ERK1/2 in Tgif1^{-/-} BMMs upon stimulation with RANKL or M-CSF without affecting the activity of MEK1/2, a kinase that phosphorylates ERK1/2. This suggested that ERK1/2 might be rapidly de-phosphorylated in the absence of Tgif1, indicating that Tgif1 controls ERK1/2 activity by inhibiting the expression of a specific phosphatase. Indeed, expression analysis of several ERK phosphatases demonstrated an increased expression of the Protein Phosphatase 2A catalytic

subunit isoform β (PP2A-C β) in *Tgif1*^{-/-} BMMs compared to control cells. Mechanistically, pharmacological inhibition of PP2A using Okadaic acid or targeted silencing of the specific C β isoform using the GapmeR technology normalized the level of phosphorylated ERK1/2 in *Tgif1*^{-/-} BMMs. Furthermore, inhibition of PP2A activity restored the impaired differentiation of *Tgif1*^{-/-} BMMs, demonstrating that *Tgif1* promotes osteoclast differentiation in an ERK1/2-dependent manner. In summary, *Tgif1*-deficiency in osteoclasts reduces ERK1/2 signaling thereby inhibiting osteoclast function and bone resorption. Thus, *Tgif1* is a novel regulator of bone remodeling with an important function in aging-related bone loss.

Tgif1 has been reported to function as a transcriptional co-repressor in retinoic acid and TGF- β signaling^{287,288}. Since both pathways are also implicated in osteoclast function^{181,289-291}, the possibility exist that these two pathways may mediate at least some of the effects in osteoclast differentiation and function in the absence of *Tgif1*. However, we could not observe any difference in the expression of the TGF- β -induced gene PAI-1 or the phosphorylation of Smad2 between *Tgif1*^{-/-} or control osteoclast precursor cells. Furthermore, TGF- β signaling induces osteoclast apoptosis²⁹², but *Tgif1*-deficient osteoclasts undergo apoptosis later than control osteoclasts.

Retinoic acid signaling is restricted by *Tgif1* through the recruitment of CtBP to RXR α retinoid receptor. Since retinoic acids stimulates osteoclast activity and because *Tgif1*-deficient mice are expected to have an increased retinoic acid signaling activity, osteoclast function and the expression of osteoclast-related genes including NFATc1 and Cathepsin K should be increased in the absence of *Tgif1*. However, we found the opposite that osteoclast function and the expression of NFATc1 and Cathepsin K are decreased in *Tgif1*-deficient osteoclasts. Although these data do not fully exclude the participation of the TGF- β and retinoic acid signaling pathways in the phenotypic findings reported in this thesis, they greatly reduce the

likelihood of a major influence. It is possible that the implication of *Tgif1* in the regulation of TGF- β signaling is cell type- and context-dependent. For instance, although *Tgif1* suppresses TGF- β in various cell types such as hematopoietic stem cells²⁶⁰, MEFs (mouse embryonic fibroblasts)²⁸⁸, HL60 cells (human promyelocytic leukemia cells)²⁹³ and A549 cells (adenocarcinomic human alveolar basal epithelial cells)²⁹⁴, it seems to be largely dispensable for TGF- β signaling in murine osteoclasts.

Our *in vivo* data, in particular the data obtained from *Ctsk-Cre⁺;Tgif1^{loxP/loxP}* mice, firmly establish an important role of *Tgif1* in bone resorption and bone remodeling. Deletion of *Tgif1* *in vivo* under the control of the *Ctsk*-promoter attenuated the aging-related loss of bone mass due to an impaired osteoclast activity. We also investigated *LysM-Cre⁺;Tgif1^{loxP/loxP}* mice as another model of an osteoclast-targeted *Tgif1* deficiency. Although deletion of *Tgif1* under the control of the *LysM*-promoter caused a trend towards a higher bone mass in aged mice, this effect was not significant and the osteoclast activity was also not inhibited as it was in *Ctsk-Cre⁺;Tgif1^{loxP/loxP}* mice. Since the data obtained from *Tgif1^{-/-}* mice and all *in vitro* findings support an important role of *Tgif1* in osteoclast differentiation and function, it is very likely that the modest phenotype caused by the lack of *Tgif1* in *LysM-Cre⁺;Tgif1^{loxP/loxP}* mice is due to other circumstances. For instance, *Lysosome M* is expressed in cells of the myeloid lineage including macrophages, myeloblasts and neutrophils, while *Cathepsin K* is highly expressed in mature osteoclasts. This implies that the respective promoters used to drive the expression of the cre recombinase might be activated in different cell populations. This points to an important role of *Tgif1* in committed osteoclasts while its function in the myeloid cell lineage might be less critical. Overall, it is interesting to note that a higher bone mass phenotype in mice with an osteoclast-targeted *Tgif1*-deficiency appears rather at an older age than during growth and adolescence. This finding is difficult to interpret but it could be due to a high bone remodeling

rate with a relatively higher bone formation during growth, while during aging bone resorption is more prominent than bone formation and the main determinant of aging-related bone loss.

Actin ring formation during osteoclast differentiation is induced by RANK signaling and mediated by src to $\alpha_v\beta_3$ integrin^{275,295}. Tgif1-deficient osteoclasts have a reduced expression of src and an impaired formation of the actin ring until day 4 of culture compared to control. By day 5 of culture, expression of src and actin ring formation is similar to control cells, suggesting that the effect of Tgif1-deficiency on src expression and actin ring formation is only transient and potentially a consequence of the overall delayed differentiation of osteoclasts lacking Tgif1.

Deletion of Tgif1 in osteoclasts not only reduces osteoclast differentiation, it also impairs osteoclast fusion, which both could be dependent on each other. While increasing the number of control precursor cells stimulated cell fusion and increased the number of nuclei per osteoclast, Tgif1-deficient osteoclast precursor cells were resistant to fuse even if the cell density was increased. Expression of DC-STAMP, a regulator of cell fusion, was unchanged in the absence of Tgif1. This demonstrates that although Tgif1 is not a regulator of DC-STAMP expression, it still affects cell fusion by a different mechanism that has to be determined.

Despite all novel findings, this study leaves open some questions. Mechanistically, our data demonstrate that Tgif1 represses PP2A-C β expression. An *in silico* analysis of the PP2A-C β promoter region revealed five potential Tgif1 binding sites 2.1 kb upstream of the transcriptional start site. This implies that Tgif1 might associate with the promoter region of the PP2A-C β gene and regulate its expression. Nevertheless, a functional investigation using gene reporter assays with the wild type promoter sequence and disabled Tgif1 binding sites would be helpful to further address this question. Furthermore, the functional relevance if this

mechanism *in vivo* also needs to be determined using an appropriate animal model. However, these experiments are beyond the scope of this thesis and can be addressed in subsequent studies.

Taken together, *Tgif1* suppresses PP2A-C β expression and therefore sustains ERK1/2 signaling activity in response to RANKL and M-CSF stimulation, which is important for osteoclast differentiation and function. In the absence of *Tgif1*, osteoclasts are impaired in their differentiation capacity due to a high abundance of PP2A-C β . This causes a de-phosphorylation of ERK1/2 and decreases its signaling activity and therefore the expression of the downstream target genes NFATc1 and Cathepsin K, which are important for the osteoclast phenotype. The work presented here identified *Tgif1* as a key factor regulating osteoclast function and bone resorption and does therefore provide novel and important information on bone remodeling and skeletal integrity. This knowledge improves our understanding of bone biology and is likely to be of future value.

6 List of Abbreviations

6.1 Generic Abbreviations

Table 6.1. Generic Abbreviations

Abbreviation	Full name (<i>Origin of the name</i>)
A	
abs.	absolute
ADP	adenosine diphosphate
AG	Aktiengesellschaft (=public company)
Akt	protein kinase B (PKB), (<i>human homolog of transforming retrovirus identified from AKR mouse</i>)
ALP	alkaline phosphatase
α MEM	alpha-modified minimum essential medium
ANK	ankyrin repeat
ANOVA	analysis of variance
AP-1	activator protein-1
app.	approximately
APS	ammonium peroxydisulfate
ASBMR	American Society for Bone and Mineral Research
ATF4	activating transcription factor 4
ATP	adenosine triphosphate
B	
BCA	bicinchoninic acid
BD	Becton Dickinson Behörde für Gesundheit und Verbraucherschutz (=Authority for Health and
BGV	Consumer Protection)
BM	bone marrow
BMD	bone mineral density
BMM	bone marrow macrophage
BMP	bone morphogenetic protein
BMU	basic multicellular unit
bp	base pairs
BPO	benzoyl peroxide
BSA	bovine serum albumin
BSP	bone sialoprotein
C	
CAII	carbonic anhydrase II
cAMP	cyclic adenocine monophosphate
Cbfa1	core binding factor alpha 1
CD	cluster of differentiation
cDNA	complementary DNA
c-fms	colony-stimulating factor 1 receptor
c-Fos	cellular homolog of Finkel-Biskis-Jinkins (FBJ) murine osteosarcoma virus oncogene

List of Abbreviations

CFU	colony forming unit
CIC-7	chloride channel-7
CLP	common lymphoid progenitor
CMP	common myeloid progenitor
Corp.	corporation
CR3	complement receptor 3
Cre	cyclization recombination recombinase enzyme
CREB	cAMP response element-binding protein
Csk	C-terminal Src kinase
Ct	cycle threshold
CtBP	C-terminal-binding protein
C-terminal	carboxy(l)-terminal, COOH-terminal
CtsK	cathepsin K

D

Da	dalton
DABA	dual action bone agent
DAPI	4',6-diamidino-2-phenylindole
DC-STAMP	dendritic cell specific transmembrane protein
DE loop	aspartic acid-glutamic acid loop
dH ₂ O	distilled water
DMSO	dimethylsulfoxide
DNA	deoxyribonucleic acid
dNTP	deoxynucleoside triphosphate
DTT	dithiothreitol
DXA	dual-energy X-ray absorptiometry

E

e.g.	<i>exempli gratiā</i> (=for example)
ECL	enhanced chemiluminescence
ECM	extracellular matrix
ECTS	European Calcified Tissue Society
EDTA	ethylenediaminetetraacetic acid
EFF	Endocrine Fellows Foundation
ERK	extracellular signal-regulated kinase
<i>et al.</i>	<i>et alii</i> (masculine plural), <i>et aliae</i> (feminine plural), <i>et alia</i> (neuter plural) (=and others)
<i>etc.</i>	<i>et cetera</i> (=and so on)
ETA1	early T-cell activation 1

F

FACS	fluorescence activated cell sorting
FAK	focal adhesion kinase
FBS	fetal bovine serum
FDA	Food and Drug Administration

Fig.	figure
Fra	Fos-related antigen
fwd	forward
G	
GAPDH	glyceraldehyde-3-phosphate dehydrogenase
GFP	green fluorescent protein
GmbH	Gesellschaft mit beschränkter Haftung (=Company with limited liability)
GM-CFU	granuloma macrophage colony forming units
GRB2	growth factor receptor bound protein 2
H	
HBSS	Hank's Balanced Salt Solution
HDAC	histone deacetylase
HE	haematoxylin and eosin
HEPES	2-[4-(2-hydroxyethyl)piperazin-1-yl]ethanesulfonic acid
hi.	high
HPE	holoprosencephaly
HR	high resolution
HRP	horseradish peroxidase
HRT	hormone replacement therapy
HSC	hematopoietic stem cell
I	
i.e.	<i>id est</i> (=that is)
i.p.	intraperitoneal injection
IC50	half maximal inhibitory concentration
ICAM-1	intercellular adhesion molecule 1
IF	immunofluorescence
IFN	interferon
IgG	immunoglobulin G
I κ B	inhibitor of NF- κ B
IKK	inhibitor of NF- κ B (I κ B) kinase
IL	interleukin
Inc.	incorporated
J	
JNK	c-Jun N-terminal kinase
K	
kb	kilo base pairs
kDa	kilo dalton
KO	knockout
L	
LNA	locked nucleic acid
lncRNA	long non-coding RNA

List of Abbreviations

lo.	low
loxP	locus of crossover P1 bacteriophage
Lrp	lipoprotein-related protein
Ltd.	limited
LysM	lysosome M
M	
Mac-1	macrophage-1 antigen
MAP	mitogen-activated protein
MAPK	mitogen-activated protein kinase
MATH	meprin and TRAF homology
M-CSF	macrophage-colony stimulating factor
μCT	micro-computed tomography
MEF	mouse embryonic fibroblast
Mef	myeloid Elf-1 like factor
MEK	mitogen-activated protein kinase kinase
MEP	megakaryocyte-erythrocyte progenitor
MH2	Mad homology 2
min	minute(s)
MITF	microphthalmia-associated transcription factor
MKK	MAPK-related kinase
MMA	methyl methacrylate
MMP-9	matrix metalloproteinase-9
MNC	multi-nucleated cell
MPP	multipotent progenitor
mRNA	messenger RNA
MSC	mesenchymal stem cell
Mst	Mammalian Sterile 20-like
MW	molecular weight
N	
NCBI	National Center for Biotechnology Information (<i>NIH</i>)
NFAT	nuclear factor of activated T cells
NF-κB	nuclear factor-κB
NHR	NFAT-homology region
NIH	National Institutes of Health
NIK	NF-κB-inducing kinase
NLS	nuclear localization signal/sequence
NP-40	nonidet P-40 (octyl phenoxypolyethoxyethanol)
N-terminal	amino-terminal, NH ₂ -terminal
O	
OC	osteoclast
OC-STAMP	osteoclast stimulatory transmembrane protein
OKA	okadaic acid

List of Abbreviations

OPG	osteoprotegerin
OPN	osteopontin
Osx	osterix
OVX	overiectomy
<i>P</i>	
p-	phosphorylated
P/S	Penicillin/Streptomycin
p38	protein 38
PAGE	polyacrylamide gel electrophoresis
PAI-1	plasmitogen activator inhibitor type-1
PBS	phosphate-buffered saline
PCR	polymerase chain reaction
pH	<i>(power of hydrogen)</i>
Pi	inorganic phosphate
PI3K	Phosphoinositide 3-kinase
PLDLS motif	Proline-Leucine-Aspartate-Leucine-Serine motif
PP	protein phosphatase
PP2A-C	protein phosphatase 2A catalytic subunit
PS bond	phosphorothioate bond
PTH	parathyroid hormone
PTH1R	parathyroid hormone 1 receptor, parathyroid hormone/paratyroid hormone-related peptide receptor
PTHrP	parathyroid hormone-related protein/peptide
PTP	protein-tyrosine phosphatase
<i>p</i> -value	probability value
PVDF	polyvinylidene fluoride
PYK	preotein tyrosine kinase
<i>Q</i>	
qRT-PCR	quantitative reverse transcription polymerase chain reaction
<i>R</i>	
RANK	receptor activator of NF- κ B
RANKL	receptor activator of NF- κ B ligand
RD	repression domain
rev	reverse
RGD	Arginine-Glycine-Aspartate
RHD	Rel homology domain
RHR	Rel-homology region
RIPA	radio-immunoprecipitation assay
RNA	ribonucleic acid
RNase	ribonuclease
ROI	region of interest
RSK	ribosomal S6 kinase

List of Abbreviations

RT	room temperature
RT	reverse transcription
Runx	Runt-related transcription factor
RXR α	Retinoid X receptor alpha
RZF	ring and zinc finger
S	
s.c.	subcutaneous injection
SARM	selective androgen receptor modulator
SD	standard deviation
SDS	sodium dodecyl sulfate
SDS-PAGE	sodium dodecyl sulfate - polyacrylamide gel electrophoresis
sec	second(s)
SEM	scanning electron microscopy
SERM	selective estrogen receptor modulator
SH	Src homology
SHH	sonic hedgehog
Smad	Sma and Mad related (protein)
SNIP1	Smad nuclear interacting protein
Sox	Sry-related HMG (high mobility group) box
Sp	specificity protein
SPP1	secreted phosphoprotein 1
T	
TA	transcriptional activation
TAB	TAK-1 binding protein
TAE	Tris base/Acetate/ EDTA
TAK1	TGF- β -activated kinase 1
TALE	three-amino-acid loop extension
Taq	Thermus aquaticus
Tbp	TATA-binding protein
TBS	tris-buffered saline
TBS-T	tris-buffered saline with tween 20
Tcf	tanscription factor
TEMED	<i>N,N,N',N'</i> -tetramethylethylenediamine
TFE3	transcription factor E3
TGF- β	transforming growth factor- β
Tgif	TG-interacting factor, TGF- β -induced factor
TGS	Tris/Glycine/SDS
TLR	Toll-like receptor
TM	Trademark
Tm	melting temperature
TNF	tumor necrosis factor
TonEBP	tonicity-responsive enhancer-binding protein
TRAF	TNF receptor-associated factor

TRAIL	TNF-related apoptosis-inducing ligand
TRAP	tartrate resistant acid phosphatase
Tris	tris-hydroxymethyl-aminomethane
TSS	transcription starting site
U	
U	unit
Ubc	ubiquitin-conjugating enzyme
Uev	ubiquitin-conjugating enzyme variant
UKE	Universitätsklinikum Hamburg-Eppendorf (University Medical Center Hamburg-Eppendorf)
US	United States
UV	ultraviolet
V	
v-ATPase	vacuolar-type H ⁺ -ATPase
vs	versus
W	
WB	western blot
WD	tryptophan-aspartic acid (dipeptide)
WHO	World Health Organization
Wnt	(<i>wingless</i> + <i>int-1</i>)
WT	wild type
#	
®	registered
2D	two dimensional
3D	three dimensional

6.2 Abbreviations in Histomorphometry

Table 6.2. Abbreviations in Histomorphometry

Abbreviation	Parameter	Units
B.Ar	bone area	mm ²
B.Pm	bone perimeter	µm
BFR/BS	Bone formation rate/bone surface	µm ³ /µm ² /day
BFR/BV	Bone formation rate/bone volume	%/year
BS/TV	bone surface/total volume	mm ² /mm ³
BV/TV	bone volume/total volume	%
Ct.Po	cortical porosity	%
Ct.Th	cortical thickness	µm
ES/BS	eroded surface/bone surface	%
MAR	mineral apposition rate	µm/day
MS/BS	mineralizing surface/bone surface	%

List of Abbreviations

MS/OS	mineralizing surface/osteoid surface	%
N.Ob/B.Pm	osteoblast number/bone perimeter	/μm
N.Ob/BS	osteoblast number/bone surface	/mm
N.Oc/B.Pm	osteoclast number/bone perimeter	/μm
N.Oc/T.A	osteoclast number/tissue area	/mm ²
O.Th	osteoid thickness	μm
Ob.S/BS	osteoblast surface/bone surface	%
Oc.S/BS	osteoclast surface/bone surface	%
OS/BS	osteoid surface/bone surface	%
OV/BV	osteoid volume/bone volume	%
T.Ar	tissue area	mm ²
Tb.N	trabecular number	mm
Tb.Sp.	trabecular separation	mm
Tb.Th.	trabecular thickness	mm

6.3 Abbreviations of Peptide sequence/Amino acid sequence

Table 6.3. Abbreviations of Peptide sequence

Alphabet	Abbreviation	Amino acid
A	Ala	Alanine
R	Arg	Arginine
N	Asn	Asparagine
D	Asp	Aspartic acid (Aspartate)
C	Cys	Cysteine
Q	Gln	Glutamine
E	Glu	Glutamic acid (Glutamate)
G	Gly	Glycine
H	His	Histidine
I	Ile	Isoleucine
L	Leu	Leucine
K	Lys	Lysine
M	Met	Methionine
F	Phe	Phenylalanine
P	Pro	Proline
S	Ser	Serine
T	Thr	Threonine
W	Trp	Tryptophan
Y	Tyr	Tyrosine
V	Val	Valine
B	Asx	Aspartic acid (Asparagine)
Z	Glx	Glutamic acid (Glutamine)
X	Xaa	Any amino acid.

7 Bibliography

1. Loveridge, N. Bone: more than a stick. *J. Anim. Sci.* **77 Suppl 2**, 190–6 (1999).
2. Taichman, R. S. Blood and bone: two tissues whose fates are intertwined to create the hematopoietic stem-cell niche. *Blood* **105**, 2631–9 (2005).
3. Quarles, L. D. Endocrine functions of bone in mineral metabolism regulation. *J. Clin. Invest.* **118**, 3820–3828 (2008).
4. DiGirolamo, D. J., Clemens, T. L. & Kousteni, S. The skeleton as an endocrine organ. *Nat. Rev. Rheumatol.* **8**, 674–683 (2012).
5. Manolagas, S. C. Birth and Death of Bone Cells: Basic Regulatory Mechanisms and Implications for the Pathogenesis and Treatment of Osteoporosis ¹. *Endocr. Rev.* **21**, 115–137 (2000).
6. Bar-Shavit, Z. The osteoclast: A multinucleated, hematopoietic-origin, bone-resorbing osteoimmune cell. *J. Cell. Biochem.* **102**, 1130–1139 (2007).
7. Wei, Y. & Sun, Y. Aging of the Bone. in *Advances in experimental medicine and biology* **1086**, 189–197 (2018).
8. Clarke, B. Normal Bone Anatomy and Physiology. *Clin. J. Am. Soc. Nephrol.* **3**, S131–S139 (2008).
9. Korkia, P. Osteoporosis: process, prevention, and treatment. *J. Bodyw. Mov. Ther.* **6**, 156–169 (2002).
10. Ascenzi, M.-G. & Roe, A. K. The osteon: the micromechanical unit of compact bone. *Front. Biosci. (Landmark Ed.)* **17**, 1551–81 (2012).
11. L Newton, A., J Hanks, L., Davis, M. & Casazza, K. The relationships among total body fat, bone mineral content and bone marrow adipose tissue in early-pubertal girls. *Bonekey Rep.* **2**, 315 (1-7) (2013).
12. Moore, S. G. & Dawson, K. L. Red and yellow marrow in the femur: age-related changes in appearance at MR imaging. *Radiology* **175**, 219–223 (1990).
13. Waitches, G., Zawin, J. K. & Poznanski, A. K. Sequence and rate of bone marrow conversion in the femora of children as seen on MR imaging: Are accepted standards accurate? *Am. J. Roentgenol.* **162**, 1399–1406 (1994).
14. Ellis, R. E. The Distribution of Active Bone Marrow in the Adult. *Phys. Med. Biol.* **5**, 255–258 (1961).
15. Cristy, M. Active bone marrow distribution as a function of age in humans. *Phys. Med. Biol.* **26**, 389–400 (1981).
16. Ornitz, D. M. & Marie, P. J. FGF signaling pathways in endochondral and intramembranous bone development and human genetic disease. *Genes Dev.* **16**, 1446–65 (2002).
17. Karaplis, A. C. Embryonic Development of Bone and Regulation of Intramembranous and Endochondral Bone Formation. in *Principles of Bone Biology. 3rd Edition* 53–84 (Academic Press, 2008). doi:10.1016/B978-0-12-373884-4.00025-2
18. McKibbin, B. The biology of fracture healing in long bones. *J. Bone Joint Surg. Br.* **60–B**, 150–62 (1978).
19. Schindeler, Aaron; McDonald, Michelle; Bokko, Paul; Little, D. Bone remodeling during fracture repair: The cellular picture. *Semin. Cell Dev. Biol.* **19**, 459–466 (2008).
20. Raisz, L. G. Physiology and pathophysiology of bone remodeling. *Clin. Chem.* **45**, 1353–8 (1999).
21. HADJIDAKIS, D. J. & ANDROULAKIS, I. I. Bone Remodeling. *Ann. N. Y. Acad. Sci.* **1092**, 385–396 (2006).
22. Franz-Odenaal, T. A., Hall, B. K. & Witten, P. E. Buried alive: How osteoblasts become osteocytes. *Dev. Dyn.* **235**, 176–190 (2006).
23. Dallas, S. L. & Bonewald, L. F. Dynamics of the transition from osteoblast to osteocyte.

- Ann. N. Y. Acad. Sci.* **1192**, 437–443 (2010).
24. Jilka, R. L., Weinstein, R. S., Bellido, T., Parfitt, A. M. & Manolagas, S. C. Osteoblast Programmed Cell Death (Apoptosis): Modulation by Growth Factors and Cytokines. *J. Bone Miner. Res.* **13**, 793–802 (1998).
 25. Yasuda, H. *et al.* Osteoclast differentiation factor is a ligand for osteoprotegerin/osteoclastogenesis-inhibitory factor and is identical to TRANCE/RANKL. *Proc. Natl. Acad. Sci. U. S. A.* **95**, 3597–602 (1998).
 26. Lacey, D. . *et al.* Osteoprotegerin Ligand Is a Cytokine that Regulates Osteoclast Differentiation and Activation. *Cell* **93**, 165–176 (1998).
 27. Katagiri, T. & Takahashi, N. Regulatory mechanisms of osteoblast and osteoclast differentiation. *Oral Dis.* **8**, 147–159 (2002).
 28. Sims, N. A. & Martin, T. J. Coupling the activities of bone formation and resorption: a multitude of signals within the basic multicellular unit. *Bonekey Rep.* **3**, #481 (2014).
 29. Henriksen, K., Neutzky-Wulff, A. V., Bonewald, L. F. & Karsdal, M. A. Local communication on and within bone controls bone remodeling. *Bone* **44**, 1026–1033 (2009).
 30. Bachrach, L. K. Acquisition of optimal bone mass in childhood and adolescence. *Trends Endocrinol. Metab.* **12**, 22–28 (2001).
 31. Seeman, E. & Delmas, P. D. Bone Quality — The Material and Structural Basis of Bone Strength and Fragility. *N. Engl. J. Med.* **354**, 2250–2261 (2006).
 32. Harada, S. & Rodan, G. A. Control of osteoblast function and regulation of bone mass. *Nature* **423**, 349–355 (2003).
 33. Boskey, A. L. & Imbert, L. Bone quality changes associated with aging and disease: a review. *Ann. N. Y. Acad. Sci.* **1410**, 93–106 (2017).
 34. Recker, R. R. *et al.* Static and tetracycline-based bone histomorphometric data from 34 normal postmenopausal females. *J. Bone Miner. Res.* **3**, 133–144 (2009).
 35. Kanis, J. A., Melton, L. J., Christiansen, C., Johnston, C. C. & Khaltaev, N. The diagnosis of osteoporosis. *J. Bone Miner. Res.* **9**, 1137–1141 (1994).
 36. Johnell, O. & Kanis, J. A. An estimate of the worldwide prevalence and disability associated with osteoporotic fractures. *Osteoporos. Int.* **17**, 1726–33 (2006).
 37. Bliuc, D. *et al.* Mortality Risk Associated With Low-Trauma Osteoporotic Fracture and Subsequent Fracture in Men and Women. *JAMA* **301**, 513–521 (2009).
 38. World Health Organization. Assessment of fracture risk and its application to screening for postmenopausal osteoporosis: Synopsis of a WHO report. *World Health Organization Technical Report Series* **843**, 1–129 (1994).
 39. Fitzpatrick, L. A. Secondary Causes of Osteoporosis. *Mayo Clin. Proc.* **77**, 453–468 (2002).
 40. Walsh, L. J., Wong, C. A., Pringle, M. & Tattersfield, A. E. Use of oral corticosteroids in the community and the prevention of secondary osteoporosis: a cross sectional study. *BMJ* **313**, 344–6 (1996).
 41. Harvey, N., Dennison, E. & Cooper, C. Osteoporosis: impact on health and economics. *Nat. Rev. Rheumatol.* **6**, 99–105 (2010).
 42. Stark, Z. & Savarirayan, R. Osteopetrosis. *Orphanet J. Rare Dis.* **4**, 5 (2009).
 43. Jochum, W. *et al.* Increased bone formation and osteosclerosis in mice overexpressing the transcription factor Fra-1. *Nat. Med.* **6**, 980–984 (2000).
 44. Suda, T. *et al.* Modulation of osteoclast differentiation and function by the new members of the tumor necrosis factor receptor and ligand families. *Endocr. Rev.* **20**, 345–57 (1999).
 45. Nakashima, T., Hayashi, M. & Takayanagi, H. New insights into osteoclastogenic signaling mechanisms. *Trends Endocrinol. Metab.* **23**, 582–590 (2012).

46. Khosla, S. Minireview: The OPG/RANKL/RANK System. *Endocrinology* **142**, 5050–5055 (2001).
47. Boyle, W. J., Simonet, W. S. & Lacey, D. L. Osteoclast differentiation and activation. *Nature* **423**, 337–342 (2003).
48. Roskoski, R. ERK1/2 MAP kinases: Structure, function, and regulation. *Pharmacol. Res.* **66**, 105–143 (2012).
49. He, Y. *et al.* Erk1 positively regulates osteoclast differentiation and bone resorptive activity. *PLoS One* **6**, e24780 (2011).
50. Hotokezaka, H. *et al.* U0126 and PD98059, specific inhibitors of MEK, accelerate differentiation of RAW264.7 cells into osteoclast-like cells. *J. Biol. Chem.* **277**, 47366–72 (2002).
51. Franzoso, G. *et al.* Requirement for NF-kappaB in osteoclast and B-cell development. *Genes Dev.* **11**, 3482–96 (1997).
52. Xing, L. *et al.* NF-κB p50 and p52 Expression Is Not Required for RANK-Expressing Osteoclast Progenitor Formation but Is Essential for RANK- and Cytokine-Mediated Osteoclastogenesis. *J. Bone Miner. Res.* **17**, 1200–1210 (2002).
53. Grigoriadis, A. E. *et al.* c-Fos: a key regulator of osteoclast-macrophage lineage determination and bone remodeling. *Science* **266**, 443–8 (1994).
54. Karin, M., Cao, Y., Greten, F. R. & Li, Z.-W. NF-κB in cancer: from innocent bystander to major culprit. *Nat. Rev. Cancer* **2**, 301–310 (2002).
55. David, J.-P., Sabapathy, K., Hoffmann, O., Idarraga, M. H. & Wagner, E. F. JNK1 modulates osteoclastogenesis through both c-Jun phosphorylation-dependent and -independent mechanisms. *J. Cell Sci.* **115**, 4317–25 (2002).
56. Yamamoto, A. *et al.* Possible Involvement of IκB Kinase 2 and MKK7 in Osteoclastogenesis Induced by Receptor Activator of Nuclear Factor κB Ligand. *J. Bone Miner. Res.* **17**, 612–621 (2002).
57. Mansky, K. C., Sankar, U., Han, J. & Ostrowski, M. C. Microphthalmia transcription factor is a target of the p38 MAPK pathway in response to receptor activator of NF-kappa B ligand signaling. *J. Biol. Chem.* **277**, 11077–83 (2002).
58. Matsumoto, M. *et al.* Essential role of p38 mitogen-activated protein kinase in cathepsin K gene expression during osteoclastogenesis through association of NFATc1 and PU.1. *J. Biol. Chem.* **279**, 45969–79 (2004).
59. Kikuta, J. & Ishii, M. Osteoclast migration, differentiation and function: novel therapeutic targets for rheumatic diseases. *Rheumatology* **52**, 226–234 (2013).
60. Hill, T. P., Später, D., Taketo, M. M., Birchmeier, W. & Hartmann, C. Canonical Wnt/β-Catenin Signaling Prevents Osteoblasts from Differentiating into Chondrocytes. *Dev. Cell* **8**, 727–738 (2005).
61. Day, T. F., Guo, X., Garrett-Beal, L. & Yang, Y. Wnt/β-Catenin Signaling in Mesenchymal Progenitors Controls Osteoblast and Chondrocyte Differentiation during Vertebrate Skeletogenesis. *Dev. Cell* **8**, 739–750 (2005).
62. Chen, G., Deng, C. & Li, Y.-P. TGF-β and BMP signaling in osteoblast differentiation and bone formation. *Int. J. Biol. Sci.* **8**, 272–88 (2012).
63. Rahman, M. S., Akhtar, N., Jamil, H. M., Banik, R. S. & Asaduzzaman, S. M. TGF-β/BMP signaling and other molecular events: regulation of osteoblastogenesis and bone formation. *Bone Res.* **3**, 15005 (2015).
64. Wu, M., Chen, G. & Li, Y.-P. TGF-β and BMP signaling in osteoblast, skeletal development and bone formation, homeostasis and disease. *Bone Res.* **4**, 16009 (2016).
65. Bonewald, L. F. The amazing osteocyte. *J. Bone Miner. Res.* **26**, 229–238 (2011).
66. Bonewald, L. F. & Johnson, M. L. Osteocytes, mechanosensing and Wnt signaling. *Bone* **42**, 606–615 (2008).

67. Nakashima, T. *et al.* Evidence for osteocyte regulation of bone homeostasis through RANKL expression. *Nat. Med.* **17**, 1231–4 (2011).
68. Xiong, J. & O'Brien, C. A. Osteocyte RANKL: new insights into the control of bone remodeling. *J. Bone Miner. Res.* **27**, 499–505 (2012).
69. Winkler, D. G. *et al.* Osteocyte control of bone formation via sclerostin, a novel BMP antagonist. *EMBO J.* **22**, 6267–76 (2003).
70. Li, X. *et al.* Sclerostin binds to LRP5/6 and antagonizes canonical Wnt signaling. *J. Biol. Chem.* **280**, 19883–7 (2005).
71. Fakhry, M., Hamade, E., Badran, B., Buchet, R. & Magne, D. Molecular mechanisms of mesenchymal stem cell differentiation towards osteoblasts. *World J. Stem Cells* **5**, 136 (2013).
72. Komori, T. Animal models for osteoporosis. *Eur. J. Pharmacol.* **759**, 287–294 (2015).
73. Kawane, T. *et al.* Dlx5 and Mef2 Regulate a Novel Runx2 Enhancer for Osteoblast-Specific Expression. *J. Bone Miner. Res.* **29**, 1960–1969 (2014).
74. Nakashima, K. *et al.* The novel zinc finger-containing transcription factor osterix is required for osteoblast differentiation and bone formation. *Cell* **108**, 17–29 (2002).
75. Ulsamer, A. *et al.* BMP-2 Induces Osterix Expression through Up-regulation of Dlx5 and Its Phosphorylation by p38. *J. Biol. Chem.* **283**, 3816–3826 (2008).
76. Xiao, G. *et al.* Cooperative Interactions between Activating Transcription Factor 4 and Runx2/Cbfa1 Stimulate Osteoblast-specific Osteocalcin Gene Expression. *J. Biol. Chem.* **280**, 30689–30696 (2005).
77. Yu, S. *et al.* Critical Role of Activating Transcription Factor 4 in the Anabolic Actions of Parathyroid Hormone in Bone. *PLoS One* **4**, e7583 (2009).
78. Yang, X. *et al.* ATF4 Is a Substrate of RSK2 and an Essential Regulator of Osteoblast Biology: Implication for Coffin-Lowry Syndrome. *Cell* **117**, 387–398 (2004).
79. Brunkow, M. E. *et al.* Bone Dysplasia Sclerosteosis Results from Loss of the SOST Gene Product, a Novel Cystine Knot-Containing Protein. *Am. J. Hum. Genet.* **68**, 577–589 (2001).
80. Balemans, W. *et al.* Increased bone density in sclerosteosis is due to the deficiency of a novel secreted protein (SOST). *Hum. Mol. Genet.* **10**, 537–544 (2001).
81. Bellido, T. *et al.* Chronic Elevation of Parathyroid Hormone in Mice Reduces Expression of Sclerostin by Osteocytes: A Novel Mechanism for Hormonal Control of Osteoblastogenesis. *Endocrinology* **146**, 4577–4583 (2005).
82. Bellido, T. Downregulation of SOST/sclerostin by PTH: a novel mechanism of hormonal control of bone formation mediated by osteocytes. *J. Musculoskelet Neuronal Interact* **6**, 358–359 (2006).
83. Robling, A. G. *et al.* Mechanical Stimulation of Bone in Vivo Reduces Osteocyte Expression of Sost/Sclerostin. *J. Biol. Chem.* **283**, 5866–5875 (2008).
84. Lin, C. *et al.* Sclerostin Mediates Bone Response to Mechanical Unloading Through Antagonizing Wnt/ β -Catenin Signaling. *J. Bone Miner. Res.* **24**, 1651–1661 (2009).
85. Sølling, A. S. K., Harsløf, T. & Langdahl, B. The clinical potential of romosozumab for the prevention of fractures in postmenopausal women with osteoporosis. *Ther. Adv. Musculoskelet. Dis.* **10**, 105–115 (2018).
86. Oldberg, A., Franzén, A. & Heinegård, D. Cloning and sequence analysis of rat bone sialoprotein (osteopontin) cDNA reveals an Arg-Gly-Asp cell-binding sequence. *Proc. Natl. Acad. Sci.* **83**, 8819–8823 (1986).
87. Noda, M. *et al.* Identification of a DNA sequence responsible for binding of the 1,25-dihydroxyvitamin D₃ receptor and 1,25-dihydroxyvitamin D₃ enhancement of mouse secreted phosphoprotein 1 (SPP-1 or osteopontin) gene expression. *Proc. Natl. Acad. Sci. U. S. A.* **87**, 9995–9 (1990).

88. Noda, M., Yoon, K., Prince, C. W., Butler, W. T. & Rodan, G. A. Transcriptional regulation of osteopontin production in rat osteosarcoma cells by type beta transforming growth factor. *J. Biol. Chem.* **263**, 13916–13921 (1988).
89. Sodek, J., Ganss, B. & McKee, M. D. Osteopontin. *Crit. Rev. Oral Biol. Med.* **11**, 279–303 (2000).
90. Reinholt, F. P., Hultenby, K., Oldberg, A. & Heinegård, D. Osteopontin--a possible anchor of osteoclasts to bone. *Proc. Natl. Acad. Sci. U. S. A.* **87**, 4473–5 (1990).
91. Rittling, S. R. *et al.* Mice Lacking Osteopontin Show Normal Development and Bone Structure but Display Altered Osteoclast Formation In Vitro. *J. Bone Miner. Res.* **13**, 1101–1111 (1998).
92. Yoshitake, H., Rittling, S. R., Denhardt, D. T. & Noda, M. Osteopontin-deficient mice are resistant to ovariectomy-induced bone resorption. *Proc. Natl. Acad. Sci. U. S. A.* **96**, 8156–60 (1999).
93. Mannstadt, M., Jüppner, H. & Gardella, T. J. Receptors for PTH and PTHrP: their biological importance and functional properties. *Am. J. Physiol. Physiol.* **277**, F665–F675 (1999).
94. Lee, K., Deeds, J. D. & Segre, G. V. Expression of parathyroid hormone-related peptide and its receptor messenger ribonucleic acids during fetal development of rats. *Endocrinology* **136**, 453–463 (1995).
95. PARTRIDGE, N. C., KEMP, B. E., VERONI, M. C. & MARTIN, T. J. Activation of Adenosine 3',5'-Monophosphate-Dependent Protein Kinase in Normal and Malignant Bone Cells by Parathyroid Hormone, Prostaglandin E₂, and Prostacyclin*. *Endocrinology* **108**, 220–225 (1981).
96. Majeska, R. J. & Rodan, G. A. Alkaline phosphatase inhibition by parathyroid hormone and isoproterenol in a clonal rat osteosarcoma cell line. Possible mediation by cyclic AMP. *Calcif. Tissue Int.* **34**, 59–66 (1982).
97. Fermor, B. & Skerry, T. M. PTH/PTHrP receptor expression on osteoblasts and osteocytes but not resorbing bone surfaces in growing rats. *J. Bone Miner. Res.* **10**, 1935–1943 (2009).
98. Martin, T. J. Osteoblast-derived PTHrP is a physiological regulator of bone formation. *J. Clin. Invest.* **115**, 2322–4 (2005).
99. Huang, J. C. *et al.* PTH Differentially Regulates Expression of RANKL and OPG. *J. Bone Miner. Res.* **19**, 235–244 (2003).
100. Amizuka, N. *et al.* Haploinsufficiency of Parathyroid Hormone-Related Peptide (PTHrP) Results in Abnormal Postnatal Bone Development. *Dev. Biol.* **175**, 166–176 (1996).
101. Miao, D. *et al.* Parathyroid Hormone-Related Peptide Is Required for Increased Trabecular Bone Volume in Parathyroid Hormone-Null Mice. *Endocrinology* **145**, 3554–3562 (2004).
102. Seita, J. & Weissman, I. L. Hematopoietic stem cell: self-renewal versus differentiation. *Wiley Interdiscip. Rev. Syst. Biol. Med.* **2**, 640–653 (2010).
103. Arai, F. *et al.* Commitment and differentiation of osteoclast precursor cells by the sequential expression of c-Fms and receptor activator of nuclear factor kappaB (RANK) receptors. *J. Exp. Med.* **190**, 1741–54 (1999).
104. Diamond, M. S. *et al.* ICAM-1 (CD54): a counter-receptor for Mac-1 (CD11b/CD18). *J. Cell Biol.* **111**, 3129–39 (1990).
105. Ono, T. & Nakashima, T. Recent advances in osteoclast biology. *Histochem. Cell Biol.* **149**, 325–341 (2018).
106. Perkins, S. L., Gibbons, R., Kling, S. & Kahn, A. J. Age-related bone loss in mice is associated with an increased osteoclast progenitor pool. *Bone* **15**, 65–72
107. Galson, D. L. & Roodman, G. D. Origins of Osteoclasts. in *Osteoimmunology* 7–41

- (Elsevier, 2011). doi:10.1016/B978-0-12-375670-1.10002-0
108. Väänänen, H. K. & Horton, M. The osteoclast clear zone is a specialized cell-extracellular matrix adhesion structure. *J. Cell Sci.* **108**, 2729–2732 (1995).
 109. Baron, R., Neff, L., Louvard, D. & Courtoy, P. J. Cell-mediated extracellular acidification and bone resorption: evidence for a low pH in resorbing lacunae and localization of a 100-kD lysosomal membrane protein at the osteoclast ruffled border. *J. Cell Biol.* **101**, 2210–22 (1985).
 110. Quinn, J. M. W., Elliott, J., Gillespie, M. T. & Martin, T. J. A Combination of Osteoclast Differentiation Factor and Macrophage-Colony Stimulating Factor Is Sufficient for both Human and Mouse Osteoclast Formation *in Vitro*. *Endocrinology* **139**, 4424–4427 (1998).
 111. Udagawa, N. *et al.* Origin of osteoclasts: mature monocytes and macrophages are capable of differentiating into osteoclasts under a suitable microenvironment prepared by bone marrow-derived stromal cells. *Proc. Natl. Acad. Sci.* **87**, 7260–7264 (1990).
 112. Nakamichi, Y. *et al.* Spleen serves as a reservoir of osteoclast precursors through vitamin D-induced IL-34 expression in osteopetrotic op/op mice. *Proc. Natl. Acad. Sci. U. S. A.* **109**, 10006–11 (2012).
 113. Deng, P., Wang, Y.-L., Pattengale, P. K. & Rettenmier, C. W. The Role of Individual Cysteine Residues in the Processing, Structure, and Function of Human Macrophage Colony-Stimulating Factor. *Biochem. Biophys. Res. Commun.* **228**, 557–566 (1996).
 114. TAKAYANAGI, H. The Role of NFAT in Osteoclast Formation. *Ann. N. Y. Acad. Sci.* **1116**, 227–237 (2007).
 115. Ross, F. P. *et al.* Interactions between the bone matrix proteins osteopontin and bone sialoprotein and the osteoclast integrin alpha v beta 3 potentiate bone resorption. *J Biol Chem* **268**, 9901–9907 (1993).
 116. Lehenkari, P., Hentunen, T. A., Laitala-Leinonen, T., Tuukkanen, J. & Väänänen, H. K. Carbonic Anhydrase II Plays a Major Role in Osteoclast Differentiation and Bone Resorption by Effecting the Steady State Intracellular pH and Ca²⁺. *Exp. Cell Res.* **242**, 128–137 (1998).
 117. Qin, A. *et al.* V-ATPases in osteoclasts: Structure, function and potential inhibitors of bone resorption. *Int. J. Biochem. Cell Biol.* **44**, 1422–1435 (2012).
 118. Kornak, U. *et al.* Loss of the ClC-7 Chloride Channel Leads to Osteopetrosis in Mice and Man. *Trends Biochem. Sci.* **104**, 205–215 (2001).
 119. Littlewood-Evans, A. *et al.* Localization of cathepsin K in human osteoclasts by in situ hybridization and immunohistochemistry. *Bone* **20**, 81–86 (1997).
 120. Yamaza, T. *et al.* Study of immunoelectron microscopic localization of cathepsin K in osteoclasts and other bone cells in the mouse femur. *Bone* **23**, 499–509 (1998).
 121. NAGASE, H., VISSE, R. & MURPHY, G. Structure and function of matrix metalloproteinases and TIMPs. *Cardiovasc. Res.* **69**, 562–573 (2006).
 122. Lee, S. K., Goldring, S. R. & Lorenzo, J. A. Expression of the calcitonin receptor in bone marrow cell cultures and in bone: a specific marker of the differentiated osteoclast that is regulated by calcitonin. *Endocrinology* **136**, 4572–4581 (1995).
 123. Wada, T., Nakashima, T., Hiroshi, N. & Penninger, J. M. RANKL–RANK signaling in osteoclastogenesis and bone disease. *Trends Mol. Med.* **12**, 17–25 (2006).
 124. Lee, Z. H. & Kim, H.-H. Signal transduction by receptor activator of nuclear factor kappa B in osteoclasts. *Biochem. Biophys. Res. Commun.* **305**, 211–214 (2003).
 125. Li, X. *et al.* p38 MAPK-Mediated Signals Are Required for Inducing Osteoclast Differentiation But Not for Osteoclast Function. *Endocrinology* **143**, 3105–3113 (2002).
 126. Teitelbaum, S. L. Bone Resorption by Osteoclasts. *Science (80-.)*. **289**, 1504–1508 (2000).

127. Halleen, J. M. *et al.* Tartrate-Resistant Acid Phosphatase 5b: A Novel Serum Marker of Bone Resorption. *J. Bone Miner. Res.* **15**, 1337–1345 (2000).
128. Hayman, A. R. Tartrate-resistant acid phosphatase (TRAP) and the osteoclast/immune cell dichotomy. *Autoimmunity* **41**, 218–223 (2008).
129. Rico, H. & Villa, L. F. Serum tartrate-resistant acid phosphatase (TRAP) as a biochemical marker of bone remodeling. *Calcif. Tissue Int.* **52**, 149–150 (1993).
130. Weilbaecher, K. N. *et al.* Linkage of M-CSF signaling to Mitf, TFE3, and the osteoclast defect in Mitf(mi/mi) mice. *Mol. Cell* **8**, 749–58 (2001).
131. Partington, G. ., Fuller, K., Chambers, T. . & Pondel, M. Mitf–PU.1 interactions with the tartrate-resistant acid phosphatase gene promoter during osteoclast differentiation. *Bone* **34**, 237–245 (2004).
132. Hayman, A. R. *et al.* Mice lacking tartrate-resistant acid phosphatase (Acp 5) have disrupted endochondral ossification and mild osteopetrosis. *Development* **122**, 3151–62 (1996).
133. Drake, F. H. *et al.* Cathepsin K, but not cathepsins B, L, or S, is abundantly expressed in human osteoclasts. *J. Biol. Chem.* **271**, 12511–6 (1996).
134. KAFIENAH, W., BRÖMME, D., BUTTLE, D. J., CROUCHER, L. J. & HOLLANDER, A. P. Human cathepsin K cleaves native type I and II collagens at the N-terminal end of the triple helix. *Int. J. Exp. Pathol.* **79**, A33–A33 (2002).
135. Saftig, P. *et al.* Impaired osteoclastic bone resorption leads to osteopetrosis in cathepsin-K-deficient mice. *Proc. Natl. Acad. Sci. U. S. A.* **95**, 13453–8 (1998).
136. Vu, T. H. *et al.* MMP-9/Gelatinase B Is a Key Regulator of Growth Plate Angiogenesis and Apoptosis of Hypertrophic Chondrocytes. *Cell* **93**, 411–422 (1998).
137. Gelb, B. D., Shi, G. P., Chapman, H. A. & Desnick, R. J. Pycnodysostosis, a lysosomal disease caused by cathepsin K deficiency. *Science* **273**, 1236–8 (1996).
138. Boggild, M. K. *et al.* Odanacatib for the treatment of osteoporosis. *Expert Opin. Pharmacother.* **16**, 1717–1726 (2015).
139. Bone, H. G. *et al.* Odanacatib for the treatment of postmenopausal osteoporosis: development history and design and participant characteristics of LOFT, the Long-Term Odanacatib Fracture Trial. *Osteoporos. Int.* **26**, 699–712 (2015).
140. Hartgers, F. C. *et al.* DC-STAMP, a novel multimembrane-spanning molecule preferentially expressed by dendritic cells. *Eur. J. Immunol.* **30**, 3585–3590 (2000).
141. Yang, M. *et al.* Osteoclast stimulatory transmembrane protein (OC-STAMP), a novel protein induced by RANKL that promotes osteoclast differentiation. *J. Cell. Physiol.* **215**, 497–505 (2008).
142. Yagi, M. *et al.* DC-STAMP is essential for cell-cell fusion in osteoclasts and foreign body giant cells. *J. Exp. Med.* **202**, 345–51 (2005).
143. Miyamoto, H. *et al.* Osteoclast stimulatory transmembrane protein and dendritic cell-specific transmembrane protein cooperatively modulate cell-cell fusion to form osteoclasts and foreign body giant cells. *J. Bone Miner. Res.* **27**, 1289–1297 (2012).
144. Miyamoto, T. The dendritic cell-specific transmembrane protein DC-STAMP is essential for osteoclast fusion and osteoclast bone-resorbing activity. *Mod. Rheumatol.* **16**, 341–342 (2006).
145. Thomas, S. M. & Brugge, J. S. Cellular Functions Regulated By Src Family Kinases. *Annu. Rev. Cell Dev. Biol.* **13**, 513–609 (1997).
146. Collett, M. S. & Erikson, R. L. Protein kinase activity associated with the avian sarcoma virus src gene product. *Proc. Natl. Acad. Sci. U. S. A.* **75**, 2021–4 (1978).
147. Levinson, A. D., Oppermann, H., Levintow, L., Varmus, H. E. & Bishop, J. M. Evidence that the transforming gene of avian sarcoma virus encodes a protein kinase associated with a phosphoprotein. *Cell* **15**, 561–572 (1978).

148. Oppermann, H., Levinson, A. D., Varmus, H. E., Levintow, L. & Bishop, J. M. Uninfected vertebrate cells contain a protein that is closely related to the product of the avian sarcoma virus transforming gene (src). *Proc. Natl. Acad. Sci.* **76**, 1804–1808 (1979).
149. Brown, M. T. & Cooper, J. A. Regulation, substrates and functions of src. *Biochim. Biophys. Acta - Rev. Cancer* **1287**, 121–149 (1996).
150. Cross, F. R., Garber, E. A., Pellman, D. & Hanafusa, H. A short sequence in the p60src N terminus is required for p60src myristylation and membrane association and for cell transformation. *Mol. Cell. Biol.* **4**, 1834–42 (1984).
151. David-Pfeuty, T., Bagrodia, S. & Shalloway, D. Differential localization patterns of myristoylated and nonmyristoylated c-Src proteins in interphase and mitotic c-Src overexpresser cells. *J. Cell Sci.* **105**, 613–628 (1993).
152. Koch, C. A., Anderson, D., Moran, M. F., Ellis, C. & Pawson, T. SH2 and SH3 domains: elements that control interactions of cytoplasmic signaling proteins. *Science* **252**, 668–74 (1991).
153. Okada, M. Regulation of the Src Family Kinases by Csk. *Int. J. Biol. Sci.* **8**, 1385–1397 (2012).
154. Chellaiah, M. A. *et al.* Rho-A is critical for osteoclast podosome organization, motility, and bone resorption. *J. Biol. Chem.* **275**, 11993–2002 (2000).
155. Chellaiah, M. A. Regulation of Actin Ring Formation by Rho GTPases in osteoclasts. *J. Biol. Chem.* **280**, 32930–32943 (2005).
156. Huveneers, S. & Danen, E. H. J. Adhesion signaling - crosstalk between integrins, Src and Rho. *J. Cell Sci.* **122**, 1059–69 (2009).
157. Soriano, P., Montgomery, C., Geske, R. & Bradley, A. Targeted disruption of the c-src proto-oncogene leads to osteopetrosis in mice. *Cell* **64**, 693–702 (1991).
158. Miyazaki, T. *et al.* Src Kinase Activity Is Essential for Osteoclast Function. *J. Biol. Chem.* **279**, 17660–17666 (2004).
159. Horne, W. C., Sanjay, A., Bruzzaniti, A. & Baron, R. The role(s) of Src kinase and Cbl proteins in the regulation of osteoclast differentiation and function. *Immunol. Rev.* **208**, 106–125 (2005).
160. Miyazaki, T., Tanaka, S., Sanjay, A. & Baron, R. The role of c-Src kinase in the regulation of osteoclast function. *Mod. Rheumatol.* **16**, 68–74 (2006).
161. Zotti, T., Vito, P. & Stilo, R. The seventh ring: exploring TRAF7 functions. *J. Cell. Physiol.* **227**, 1280–4 (2012).
162. Lomaga, M. A. *et al.* TRAF6 deficiency results in osteopetrosis and defective interleukin-1, CD40, and LPS signaling. *Genes Dev.* **13**, 1015–24 (1999).
163. Xie, P. TRAF molecules in cell signaling and in human diseases. *J. Mol. Signal.* **8**, 7 (2013).
164. Deng, L. *et al.* Activation of the I κ B Kinase Complex by TRAF6 Requires a Dimeric Ubiquitin-Conjugating Enzyme Complex and a Unique Polyubiquitin Chain. *Cell* **103**, 351–361 (2000).
165. Moriguchi, T. *et al.* A novel kinase cascade mediated by mitogen-activated protein kinase kinase 6 and MKK3. *J. Biol. Chem.* **271**, 13675–9 (1996).
166. Sakurai, H., Shigemori, N., Hasegawa, K. & Sugita, T. TGF- β -Activated Kinase 1 Stimulates NF- κ B Activation by an NF- κ B-Inducing Kinase-Independent Mechanism. *Biochem. Biophys. Res. Commun.* **243**, 545–549 (1998).
167. Ninomiya-Tsuji, J. *et al.* The kinase TAK1 can activate the NIK-I κ B as well as the MAP kinase cascade in the IL-1 signalling pathway. *Nature* **398**, 252–256 (1999).
168. Häcker, H., Tseng, P.-H. & Karin, M. Expanding TRAF function: TRAF3 as a tri-faced immune regulator. *Nat. Rev. Immunol.* **11**, 457–468 (2011).

169. Uren, A. G. & Vaux, D. L. TRAF proteins and meprins share a conserved domain. *Trends Biochem. Sci.* **21**, 244–5 (1996).
170. Sunnerhagen, M., Pursglove, S. & Fladvad, M. The new MATH: homology suggests shared binding surfaces in meprin tetramers and TRAF trimers. *FEBS Lett.* **530**, 1–3 (2002).
171. Gohda, J. *et al.* RANK-mediated amplification of TRAF6 signaling leads to NFATc1 induction during osteoclastogenesis. *EMBO J.* **24**, 790–9 (2005).
172. Kim, H. H. *et al.* Receptor activator of NF-kappaB recruits multiple TRAF family adaptors and activates c-Jun N-terminal kinase. *FEBS Lett.* **443**, 297–302 (1999).
173. Kanazawa, K., Azuma, Y., Nakano, H. & Kudo, A. TRAF5 Functions in Both RANKL- and TNF α -Induced Osteoclastogenesis. *J. Bone Miner. Res.* **18**, 443–450 (2003).
174. Wang, K. Z. Q. *et al.* TRAF6 activation of PI 3-kinase-dependent cytoskeletal changes is cooperative with Ras and is mediated by an interaction with cytoplasmic Src. *J. Cell Sci.* **119**, 1579–91 (2006).
175. Wong, B. R. *et al.* TRANCE, a TNF Family Member, Activates Akt/PKB through a Signaling Complex Involving TRAF6 and c-Src. *Mol. Cell* **4**, 1041–1049 (1999).
176. Naito, A. *et al.* Severe osteopetrosis, defective interleukin-1 signalling and lymph node organogenesis in TRAF6-deficient mice. *Genes Cells* **4**, 353–62 (1999).
177. Neer, E. J., Schmidt, C. J., Nambudripad, R. & Smith, T. F. The ancient regulatory-protein family of WD-repeat proteins. *Nature* **371**, 297–300 (1994).
178. Tang, Y. *et al.* TGF- β 1-induced migration of bone mesenchymal stem cells couples bone resorption with formation. *Nat. Med.* **15**, 757–765 (2009).
179. Dallas, S. L., Rosser, J. L., Mundy, G. R. & Bonewald, L. F. Proteolysis of latent transforming growth factor-beta (TGF-beta)-binding protein-1 by osteoclasts. A cellular mechanism for release of TGF-beta from bone matrix. *J. Biol. Chem.* **277**, 21352–60 (2002).
180. Quinn, J. M. W. *et al.* Transforming Growth Factor β Affects Osteoclast Differentiation via Direct and Indirect Actions. *J. Bone Miner. Res.* **16**, 1787–1794 (2001).
181. Karsdal, M. A. *et al.* Transforming growth factor-beta controls human osteoclastogenesis through the p38 MAPK and regulation of RANK expression. *J. Biol. Chem.* **278**, 44975–87 (2003).
182. Dennler, S. *et al.* Direct binding of Smad3 and Smad4 to critical TGFbeta -inducible elements in the promoter of human plasminogen activator inhibitor-type 1 gene. *EMBO J.* **17**, 3091–3100 (1998).
183. Waltz, D. A., Natkin, L. R., Fujita, R. M., Wei, Y. & Chapman, H. A. Plasmin and plasminogen activator inhibitor type 1 promote cellular motility by regulating the interaction between the urokinase receptor and vitronectin. *J. Clin. Invest.* **100**, 58–67 (1997).
184. Czekay, R.-P., Aertgeerts, K., Curriden, S. A. & Loskutoff, D. J. Plasminogen activator inhibitor-1 detaches cells from extracellular matrices by inactivating integrins. *J. Cell Biol.* **160**, 781–91 (2003).
185. Hocevar, B. A., Brown, T. L. & Howe, P. H. TGF-beta induces fibronectin synthesis through a c-Jun N-terminal kinase-dependent, Smad4-independent pathway. *EMBO J.* **18**, 1345–56 (1999).
186. Yasui, T. *et al.* Regulation of RANKL-induced osteoclastogenesis by TGF- β through molecular interaction between Smad3 and Traf6. *J. Bone Miner. Res.* **26**, 1447–1456 (2011).
187. Macián, F., López-Rodríguez, C. & Rao, A. Partners in transcription: NFAT and AP-1. *Oncogene* **20**, 2476–2489 (2001).
188. Lopez-Rodríguez, C., Aramburu, J., Rakeman, A. S. & Rao, A. NFAT5, a constitutively

- nuclear NFAT protein that does not cooperate with Fos and Jun. *Proc. Natl. Acad. Sci. U. S. A.* **96**, 7214–9 (1999).
189. Okamura, H. *et al.* Concerted Dephosphorylation of the Transcription Factor NFAT1 Induces a Conformational Switch that Regulates Transcriptional Activity. *Mol. Cell* **6**, 539–550 (2000).
 190. Hogan, P. G., Chen, L., Nardone, J. & Rao, A. Transcriptional regulation by calcium, calcineurin, and NFAT. *Genes Dev.* **17**, 2205–32 (2003).
 191. Asagiri, M. *et al.* Autoamplification of NFATc1 expression determines its essential role in bone homeostasis. *J. Exp. Med.* **202**, 1261–9 (2005).
 192. Takayanagi, H. *et al.* Induction and Activation of the Transcription Factor NFATc1 (NFAT2) Integrate RANKL Signaling in Terminal Differentiation of Osteoclasts. *Dev. Cell* **3**, 889–901 (2002).
 193. Chen, F., Castranova, V., Shi, X. & Demers, L. M. New insights into the role of nuclear factor-kappaB, a ubiquitous transcription factor in the initiation of diseases. *Clin. Chem.* **45**, 7–17 (1999).
 194. Hayden, M. S. & Ghosh, S. NF- κ B, the first quarter-century: remarkable progress and outstanding questions. *Genes Dev.* **26**, 203–234 (2012).
 195. Fan, C.-M. & Maniatis, T. Generation of p50 subunit of NF- κ B by processing of p105 through an ATP-dependent pathway. *Nature* **354**, 395–398 (1991).
 196. Sears, C., Olesen, J., Rubin, D., Finley, D. & Maniatis, T. NF- κ B p105 processing via the ubiquitin-proteasome pathway. *J. Biol. Chem.* **273**, 1409–19 (1998).
 197. Xiao, G., Harhaj, E. W. & Sun, S.-C. NF- κ B-Inducing Kinase Regulates the Processing of NF- κ B2 p100. *Mol. Cell* **7**, 401–409 (2001).
 198. Xiao, G., Fong, A. & Sun, S.-C. Induction of p100 processing by NF- κ B-inducing kinase involves docking IkappaB kinase alpha (IKKalpha) to p100 and IKKalpha-mediated phosphorylation. *J. Biol. Chem.* **279**, 30099–105 (2004).
 199. Hatada, E. N. *et al.* The ankyrin repeat domains of the NF- κ B precursor p105 and the protooncogene bcl-3 act as specific inhibitors of NF- κ B DNA binding. *Proc. Natl. Acad. Sci. U. S. A.* **89**, 2489–93 (1992).
 200. Henkel, T. *et al.* Intramolecular masking of the nuclear location signal and dimerization domain in the precursor for the p50 NF- κ B subunit. *Cell* **68**, 1121–1133 (1992).
 201. Gilmore, T. D. Introduction to NF- κ B: players, pathways, perspectives. *Oncogene* **25**, 6680–6684 (2006).
 202. Vaira, S. *et al.* RelB is the NF- κ B subunit downstream of NIK responsible for osteoclast differentiation. *Proc. Natl. Acad. Sci. U. S. A.* **105**, 3897–902 (2008).
 203. Sun, S.-C. Non-canonical NF- κ B signaling pathway. *Cell Res.* **21**, 71–85 (2011).
 204. Jain, J., Burgeon, E., Badalian, T. M., Hogan, P. G. & Rao, A. A similar DNA-binding motif in NFAT family proteins and the Rel homology region. *J. Biol. Chem.* **270**, 4138–45 (1995).
 205. Sha, W. C., Liou, H.-C., Tuomanen, E. I. & Baltimore, D. Targeted disruption of the p50 subunit of NF- κ B leads to multifocal defects in immune responses. *Cell* **80**, 321–330 (1995).
 206. Franzoso, G. *et al.* Mice deficient in nuclear factor (NF)- κ B/p52 present with defects in humoral responses, germinal center reactions, and splenic microarchitecture. *J. Exp. Med.* **187**, 147–59 (1998).
 207. Iotsova, V. *et al.* Osteopetrosis in mice lacking NF- κ B1 and NF- κ B2. *Nat. Med.* **3**, 1285–1289 (1997).
 208. Hess, J. AP-1 subunits: quarrel and harmony among siblings. *J. Cell Sci.* **117**, 5965–5973 (2004).
 209. Busch, S. J. & Sassone-Corsi, P. Dimers, leucine zippers and DNA-binding domains.

- Trends Genet.* **6**, 36–40 (1990).
210. Ellenberger, T. Getting a grip on DNA recognition: structures of the basic region leucine zipper, and the basic region helix-loop-helix DNA-binding domains. *Curr. Opin. Struct. Biol.* **4**, 12–21 (1994).
 211. Chen, R. H., Sarnecki, C. & Blenis, J. Nuclear localization and regulation of erk- and rsk-encoded protein kinases. *Mol. Cell. Biol.* **12**, 915–27 (1992).
 212. Deng, T. & Karin, M. c-Fos transcriptional activity stimulated by H-Ras-activated protein kinase distinct from JNK and ERK. *Nature* **371**, 171–175 (1994).
 213. Minden, a *et al.* c-Jun N-terminal phosphorylation correlates with activation of the JNK subgroup but not the ERK subgroup of mitogen-activated protein kinases. *Mol. Cell. Biol.* **14**, 6683–8 (1994).
 214. Ikeda, F. *et al.* Critical roles of c-Jun signaling in regulation of NFAT family and RANKL-regulated osteoclast differentiation. *J. Clin. Invest.* **114**, 475–84 (2004).
 215. Matsuo, K. *et al.* Fos11 is a transcriptional target of c-Fos during osteoclast differentiation. *Nat. Genet.* **24**, 184–187 (2000).
 216. Matsuo, K. *et al.* Nuclear factor of activated T-cells (NFAT) rescues osteoclastogenesis in precursors lacking c-Fos. *J. Biol. Chem.* **279**, 26475–80 (2004).
 217. Kearbey, J. D. *et al.* Selective Androgen Receptor Modulator (SARM) Treatment Prevents Bone Loss and Reduces Body Fat in Ovariectomized Rats. *Pharm. Res.* **24**, 328–335 (2007).
 218. Ettinger, B. *et al.* Reduction of Vertebral Fracture Risk in Postmenopausal Women With Osteoporosis Treated With Raloxifene -Results From a 3-Year Randomized Clinical Trial-. *JAMA* **282**, 637–645 (1999).
 219. Dawson-Hughes, B., Harris, S. S., Krall, E. A. & Dallal, G. E. Effect of Calcium and Vitamin D Supplementation on Bone Density in Men and Women 65 Years of Age or Older. *N. Engl. J. Med.* **337**, 670–676 (1997).
 220. Tang, B. M., Eslick, G. D., Nowson, C., Smith, C. & Bensoussan, A. Use of calcium or calcium in combination with vitamin D supplementation to prevent fractures and bone loss in people aged 50 years and older: a meta-analysis. *Lancet* **370**, 657–666 (2007).
 221. Tilyard, M. W., Spears, G. F. S., Thomson, J. & Dovey, S. Treatment of Postmenopausal Osteoporosis with Calcitriol or Calcium. *N. Engl. J. Med.* **326**, 357–362 (1992).
 222. Abrahamsen, B., Grove, E. L. & Vestergaard, P. Nationwide registry-based analysis of cardiovascular risk factors and adverse outcomes in patients treated with strontium ranelate. *Osteoporos. Int.* **25**, 757–762 (2014).
 223. Bjarnason, K., Cerin, Å., Lindgren, R. & Weber, T. Adverse endometrial effects during long cycle hormone replacement therapy. *Maturitas* **32**, 161–170 (1999).
 224. Fleisch, H. Bisphosphonates--history and experimental basis. *Bone* **8 Suppl 1**, S23-8 (1987).
 225. Russell, R. G. . & Rogers, M. . Bisphosphonates: from the laboratory to the clinic and back again. *Bone* **25**, 97–106 (1999).
 226. Reszka, A. A., Halasy-Nagy, J. M., Masarachia, P. J. & Rodan, G. A. Bisphosphonates act directly on the osteoclast to induce caspase cleavage of mst1 kinase during apoptosis. A link between inhibition of the mevalonate pathway and regulation of an apoptosis-promoting kinase. *J. Biol. Chem.* **274**, 34967–73 (1999).
 227. Benford, H. ., McGowan, N. W. ., Helfrich, M. ., Nuttall, M. . & Rogers, M. . Visualization of bisphosphonate-induced caspase-3 activity in apoptotic osteoclasts in vitro. *Bone* **28**, 465–473 (2001).
 228. RUSSELL, R. G. G. Bisphosphonates: From Bench to Bedside. *Ann. N. Y. Acad. Sci.* **1068**, 367–401 (2006).
 229. Luckman, S. P., Hughes, D. E., Coxon, F. P., Russell, R. G. G. & Rogers, M. J. Nitrogen-

- Containing Bisphosphonates Inhibit the Mevalonate Pathway and Prevent Post-Translational Prenylation of GTP-Binding Proteins, Including Ras. *J. Bone Miner. Res.* **13**, 581–589 (1998).
230. Plotkin, L. I. *et al.* Prevention of osteocyte and osteoblast apoptosis by bisphosphonates and calcitonin. *J. Clin. Invest.* **104**, 1363–74 (1999).
231. Plotkin, L. I., Aguirre, J. I., Kousteni, S., Manolagas, S. C. & Bellido, T. Bisphosphonates and estrogens inhibit osteocyte apoptosis via distinct molecular mechanisms downstream of extracellular signal-regulated kinase activation. *J. Biol. Chem.* **280**, 7317–25 (2005).
232. Sahni, M., Guenther, H. L., Fleisch, H., Collin, P. & Martin, T. J. Bisphosphonates act on rat bone resorption through the mediation of osteoblasts. *J. Clin. Invest.* **91**, 2004–11 (1993).
233. Vitte, C., Fleisch, H. & Guenther, H. L. Bisphosphonates induce osteoblasts to secrete an inhibitor of osteoclast-mediated resorption. *Endocrinology* **137**, 2324–2333 (1996).
234. Giuliani, N., Pedrazzoni, M., Passeri, G. & Girasole, G. Bisphosphonates inhibit IL-6 production by human osteoblast-like cells. *Scand. J. Rheumatol.* **27**, 38–41 (1998).
235. Lacey, D. L. *et al.* Bench to bedside: elucidation of the OPG–RANK–RANKL pathway and the development of denosumab. *Nat. Rev. Drug Discov.* **11**, 401–419 (2012).
236. Kostenuik, P. J. *et al.* Denosumab, a Fully Human Monoclonal Antibody to RANKL, Inhibits Bone Resorption and Increases BMD in Knock-In Mice That Express Chimeric (Murine/Human) RANKL*. *J. Bone Miner. Res.* **24**, 182–195 (2009).
237. Seeman, E. *et al.* Microarchitectural deterioration of cortical and trabecular bone: Differing effects of denosumab and alendronate. *J. Bone Miner. Res.* **25**, 1886–1894 (2010).
238. Berg, C., Neumeyer, K. & Kirkpatrick, P. Teriparatide. *Nat. Rev. Drug Discov.* **2**, 257–258 (2003).
239. Miller, S. C. The rapid appearance of acid phosphatase activity at the developing ruffled border of parathyroid hormone activated medullary bone osteoclasts. *Calcif. Tissue Int.* **37**, 526–529 (1985).
240. Lee, S.-K. & Lorenzo, J. A. Parathyroid Hormone Stimulates TRANCE and Inhibits Osteoprotegerin Messenger Ribonucleic Acid Expression in Murine Bone Marrow Cultures: Correlation with Osteoclast-Like Cell Formation 1. *Endocrinology* **140**, 3552–3561 (1999).
241. TAM, C. S., HEERSCHKE, J. N. M., MURRAY, T. M. & PARSONS, J. A. Parathyroid Hormone Stimulates the Bone Apposition Rate Independently of Its Resorptive Action: Differential Effects of Intermittent and Continuous Administration*. *Endocrinology* **110**, 506–512 (1982).
242. Teriparatide (forteo) for osteoporosis. *Med. Lett. Drugs Ther.* **45**, 9–10 (2003).
243. Vahle, J. L. *et al.* Skeletal Changes in Rats Given Daily Subcutaneous Injections of Recombinant Human Parathyroid Hormone (1-34) for 2 Years and Relevance to Human Safety. *Toxicol. Pathol.* **30**, 312–321 (2002).
244. Tella, S. H., Kommalapati, A. & Correa, R. Profile of Abaloparatide and Its Potential in the Treatment of Postmenopausal Osteoporosis. *Cureus* **9**, e1300 (2017).
245. Ferrandon, S. *et al.* Sustained cyclic AMP production by parathyroid hormone receptor endocytosis. *Nat. Chem. Biol.* **5**, 734–742 (2009).
246. Miller, P. D. *et al.* Effect of Abaloparatide vs Placebo on New Vertebral Fractures in Postmenopausal Women With Osteoporosis. *JAMA* **316**, 722–733 (2016).
247. Shirley, M. Abaloparatide: First Global Approval. *Drugs* **77**, 1363–1368 (2017).
248. Krishnan, V., Bryant, H. U. & Macdougald, O. A. Regulation of bone mass by Wnt signaling. *J. Clin. Invest.* **116**, 1202–1209 (2006).

249. Baron, R. & Rawadi, G. Targeting the Wnt/ β -Catenin Pathway to Regulate Bone Formation in the Adult Skeleton. *Endocrinology* **148**, 2635–2643 (2007).
250. Glass, D. A. *et al.* Canonical Wnt Signaling in Differentiated Osteoblasts Controls Osteoclast Differentiation. *Dev. Cell* **8**, 751–764 (2005).
251. ten Dijke, P., Krause, C., de Gorter, D. J., Löwik, C. W. & van Bezooijen, R. L. Osteocyte-Derived Sclerostin Inhibits Bone Formation: Its Role in Bone Morphogenetic Protein and Wnt Signaling. *J. Bone Jt. Surgery-American Vol.* **90**, 31–35 (2008).
252. Lim, S. Y. & Bolster, M. B. Profile of romosozumab and its potential in the management of osteoporosis. *Drug Des. Devel. Ther.* **11**, 1221–1231 (2017).
253. Hadaya, D. *et al.* Clinically Relevant Doses of Sclerostin-Antibody do not Induce Osteonecrosis of the Jaw (ONJ) in Rats with Experimental Periodontitis. *J. Bone Miner. Res.* (2018). doi:10.1002/jbmr.3581
254. Bertolino, E., Reimund, B., Wildt-Perinic, D. & Clerc, R. G. A novel homeobox protein which recognizes a TGT core and functionally interferes with a retinoid-responsive motif. *J. Biol. Chem.* **270**, 31178–88 (1995).
255. Bürglin, T. R. Analysis of TALE superclass homeobox genes (MEIS, PBC, KNOX, Iroquois, TGIF) reveals a novel domain conserved between plants and animals. *Nucleic Acids Res.* **25**, 4173–4180 (1997).
256. Zhang, M.-Z. *et al.* TGIF Governs a Feed-Forward Network that Empowers Wnt Signaling to Drive Mammary Tumorigenesis. *Cancer Cell* **27**, 547–560 (2015).
257. Razzaque, M. S. & Atfi, A. TGIF function in oncogenic Wnt signaling. *Biochim. Biophys. Acta - Rev. Cancer* **1865**, 101–104 (2016).
258. Powers, S. E. *et al.* Tgif1 and Tgif2 regulate Nodal signaling and are required for gastrulation. *Development* **137**, 249–59 (2010).
259. Derynck, R. & Zhang, Y. E. Smad-dependent and Smad-independent pathways in TGF- β family signalling. *Nature* **425**, 577–584 (2003).
260. Yan, L. *et al.* Tgif1 regulates quiescence and self-renewal of hematopoietic stem cells. *Mol. Cell. Biol.* **33**, 4824–33 (2013).
261. Taniguchi, K., Anderson, A. E., Sutherland, A. E. & Wotton, D. Loss of Tgif Function Causes Holoprosencephaly by Disrupting the Shh Signaling Pathway. *PLoS Genet.* **8**, e1002524 (2012).
262. Imoto, I. *et al.* Amplification and Overexpression of TGIF2, a Novel Homeobox Gene of the TALE Superclass, in Ovarian Cancer Cell Lines. *Biochem. Biophys. Res. Commun.* **276**, 264–270 (2000).
263. Melhuish, T. A., Gallo, C. M. & Wotton, D. TGIF2 interacts with histone deacetylase 1 and represses transcription. *J. Biol. Chem.* **276**, 32109–14 (2001).
264. Krzeszinski, J. Y. *et al.* miR-34a blocks osteoporosis and bone metastasis by inhibiting osteoclastogenesis and Tgif2. *Nature* **512**, 431–435 (2014).
265. Taipaleenmäki, H. *et al.* Tgif1 Controls Bone Remodeling and Anabolic Response to Parathyroid Hormone. FR0168, SA0168 (2017).
266. Shen, J. & Walsh, C. A. Targeted disruption of Tgif, the mouse ortholog of a human holoprosencephaly gene, does not result in holoprosencephaly in mice. *Mol. Cell. Biol.* **25**, 3639–47 (2005).
267. Clausen, B. E., Burkhardt, C., Reith, W., Renkawitz, R. & Förster, I. Conditional gene targeting in macrophages and granulocytes using LysMcre mice. *Transgenic Res.* **8**, 265–277 (1999).
268. Nakamura, T. *et al.* Estrogen prevents bone loss via estrogen receptor alpha and induction of Fas ligand in osteoclasts. *Cell* **130**, 811–23 (2007).
269. Suganuma, M. *et al.* Okadaic acid: an additional non-phorbol-12-tetradecanoate-13-acetate-type tumor promoter. *Proc. Natl. Acad. Sci. U. S. A.* **85**, 1768–71 (1988).

270. Fazil, M. H. U. T. *et al.* GapmeR cellular internalization by macropinocytosis induces sequence-specific gene silencing in human primary T-cells. *Sci. Rep.* **6**, 37721 (2016).
271. Parfitt, A. M. *et al.* Bone histomorphometry: Standardization of nomenclature, symbols, and units: Report of the ASBMR histomorphometry nomenclature committee. *J. Bone Miner. Res.* **2**, 595–610 (1987).
272. Dempster, D. W. *et al.* Standardized nomenclature, symbols, and units for bone histomorphometry: A 2012 update of the report of the ASBMR Histomorphometry Nomenclature Committee. *J. Bone Miner. Res.* **28**, 1–16 (2013).
273. Park, J. H., Lee, N. K. & Lee, S. Y. Current Understanding of RANK Signaling in Osteoclast Differentiation and Maturation. *Mol. Cells* **40**, 706–713 (2017).
274. Lakkakorpi, P. T. & Väänänen, H. K. Cytoskeletal changes in osteoclasts during the resorption cycle. *Microsc. Res. Tech.* **33**, 171–181 (1996).
275. Väänänen, H. K., Zhao, H., Mulari, M. & Halleen, J. M. The cell biology of osteoclast function. *J. Cell Sci.* **113** (Pt 3, 377–81 (2000).
276. Sanjay, A. *et al.* Cbl associates with Pyk2 and Src to regulate Src kinase activity, alpha(v)beta(3) integrin-mediated signaling, cell adhesion, and osteoclast motility. *J. Cell Biol.* **152**, 181–95 (2001).
277. Feng, X. RANKing intracellular signaling in osteoclasts. *IUBMB Life* **57**, 389–95 (2005).
278. Crews, C. M., Alessandrini, A. & Erikson, R. L. The primary structure of MEK, a protein kinase that phosphorylates the ERK gene product. *Science* **258**, 478–80 (1992).
279. Zassadowski, F., Rochette-Egly, C., Chomienne, C. & Cassinat, B. Regulation of the transcriptional activity of nuclear receptors by the MEK/ERK1/2 pathway. *Cell. Signal.* **24**, 2369–2377 (2012).
280. Kiely, M. & Kiely, P. PP2A: The Wolf in Sheep's Clothing? *Cancers (Basel)*. **7**, 648–669 (2015).
281. Frydrychowski, V. A., Urbanek, R. A., Dounay, A. B. & Forsyth, C. J. Importance of the C28–C38 hydrophobic domain of okadaic acid for potent inhibition of protein serine-threonine phosphatases 1 and 2A. *Bioorg. Med. Chem. Lett.* **11**, 647–649 (2001).
282. Tanti, J. F., Grémeaux, T., Van Obberghen, E. & Le Marchand-Brustel, Y. Effects of okadaic acid, an inhibitor of protein phosphatases-1 and -2A, on glucose transport and metabolism in skeletal muscle. *J. Biol. Chem.* **266**, 2099–103 (1991).
283. Bialojan, C. & Takai, A. Inhibitory effect of a marine-sponge toxin, okadaic acid, on protein phosphatases. Specificity and kinetics. *Biochem. J.* **256**, 283–90 (1988).
284. Feyen, J. H. & Kuntzelmann, G. M. Inhibitory effect of okadaic acid on bone resorption in neonatal mouse calvaria in vitro. Protein dephosphorylation as an important regulatory mechanism in the bone resorption process. *Biochem. Biophys. Res. Commun.* **178**, 758–63 (1991).
285. International Osteoporosis Foundation. *IOF Compendium of Osteoporosis*. (2017).
286. Tashjian, A. H. & Gagel, R. F. Teriparatide [Human PTH(1-34)]: 2.5 Years of Experience on the Use and Safety of the Drug for the Treatment of Osteoporosis. *J. Bone Miner. Res.* **21**, 354–365 (2005).
287. Bartholin, L. *et al.* TGIF inhibits retinoid signaling. *Mol. Cell. Biol.* **26**, 990–1001 (2006).
288. Zerlanko, B. J., Bartholin, L., Melhuish, T. A. & Wotton, D. Premature Senescence and Increased TGFβ Signaling in the Absence of Tgif1. *PLoS One* **7**, e35460 (2012).
289. Saneshige, S. *et al.* Retinoic acid directly stimulates osteoclastic bone resorption and gene expression of cathepsin K/OC-2. *Biochem. J.* **309** (Pt 3, 721–4 (1995).
290. Hu, L., Lind, T., Sundqvist, A., Jacobson, A. & Melhus, H. Retinoic acid increases proliferation of human osteoclast progenitors and inhibits RANKL-stimulated osteoclast differentiation by suppressing RANK. *PLoS One* **5**, e13305 (2010).

Bibliography

291. Menéndez-Gutiérrez, M. P. *et al.* Retinoid X receptors orchestrate osteoclast differentiation and postnatal bone remodeling. *J. Clin. Invest.* **125**, 809–23 (2015).
292. Houde, N., Chamoux, E., Bisson, M. & Roux, S. Transforming growth factor-beta1 (TGF-beta1) induces human osteoclast apoptosis by up-regulating Bim. *J. Biol. Chem.* **284**, 23397–404 (2009).
293. Hamid, R. & Brandt, S. J. Transforming growth-interacting factor (TGIF) regulates proliferation and differentiation of human myeloid leukemia cells. *Mol. Oncol.* **3**, 451–463 (2009).
294. Wotton, D., Lo, R. S., Lee, S. & Massagué, J. A Smad Transcriptional Corepressor. *Cell* **97**, 29–39 (1999).
295. Destaing, O. *et al.* The Tyrosine Kinase Activity of c-Src Regulates Actin Dynamics and Organization of Podosomes in Osteoclasts. *Mol. Biol. Cell* **19**, 394–404 (2008).

8 Summary

8.1 Summary in English

High resorption activity is a key component of bone loss during aging. We identified an increased expression of the homeodomain protein TG-interacting factor 1 (Tgif1) in osteoclasts after RANKL/M-CSF stimulation, suggesting a functional role of Tgif1 in osteoclast differentiation. To test this hypothesis, we deleted Tgif1 in the germline (Tgif1^{-/-}) and in the osteoclast lineage (Ctsk-Cre⁺;Tgif1^{loxP/loxP}). Interestingly, 8-month old Ctsk-Cre⁺;Tgif1^{loxP/loxP} mice were protected from aging-related bone loss due to a reduced osteoclast number and bone resorption (p<0.05). Furthermore, in vitro differentiation of bone marrow macrophages (BMMs) obtained from Tgif1^{-/-} or Ctsk-Cre⁺;Tgif1^{loxP/loxP} mice demonstrated a decreased number and size of osteoclasts (p<0.05) and a reduced expression of osteoclast-related genes such as NFATc1 and Cathepsin K, leading to fewer and shallower resorption pits. These findings indicate that Tgif1 promotes osteoclast differentiation and function in a cell-autonomous manner and establish Tgif1 as a novel regulator of bone resorption. To elucidate the underlying molecular mechanism, we performed signaling analyses, which revealed a reduction of phosphorylated ERK1/2 in Tgif1^{-/-} BMMs. While the de novo phosphorylation of ERK1/2 in response to RANKL/M-CSF stimulation was comparable between wild-type and Tgif1^{-/-} BMMs, ERK1/2 was rapidly de-phosphorylated in the absence of Tgif1. This suggests that Tgif1 controls ERK1/2 activity by inhibiting the expression of a specific phosphatase. Indeed, expression analysis of several ERK phosphatases demonstrated an increased expression of the Protein Phosphatase 2A catalytic subunit isoform β (PP2A-C β) in Tgif1^{-/-} BMMs compared to control cells. Mechanistically, inhibition of PP2A using okadaic acid or targeted silencing of PP2A-C β using the GapmeR technology normalized the amount of phosphorylated ERK1/2 and restored the reduced osteoclast differentiation in Tgif1^{-/-} BMMs. In summary, Tgif1-deficiency in osteoclasts impairs ERK1/2 signaling and subsequently osteoclast

Summary

differentiation, function and bone resorption. Thus, *Tgif1* is a novel regulator of bone remodeling with an important function in aging-related bone loss.

8.2 Summary in German

Eine hohe Resorptionsaktivität ist eine Schlüsselkomponente für den Knochenverlust während des Alterns. Wir haben in Osteoklasten nach RANKL/M-CSF-Stimulation eine erhöhte Expression des Homeodomain-Proteins TG-interacting Factor 1 (Tgif1) festgestellt, was auf eine funktionale Rolle von Tgif1 bei der Osteoklasten-Differenzierung hindeutet. Um diese Hypothese zu testen, haben wir Tgif1 aus der Keimbahn (Tgif1^{-/-}) und in der Osteoklastenlinie (Ctsk-Cre⁺;Tgif1^{loxP/loxP}) entfernt. Interessanterweise wurden 8 Monate alte Ctsk-Cre⁺;Tgif1^{loxP/loxP}-Mäuse vor einem durch Alterung bedingten Knochenverlust aufgrund einer reduzierten Osteoklastenzahl und Knochenresorption (p<0,05) geschützt. Darüber hinaus zeigte die *in vitro* Differenzierung von Knochenmark-Makrophagen (BMMs) aus Tgif1^{-/-} oder Ctsk-Cre⁺;Tgif1^{loxP/loxP}-Mäusen eine verringerte Anzahl und Größe von Osteoklasten (p<0,05) und eine verringerte Expression von Osteoklasten-assoziierten Genen, z.B. NFATc1 und Cathepsin K, was zu weniger und flacheren Resorptionslakunen führt. Diese Ergebnisse zeigen, dass Tgif1 die Differenzierung und Funktion von Osteoklasten auf zellautonome Weise fördert und Tgif1 als neuen Regulator der Knochenresorption etabliert. Um den zugrunde liegenden molekularen Mechanismus aufzuklären, führten wir Signalanalysen durch, die eine Reduktion von phosphoryliertem ERK1/2 in Tgif1^{-/-} BMMs zeigten. Während die de-novo Phosphorylierung von ERK1/2 als Reaktion auf die RANKL/M-CSF-Stimulation zwischen Wildtyp und Tgif1^{-/-} BMMs vergleichbar war, wurde ERK1/2 in Abwesenheit von Tgif1 schnell desophoryliert. Dies legt nahe, dass Tgif1 die ERK1/2-Aktivität durch Hemmung der Expression einer spezifischen Phosphatase kontrolliert. In der Tat zeigte die Expressionsanalyse mehrerer ERK-Phosphatasen eine erhöhte Expression der Isoform β (PP2A-C β) der katalytischen Proteinphosphatase-2A-Untereinheit in Tgif1^{-/-} BMMs im Vergleich zu Kontrollzellen. Mechanistisch normalisierte die Inhibierung von PP2A unter Verwendung von Okadainsäure oder das gezielte Stummschalten von PP2A-C β unter Verwendung der GapmeR-Technologie

Summary

die Menge an phosphoryliertem ERK1/2 und stellte die reduzierte Osteoklastendifferenzierung in $Tgif1^{-/-}$ BMMs wieder her. Zusammenfassend kann gesagt werden, dass der $Tgif1$ -Mangel bei Osteoklasten die ERK1/2-Signalgebung und anschließend die Differenzierung und Funktion von Osteoklasten beeinträchtigt. Somit ist $Tgif1$ ein neuartiger Regulator des Knochenbaus mit einer wichtigen Funktion beim altersbedingten Knochenverlust.

***9 List of Publications
and Author
Contributions***

9.1 Publications

This author has contributed to four publications that do not form part of this thesis:

- **TG-interacting factor 1 (Tgif1)-deficiency attenuates bone remodeling and blunts the anabolic response to parathyroid hormone**

Saito H, Gasser A, Bolamperti S, **Maeda M**, Matthies L, Ring M, Shih Y, Jähn K, Long CL, Schlüter H, Kwiatkowski M, Johnsen SA, Nagarajan S, Kari V, Haasper C, Gehrke T, Saini V, Pajevic PD, Bellodo T, van Wijnen A, Mohammads KS, Guise T, Taipaleenmäki H and Hesse E.

Under review.

This author established osteoclast assay in our laboratory.

- **Increased levels of sodium chloride directly increase osteoclastic differentiation and resorption in mice and men**

Wu L, Luthringer BJC, Feyerabend F, Zhang Z, Machens HG, **Maeda M**, Taipaleenmäki H, Hesse E, Willumeit-Römer R, Schilling AF.

Osteoporosis International, 2017 Nov; **28** (11): 3215-3228.
doi: 10.1007/s00198-017-4163-4. Epub 2017 Aug 29.

This author helped conducting experiments of murine osteoclast *in vitro*.

- **The inhibitory effects of a RANKL-binding peptide on articular and periarticular bone loss in a murine model of collagen-induced arthritis: a bone histomorphometric study**

Kato G, Shimizu Y, Arai Y, Suzuki N, Sugamori Y, **Maeda M**, Takahashi M, Tamura Y, Wakabayashi N, Murali R, Ono T, Ohya K, Mise-Omata S, Aoki K.

Arthritis Res Ther. 2015 Sep 12; **17**: 251 (1-14).
doi: 10.1186/s13075-015-0753-8.

This author helped conducting experiments *in vivo*.

- **A disulfide bond replacement strategy enables the efficient design of artificial therapeutic peptides**

Aoki K, **M. Maeda M**, Nakae T, Okada Y, Ohya K and Chiba K.

Tetrahedron, 2014 Oct 21, **70** (42): 7774-7779.
doi.org/10.1016/j.tet.2014.05.079.

This author carried out all evaluations of modified peptides *in vitro* and *in vivo*.

9.2 Abstracts

- **Aging-related Bone Loss is Attenuated through Tgif1-ERK1/2 Signaling in Osteoclasts**

Miki Maeda, Hiroaki Saito, Hanna Taipaleenmäki, Eric Hesse

ECTS 2018, Valencia, Spain
New Investigator Award

- **Tgif1-Deficiency Attenuates Aging-Related Bone Loss through ERK1/2 Signaling in Osteoclasts**

Miki Maeda, Hiroaki Saito, Hanna Taipaleenmäki, Eric Hesse

ASBMR 2017, Denver, CO
Young Investigator Travel Grant

- **Tgif1-Deficiency Attenuates Aging-Related Bone Loss through ERK1/2 Signaling in Osteoclasts**

Miki Maeda, Hiroaki Saito, Hanna Taipaleenmäki, Eric Hesse

Eleventh ASBMR-EFF Fellows Forum on Metabolic Bone Diseases 2017, Denver, CO
Eleventh ASBMR-EFF Fellows Nomination

10 Acknowledgement

Acknowledgement

The author declares no competing financial interest.

In this thesis I report my research, which was carried out in the Molecular Skeletal Biology Laboratory (MSB-Lab) under the supervision of Prof. Dr. Dr. Eric Hesse and Dr. Hanna Taipaleenmäki in the Department of Trauma, Hand and Reconstructive Surgery at the University Medical Center Hamburg-Eppendorf. I would like to thank everyone who helped me during this long-term project. Becoming a PhD has been one of the toughest challenges of my life. I could not have made it without some key people, who I would like to recognize.

First and foremost, I would like to express my deepest gratitude to my supervisor Prof. Eric Hesse for giving me the outstanding opportunity to work on this interesting research project. Without his great knowledge and academic guidance, it would have been impossible to complete this project successfully. I am deeply grateful that I have been given the chance to work with osteoclasts, the most fascinating cells. He provided a stimulating academic environment and a well-equipped laboratory that was opened 24/7. I appreciate that he granted me ample of time to progress with my project. He also supported me to present my work as a poster and even as an oral presentation at several international conferences such as the annual meetings of the American Society for Bone and Mineral Research (ASBMR) in 2017 and of the European Calcified Tissue Society (ECTS) in 2018. This allowed me to interact with famous researchers from all over the world. One of my biggest obstacles was to talk in front of a big audience, but he trained me patiently. I feel very privileged that I received travel grants from ASBMR and the Endocrine Fellowship Foundation (EFF) in 2017. Furthermore, I was awarded the New Investigator Award from ECTS in 2018. It has truly been a pleasure, a privilege, and an honor to have Prof. Hesse as an academic mentor and to be his first PhD student.

Acknowledgement

I am equally and very deeply grateful to Dr. Hanna Taipaleenmäki for being my supervisor. She trained me very patiently, thereby ensuring that my research goes into the right direction. She helped me with establishing osteoclast assays, optimizing transfection conditions, conducting animal studies and revising my English writing. It made me very happy to see her always getting very excited when I had new results and she enjoyed it as if these were her data. She taught me the fun of research and reminded me that "all roads lead to bone."

I would also like to thank Dr. Hiroaki Saito. From the beginning of my life in Germany, he always helped me kindly to translate and explain everything in our mother language Japanese. This was really a great help for me starting a new life abroad comfortably. In addition, he also supervised me how to perform experiments, analyze data, read and interpret the results and to which papers to refer to. I appreciate that he spent so much time for discussing my data even during the coffee break. Importantly, he is one of the greatest contributor of the histomorphometry part of my project.

Special thanks are given to Saskia Schröder, my dear buddy. She is also a great contributor of my project by taking care of mouse bones for histology. Since I have worked as a technician at my former University, I know that her precise performance is amazing. Not only provided technical assistance to produce promising data, she also discussed data with researchers and provided invaluable advice. I am always impressed how much she contributes to researchers' work. We also shared fun, joy, sorrows, frustration and everything else in the laboratory and in private life. That is why I was able to survive in such a tough five years project.

I am grateful to the entire team of the MSB-Lab for introducing me into science and for sharing this remarkable experience. I am very lucky and happy to meet great, brave and smart postdocs;

Acknowledgement

especially, Dr. Simona Bolamperti, Dr. Katharina Jähn, Dr. Courtney Long and Dr. Andreas Gasser. They helped me in adapting to the new environment, which is totally different from Japan. I am proud of establishing friendship with them after a while and for sharing many fun moments. Prost! Kampai! Also, I learnt from them how important family, friends and myself are. This gave me a serious opportunity to think again about work-life balance and how to be successful as a female researcher. I respect all of them and wish them success for their future. Also, I appreciate Cordula Erdmann and “Mrs.” Diana Brandt for kindly teaching me German rules, laws and UKE regulations. I thank to Dr. Katharina Jähn for analyzing 8-week old male $\text{LysM-Cre}^-; \text{Tgfl}^{\text{loxP/loxP}}$ and $\text{LysM-Cre}^+; \text{Tgfl}^{\text{loxP/loxP}}$ mice for histomorphometry. I never forget what they have done for me and how much they encouraged me.

All past and current MSB-Lab members are deserved to my gratitude. They actively attended my lab meetings, gave me scientific advice and valuable feedback throughout. I never worked in such an international laboratory with German, Finnish, Italian, American, Austrian, Russian, Chinese and Japanese before. This environment strengthened myself in my English communication skills, broke my stereotypes and helped me to understand different cultures. The most important lesson they taught me was experience is better than learning.

I would also like to thank all past and current technical students, who worked diligently on genotyping for our laboratory. They played a crucial role in helping us to progress faster and I sincerely appreciate their determined efforts.

I am also indebted to the animal facility members Ms. Gudrun Ahrndt and Mr. Phillip Missberger. I thank them for providing mice for my experiments and for cutting tails for genotyping. Since I exchanged mice cages, filled up water bottles and fed mice by myself when

Acknowledgement

I was an undergraduate student in Japan, I know how much weight their help lifted off my shoulders.

The surface of 20 dentine slices was scanned with Contour GT-K by Dr. Lili Wu and Dr. Jorge Gonzalez at the Helmholtz-Zentrum Geesthacht – Zentrum für Material- und Küstenforschung. I appreciate their effort, time and technical help in quantifying osteoclast resorption activity. In particular, I am grateful to meet with Dr. Wu, who is an Asian female researcher working in Europe and published many papers successfully. I was inspired by her a lot with her heartwarming kindness, independence and strength.

I would like to thank Sarah Heerdmann who taught me how to work in a laboratory until how to rent a city bike at the very beginning when I joined in MSB-Lab. We shared the lab life for about one year as PhD students together at that time. Although we all had busy days, I still remember clearly that she cared about me by asking every single day “Is everything OK?” It was a very pleasant and comfortable feeling I got as a new incoming foreign student. I wish her all the best for her new professional life.

I thank Prof. Dr. Stefan Linder for being a member of my PhD committee and for reviewing this thesis. He always kindly supported, advised and encouraged me. I cannot thank him enough for his great support of the scientific discussions and heartwarming encouragement.

I am happy to thank Prof. Dr. Dr. Sonja Schrepfer for being a member of my PhD committee. Unfortunately, for me, she started working mainly in the U.S. after a while. However, she joined my PhD committee meetings by video.

Acknowledgement

I appreciate Prof. Dr. Dr. Sonja Loges to be my PhD committee attending to my defense. I would like to give all committee members the sincerest appreciation for taking time away from their own labs and research in order to help me.

I would like to thank the University of Medical Center Hamburg-Eppendorf. It has been a great privilege to be a member of the medical department during my PhD course. I was happy to be welcomed as a foreign student from a non-EU country like Japan.

I would also like to acknowledge the role of the PhD Program for non-medical students at UKE. I am thankful to the organizers of the program for giving me a chance and for trusting me by giving me a spot in the program. This program paved the way for all my experiences, colleagues, and friends that I made over the last several years and I appreciate all of it. This PhD program provided very useful lessons for my career path such as good scientific practice, writing skills, presentation skills, statistics and so on. Thanks to all lecturers and organizers for making me a well-rounded scientist. I have also received help from many people including Dr. Katrin Klempahn and Ms. Sabine Plech throughout the entire PhD term.

I appreciate Prof. Dr. Keiichi Ohya, Prof. Dr. Kazuhiro Aoki and Dr. Yukihiro Tamura for giving me the great opportunity to learn more about bone abroad. My road of the bone research has started from the time when I was working in the Hard-Tissue Pharmacology laboratory at the Tokyo Medical and Dental University in Tokyo, Japan. It was all new and precious experiences for me to operate DXA, μ CT, the OsteoMeasure system and metabolic cages. I was fascinated by osteoclasts from that time on in their laboratory, leading to my pure curiosity and motivation to go abroad. It was a big decision and the biggest challenge in my life. I could not have made such a big decision without their support and encouragement. I sincerely thank all

Acknowledgement

of them for their faith in me and for recommending me. I hope they will be proud of me after reading my thesis.

I cannot talk about my life in Germany without Dr. Robert Höppner. I am lucky to have met him to be able to share our similar thoughts about PhD life at the same time in Hamburg. We had lots of fun with friends and encouraged each other during our PhD time. I am very happy for him that he got his PhD in March 2018 like it is now happening to me. I am proud of us to overcome blue moments, and together we are reaching the end and become PhDs.

I would like to thank all my friends for being my biggest fans always.

I am grateful to all my family (Grandma, Mom, Dad, Junko, Masahiro, Aunt) for silently and patiently accepting my reckless decision to go abroad without family, friends and language skills. Later I experienced the difficulty and the toughness of living abroad, which they told me in advance. They were right. But I know that they always support and cheer me up, even though we had much less contact after I came to Germany. I am very happy to be able to hand in this thesis to my family finally. I hope they will be proud of me after seeing my work in this book. I wish I could have shown this book to Jisho.

I thank to Ms. A. F. who always kindly, sometimes strictly advises me and constantly takes care of me to break through the biggest wall. She provided me a pair of crutches, which strongly supports me to walk towards the goal. I believe that I have gotten a strong bone after the fracture.

Acknowledgement

I send my sincere condolences and appreciation to Dr. Andreas Meyer, who greatly supported me to stand up and to go throughout the hardest time of my PhD. I am very sorry that I could not report to him the success of my presentations at the conferences, winning Awards and completing my doctoral thesis. I wish he would be proud of me.

Last but not least, I am very thankful to Manfred Hülsmann, who helped me to find confidence and hope when I felt completely overwhelmed in the hardest moment. Whether it was trying to fix me when I was depressed, patiently listening to me complain, doing his best to understand me as a scientist, providing me comfortable environment and lighting up the path, he has been there consistently through it all. I am happy that he celebrates my success and shares my feelings as if it happened to him. Nobody said it was easy, but now I am proud of us that we walked till the end of this adventure, just like this.

I know there are many people who I have not mentioned here but who deserve my gratitude. Past and present lab members that have helped to guide me, office staff who took care of details for me and student organizations that helped lighten my stress. My degree and accomplishments do not just represent the work I did, but also of all the people who stood behind me and helped me to stay focused.

Thanks many times to everyone who was involved.

A R I G A T O.

27.11.2018
Miki Maeda

11 Curriculum Vitae

Miki Maeda, M. Sc.

CONTACT DETAILS

Date of birth: 27 December 1978

Place of birth: Chiba, Japan

Nationality: Japanese

EDUCATION

- PhD program for non-physicians, Medical Faculty
University of Medical Center Hamburg-Eppendorf, Hamburg, Germany
August 2013-Now
- Master of Science in Biosciences, Faculty of Fundamental Life Sciences
Kitasato University, Tokyo, Japan
April 2001-March 2003
- Bachelor of Science in Biosciences, School of Science
Kitasato University, Tokyo, Japan
April 1997-March 2001
- High School Diploma
Showa Gakuin Shuei High School, Chiba, Japan
April 1994-March 1997

RESEARCH POSITIONS

- August 2013 - : PhD candidate, University of Medical Center Hamburg-Eppendorf, Hamburg, Germany
- July 2012- May 2013: Assistant technician, Tokyo Medical and Dental University, Tokyo, Japan
- April 2011- May 2012: Researcher, Jitsubo Co., Ltd., Tokyo, Japan (Dispatched to Tokyo Medical and Dental University, Tokyo, Japan)
- April 2006- December 2009: Technician, the University of Tokyo, Tokyo, Japan
- April 2003- March 2006: Researcher, Japan BCG Laboratory, Tokyo, Japan

GRANT AND AWARD

- 2018 New Investigator Award, ECTS
- 2017 Young Investigator Travel Grant, ASBMR
- 2017 Eleventh ASBMR-EFF Fellows Nomination, EFF

COURSES AND CERTIFICATES

- ECTS PhD Training Course, Paris, 2017
- Course in Basics of Laboratory Animal Science (FELASA B Guidelines), Berlin, 2016
- ECTS PhD Training Course, Hamburg, 2013 as a part of the organizing hosting team

PROFESSIONAL MEMBERSHIPS

American Society for Bone and Mineral Research (ASBMR)

European Calcified Tissue Society (ECTS)

PUBLICATIONS

Wu L, Luthringer BJC, Feyerabend F, Zhang Z, Machens HG, **Maeda M**, Taipaleenmäki H, Hesse E, Willumeit-Römer R, Schilling AF. Increased levels of sodium chloride directly increase osteoclastic differentiation and resorption in mice and men. *Osteoporosis Int.* 2017; 28 (11): 3215-3228. doi: 10.1007/s00198-017-4163-4.

Kato G, Shimizu Y, Arai Y, Suzuki N, Sugamori Y, **Maeda M**, Takahashi M, Tamura Y, Wakabayashi N, Murali R, Ono T, Ohya K, Mise-Omata S, Aoki K. The inhibitory effects of a RANKL-binding peptide on articular and periarticular bone loss in a murine model of collagen-induced arthritis: a bone histomorphometric study. *Arthritis Res Ther.* 2015; 17: 251 (1-14). doi: 10.1186/s13075-015-0753-8.

Aoki K, **Maeda M**, Nakae T, Okada Y, Ohya K and Chiba K. A disulfide bond replacement strategy enables the efficient design of artificial therapeutic peptides. *Tetrahedron.* 2014; 70 (42): 7774-7779. doi: 10.1016/j.tet.2014.05.079

CONFERENCES ABSTRACTS

Miki Maeda, Hiroaki Saito, Hanna Taipaleenmäki, Eric Hesse. Aging-related Bone Loss is Attenuated through Tgfr1-ERK1/2 Signaling in Osteoclasts. ECTS, Valencia, Spain, 26-29 May 2018

New Investigator Award

Miki Maeda, Hiroaki Saito, Hanna Taipaleenmäki, Eric Hesse. Tgfr1-Deficiency Attenuates Aging-Related Bone Loss through ERK1/2 Signaling in Osteoclasts. ASBMR, Denver, CO, 8-11 September 2017

Young Investigator Travel Grant

Miki Maeda, Hiroaki Saito, Hanna Taipaleenmäki, Eric Hesse. Tgfr1-Deficiency Attenuates Aging-Related Bone Loss through ERK1/2 Signaling in Osteoclasts. Eleventh ASBMR-EFF Fellows Forum on Metabolic Bone Diseases, Denver, CO, 6-7 September 2017

Eleventh ASBMR-EFF Fellows Nomination

12 Declaration

12.1 Declaration in English

I hereby declare that I have written this work independently and without outside help, that I have not used any other sources or auxiliary means other than those stated, and that I have cited all quotations, verbatim or paraphrased, by edition (edition and year of publication), volume and page of the source.

Furthermore, I assure that I have not submitted this thesis for examination to a representative at a different university or otherwise applied for the conferral of a doctorate.

I express my agreement that my dissertation may be examined by the Dean's Office of the Faculty of Medicine with common software for plagiarism detection.

27.11.2018, Hamburg

Signature:

12.2 Declaration in German

Ich versichere ausdrücklich, dass ich die Arbeit selbständig und ohne fremde Hilfe verfasst, andere als die von mir angegebenen Quellen und Hilfsmittel nicht benutzt und die aus den benutzten Werken wörtlich oder inhaltlich entnommenen Stellen einzeln nach Ausgabe (Auflage und Jahr des Erscheinens), Band und Seite des benutzten Werkes kenntlich gemacht habe.

Ferner versichere ich, dass ich die Dissertation bisher nicht einem Fachvertreter an einer anderen Hochschule zur Überprüfung vorgelegt oder mich anderweitig um Zulassung zur Promotion beworben habe.

Ich erkläre mich einverstanden, dass meine Dissertation vom Dekanat der Medizinischen Fakultät mit einer gängigen Software zur Erkennung von Plagiaten überprüft werden kann.

27.11.2018, Hamburg

Unterschrift: